Commun Nonlinear Sci Numer Simulat 136 (2024) 108036

Contents lists available at ScienceDirect

Communications in Nonlinear Science and Numerical Simulation

journal homepage: www.elsevier.com/locate/cnsns

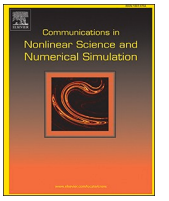

Finite-Time Adaptive Event-Triggered Output Feedback Intelligent Control for Noninteger Order Nonstrict Feedback Systems with Asymmetric Time-varying Pseudo-state Constraints and Nonsmooth Input Nonlinearities

Farouk ZOUARI [a,*], Asier Ibeas [b,*], Abdesselem Boulkroune [c], Jinde Cao [d,e]

[a] *Laboratoire de Recherche en Automatique (LARA), École Nationale d'Ingénieurs de Tunis (ENIT), Université de Tunis El Manar, BP. 37, Le Belvédère, 1002 Tunis, Tunisia*
[b] *Department of Telecommunications and Systems Engineering, Universitat Autònoma de Barcelona, 08193, Bellaterra, Barcelona, Spain*
[c] *LAJ, University of Jijel, BP. 98, Ouled-Aissa, 18000, Jijel, Algeria*
[d] *School of Mathematics, Southeast University, Nanjing 211189, China*
[e] *Ahlia University, Manama 10878, Bahrain*

ARTICLE INFO

Keywords:
Approximation-based-neural adaptive control
Event-triggering mechanism
Non-integer order non-strict feedback systems
High-gain observer
Time-varying asymmetric barrier lyapunov functions
Nussbaum-type functions

ABSTRACT

This paper addresses issues and challenges associated with approximation-based adaptive neural event-triggered output feedback control schemes for a group of non-integer order non-strict feedback systems subject to asymmetric time-varying pseudo-state constraints, unknown control directions, and input nonlinearities. The actuator nonlinearities are first approximated using Caputo fractional derivative definitions and novel continuous functions. After that, by introducing auxiliary non-integer order integrators, the original non-affine plant is transformed into an augmented affine system. Furthermore, neural networks, a high-gain observer, and Nussbaum-type functions are applied to deal with the unknown functions, the immeasurable pseudo-states, and the unknown control directions, respectively. In parallel, by utilizing non-integer order filters, the dynamic surface control technique is incorporated to eliminate the "explosion of complexity" that is frequently encountered with backstepping approaches. In addition, an event-triggered mechanism is integrated into the control design procedure to save computational resources and reduce communication burden. Time-varying asymmetric barrier Lyapunov functions are built with error variables to guarantee that the full pseudo-state constraints are not violated. Based on the Lyapunov stability theory, theoretical analysis indicates that the proposed control scheme ensures that (1) the Zeno behavior is excluded, (2) all the closed-loop signals are bounded and (3) the tracking errors converge to the origin asymptotically in finite time. This paper makes the following contributions: (1) New fractional differential inequalities are developed to extend traditional approaches for the stability analysis and the controller design procedure of integer order systems to fractional-order systems; (2) Compared with existing achievements, the proposed adaptive event-triggered control strategy is more advantageous in practice. Finally, simulation studies are worked out to prove the validity of the proposed approach and corroborate the theoretical results.

* Corresponding authors.
E-mail addresses: zouari.farouk@gmail.com, farouk.zouari@enit.utm.tn, farouk.zouari@enit.rnu.tn, farouk.zouari@fst.utm.tn (F. ZOUARI), Asier.Ibeas@uab.cat (A. Ibeas).

https://doi.org/10.1016/j.cnsns.2024.108036
Received 13 November 2023; Received in revised form 20 March 2024; Accepted 17 April 2024
Available online 1 May 2024

1. Introduction

Interest in adaptive control questions of nonlinear systems has grown significantly in recent decades since a large number of branches of science, physics and engineering including bioengineering applications, satellites, electrical networks, financial systems, missiles, planes, ships, vehicles, and so on, may be framed as output tracking issues (see [1-16] and the references therein). It is out of defiance and real-world importance to construct efficient adaptive schemes capable of guaranteeing the appropriate tracking performance of the resulting closed-loop system and of tackling the uncertainty of nonlinear system dynamics [17-33]. A large amount of research into the two existing adaptive control approaches (direct and indirect) has already been conducted recently to regulate both deterministic and continuous-time systems in real-time and stochastic discrete-time systems through adaptation and learning [34-54]. Afterwards, in view of the fact that various nonlinearities, uncertainties and disturbances are inevitable in real-world systems, various effective adaptive control protocols based on the Lyapunov stability theory have been carried out in the open access literature such as flatness-based adaptive control [4], bipartite consensus control [5], machine learning–based adaptive control [6], adaptive finite-time control [7], adaptive dynamic surface control [10,11,29,46], optimal adaptive control [13], observer-based adaptive control [12], event-triggered adaptive control [1,9,10,14,15,28,48-50], switched adaptive control [7,15,16,50], adaptive variable structure control [18], adaptive backstepping control [19], adaptive data-driven control [20], adaptive state feedback control [17], adaptive decentralized control [21], command filter-based adaptive tracking control [22,43], adaptive sliding mode control [15,23], adaptive model predictive control [6,24], adaptive model reference control [25], adaptive intelligent control [26], adaptive synchronization control [8,12,26,27,37], fault-tolerant resilient control [55], among other approaches. Within the intelligent adaptive control field, artificial neural networks and/or fuzzy logic systems are commonly applied to identify system uncertainties such as unknown disturbances, unknown function terms, or even unformed elements of the system, due to their high self-learning abilities, their strong approximation properties and their exceptional structural characteristics [2,4,9,11,17,18,22,23,26,28-30,32-39,42,44,48,49]. Additionally, fuzzy logic systems and neural networks are two universal approximators and essentials in areas of machine learning–based adaptive control techniques covering many topics such as electronic information technology, computer science, and control engineering [6,28-30, 32-39,42,44,48,49]. In the literature, current data (on-line learning), prior recorded data, and simulated data (off-line training) have been utilized to train the parameters of neural networks and fuzzy logic systems [6,11,17,18,22,23,26,28-30,32-39,42,44,48,49]. The most popular artificial neural network training algorithms are the projection-type adaptation algorithm [1], gradient descent algorithm [30], Newton method algorithm [31], Levenberg-Marquardt algorithm [33], and conjugate gradient algorithm [32]. The primary drawbacks of some of the aforesaid studies on adaptive control approaches are: (1) the control gain signs (or control directions) are expected to be known a priori (strictly negative or strictly positive with no loss of generality). (2) The systems studied in the research [1,4,5-7,19] are not taken into account in both the analysis and synthesis phases of the design of practical control systems, the presence of constraints, nonlinearities and nonaffine structures inherent in plant dynamics and/or physical actuators (inputs) or sensors and as a result, there will be a lack of practicability.

It can be drawn from the research [28,34-37] that the non-strict feedback nonlinear systems in the attendance of unknown control directions, nonaffine structures, nonsmooth functions, constraints and input nonlinearities are more prevalent than unconstrained strict feedback ones and that the conception of their controllers and the examination of their stability are exceedingly challenging tasks since they are not differentiable, and if not adequately addressed, the control performance will be adversely affected or even unstable. In practical productions and applications, unknown control directions, nonlinearities, constraints, uncertainties and nonaffine structures can have negative effects on system performance, prevent systems from achieving their objectives and aggravate the relevant control issue [34]. This aroused the interest of scholars and led to considerable progress in the control of research [35-37]. The output-constrained, input-constrained, incremental control variation-constrained, and the state-constrained are the most common constraints in practical applications and executed as performance requirements, nonlinear saturations, safety standards, restrictive conditions, and physical limits [2,3,5,34-36,41,47,48]. In the literature, nonsmooth properties such as saturation, sector nonlinearities, dead zone, hysteresis, backlash, and so on, have constrained system inputs [8,10-12,18,22,26,28,34-39]. On the other hand, as soon as the input directions or control gain signs of many practical engineering systems are complicated to detect, controller design and stability analyses will countenance new problems due to their complications [11,34-36,40]. Notwithstanding the developments in the area of adaptive control and machine learning technology, it should be noted that the constraint violations, as well as ignoring or being unaware of the control direction and input nonlinearity effects, may be a reason for poor performances or instability for controlled systems, resulting in grave issues such as huge overshoots, excessive steady-state errors, longer time responses, poorer transient responses, and process operation shutdowns [34-36]. From a theoretical and engineering perspective, the preponderance of adaptive control techniques is not directly applicable to constrained nonstrict feedback nonlinear systems subject to unknown control directions, nonaffine structures, and input nonlinearities because of their extraordinary architectures [35,36]. In the literature, six techniques have mostly been used so far for decomposing the original nonaffine plant into a nonaffine part representing generalized modeling errors and an affine plant in the control part, notably [34,42,44,46]: (1) intelligent affine models (neural networks or fuzzy logic systems), (2) the implicit function theory, (3) the mean value theorem, (4) Taylor-series expansions, (5) differentiation of the original state space systems and (6) the contraction mapping method. Recently, many constraint-handling methods [2,3,5,34-36,41, 47,48], such as (1) barrier Lyapunov functions, (2) override controls, (3) predictive controls, (4) reference governors, (5) constrained models, (6) error transformation techniques, and many others, have been developed by scientists to satisfy special requirements and to ensure that system outputs or system states do not breach the constraints. Additionally, in the practical automation industry, there are several solutions that use continuous functions to offset the detrimental effects of nonsmooth actuator nonlinearities [10-12,18,22,26, 28,34-39], such as (1) inverse compensation methods, (2) direct decomposition approaches, and so on. Also, the current techniques

used in the literature [11,34-36,40] to compensate for a lack of prior knowledge about control directions specifically are: (1) methods employing switching and monitoring functions, (2) methods employing Nussbaum-type functions; (3) methods employing hysteresis-type functions; (4) methods based on the identification of the unknown control direction; and (5) the correction-vector approach. According to the findings of the preceding works, it is obvious that: (1) methods that handle output and state constraints are incapable of addressing the issues of nonsmooth actuator nonlinearities [35,36], and (2) by using the backstepping technique, both associated Lyapunov functions and feedback controllers have been meticulously built for nonlinear systems in lower triangular form [17,18,29]. However, neither the approximation-based adaptive fuzzy logic system nor neural network backstepping control strategies solve the problem of complexity explosion caused by repeated differentiations of virtual input for the standard adaptive backstepping control methodology [10,46]. Over the last few years, three solutions for dealing with the aforementioned difficulty with the traditional adaptive backstepping design have been devised. Specifically: (1) dynamic surface control (DSC) [10,11,29,46]; (2) command filtering technology [43]; and (3) computation of virtual control inputs and their derivatives in each step using fuzzy systems or/and neural networks [34,35]. Dynamic Surface Control is an upgraded backstepping control approach with a step-by-step conception procedure [10,11,29,31,46]. At each step of the conception process to ensure input-to-state practical stability of the related subsystems, feedback controllers have been created in [1,8,11,17,21,36-40,43,47,48]. The key benefit of dynamic surface control is that by incorporating a first-order low-pass filter of the synthetic input at each stage of the typical backstepping approach it can avoid the "explosion of terms" issue associated with the backstepping conception technique [10,11,29,46]. However, the works mentioned above do not specify the means to compensate for the errors induced by the first-order filters, which decrease the control quality. It is widely known that to address the aforementioned issues command-filtered adaptive backstepping schemes have been created [43]. The restrictions on communication channel bandwidth and computational capacities in several of the practical control systems previously stated have often been challenging and ssues to resolve. It is not merely the effectiveness and good performance of controls that must be taken into account during industrial production, but it is also essential to trim down the communication costs [2,3,15,22-25,27,38,39,42,43]. It is worth noting that traditional control methods rely on continuous control inputs to ensure good system performance, which requires a large amount of communication bandwidth to transmit control signals [27,38,39,42].

Over the last decade studies on the ways to reduce the restricted network bandwidth utilization have piqued the control community's interest, particularly in the field of practical engineering applications [22–25, 27, 38, 39,]. In this sense, control issues in numerous practical plants have been studied using event-triggered, time-triggered, and self-triggered (discrete monitoring) mechanisms [3,15,22-25,27,38]. The benefit of an event-triggered mechanism over a time-triggered mechanism has been exposed in [2,27, 38,39,42,43]. As a result, employing an event-triggered mechanism is the best way to eliminate an unnecessary waste of resources and to decrease computation and communication [15,22-25,27]. It should be highlighted that previous works have employed an event-triggered strategy to eliminate continuous communication with neighbouring agents and/or decrease the number of the events (data transmissions and control updates). Numerous advanced adaptive control schemes, such as neural adaptive backstepping control, observer-based adaptive control, distributed adaptive control, model-free adaptive control, fuzzy adaptive control, sliding mode adaptive control, and finite-time adaptive control have been researched under event-triggered mechanisms as viable alternatives to traditional periodic control methods because they can achieve the desired performance in the attendance of system uncertainties with a reduced communication burden, specified performance circumstances, bandwidth limitations, and minimal resource use [2,3, 15,22-25,27,38,39,42,43]. The literature mostly discusses two ways for creating event-triggered controllers [3,15,22-25,]. The first strategy, known as codesign in the literature, entails simultaneously creating the triggering circumstance and the control rule [2,3,15, 22-25]. The second strategy is emulation design, in which the objective is to simply create the triggering circumstance and the controller is provided a priori [38,39,42,43]. During the practical implementation of event-triggered control schemes, it must be ensured that no Zeno behaviours occur because of their hybrid nature [15,22-25,27]. As is well known Zeno behaviour, which is observed as a phenomenon indicating the existence of an infinite number of events in a finite period of time, affects the normal process of the event generator [3,15,22-25,27,38]. Some of the abovementioned methods of adaptive event-triggered control schemes are limited to the state feedback scenario, which necessitates the knowledge of complete state information [15]. Because full-state measurements are not feasible in real-world applications, state feedback-based adaptive event-triggered control schemes cannot be applied in most circumstances [15]. As a result, investigating event-triggered network control systems that solely depend on the available information (measured or local signals) is essential and critical, which inspired the concept of observer-based (or dynamic-output-feedback) event-triggered control schemes. In the literature, many centralized and distributed observer-based event-triggered control schemes have already been published [15]. Specifically, state observers [51], nonlinear observers [50], high-gain observers [9], extended state observers [49], adaptive fuzzy observers [9,48], adaptive neural observers [28,49], and disturbance observers [1] have been extensively developed in recent research works. In addition, event-triggered control research has recently expanded to fractional-order systems owing to the fact that event-triggered control may result in great savings for both energy resources and computing [2,38,43].

Over the past few years, noninteger-order (fractional-order) calculus has attracted the interest of scholars in many domains of applied mathematics, engineering, and physics because it is an excellent way to improve the description of infinite memory and heredity properties of system models, as well as to better express several physical phenomena in contrast to conventional integer-order calculus [2,5,15,26,34-38,43,54-60]. Moreover, fractional calculus is frequently seen mathematically as a superset and extension of integer-order calculus [26,34-38,43,54-60]. The fractional-order derivative is nonlocal and the subsequent tates are dependent not only on the current states but also on their preceding states' histories [2,5,15,26,34,54,58-60]. Thanks to advances in current mathematical knowledge, fractional (noninteger order) differential and integral equations offer many fascinating features, such as the precision of controlling and modeling physical systems [38,43,54-60]. However, finance systems, electrical circuit systems, mechanical systems, polarization process, COVID-19 epidemic transmission, chaotic systems, diffusion waves and many practical

applications exhibit dynamic behaviours like those of fractional order systems and are well characterized by differential fractional-order models, i.e. equations that include both integer derivatives and fractional (noninteger)-order derivatives [15,26, 34-38,43,54]. Because numerous valuable mathematical techniques, such as Leibniz and Chain Rules, cannot be readily extended to fractional-order derivatives and integrals, it is difficult to generalize established methods of stability analysis and control of integer order plants to those of fractional (noninteger) order ones [34-38,43,54-60]. There are several excellent techniques for dealing with these difficulties and for studying stability controllability, and observability of fractional order systems [2,5,15,26,34-38,43,54-60], namely: (1) the linear matrix inequality (LMI) method; (2) the Laplace transform method; (3) the method based on convex Lyapunov functions; (4) the method based on Mittag-Leffler functions; (5) the method based on equivalent frequency distributed models; (6) the method based on Volterra-type Lyapunov functions; (7) the method based on Gronwall-Bellman-Bihari type inequalities; (8) the method based on Matignon's stability theorem, and so on. The results reported in [28,29,35-37] assure that the tracking errors or states asymptotically approach zero, implying that the settling time is unlimited. From a practical view, finite-time convergence is a desirable goal [7,39,45], which is why enhanced characteristics of finite-time control methods have originally been presented in [7,45]. In contrast to asymptotic stability, finite-time stability typically exhibits not just quicker convergence rates but also certain attractive qualities; for instance, stronger anti-jamming capability, higher tracking accuracy, disturbance rejection and higher robustness to uncertainties [7.39, 45]. Over the last few years, various adaptive finite-time control strategies, such as finite-timeH_∞ control [7], finite-time containment output-feedback control [39] and finite-time formation tracking control [45] have been proposed to nonlinear uncertain plants. Despite the growing body of research on adaptive control strategies for integer order plants, there has been a scarcity of studies on intelligent adaptive control approaches for fractional order systems until recently [2,5,15,26,54-57]. As far as the researchers are aware, the issues of finite-time output feedback event-triggered adaptive intelligent control schemes have not been fully investigated for noninteger order nonstrict feedback systems with unknown control directions, nonaffine structures, pseudo-state constraints and actuator nonlinearities.

Inspired by the preceding literature review, this article chiefly focuses on the issues of neural adaptive event-triggered control protocols for a class of nonaffine nonstrict feedback fractional-order systems subject to unknown control directions, unmodeled dynamics, asymmetric time-varying pseudo-state constraints and input nonlinearities. The solution starts from using the mean-value theorem and novel continuous functions, to approximate the input nonlinearities. Then, auxiliary non-integer order integrators are introduced such that the original nonaffine system is converted into an augmented affine system. To handle the unknown nonlinear system dynamics and functions, neural networks are applied. With the aid of the Lyapunov stability theory and a continuous frequency distributed equivalent model, a neural high-gain observer and a novel adaptive law are constructed for pseudo-state estimation as well as system identification. Besides, the Nussbaum gain technique is used to overcome the difficulties caused by the unknown control gain directions. On the basis of Caputo fractional derivative definitions and fractional order filters, the dynamic surface control method is exploited to address the computational complexity problem brought on by the conventional backstepping approach. Moreover, once into the control design procedure, to reduce the communication burden an event-triggered strategy is integrated with a varying threshold. Asymmetric time-varying barrier Lyapunov functions with the error variables are also introduced into the adaptive control design to prevent the violation of the full pseudo-state constraints. In addition, the adaptive mechanism is developed for overcoming any exogenous disturbances, neural approximation errors, neural adaptive observer errors, tracking errors and errors caused by the fractional-order filters. It has been proven based on the Lyapunov function method that (1) the control design avoids Zeno behaviour, (2) all closed-loop signals remain bounded and (3) the reference signals are well-tracked by the system outputs in finite time without transgression of the constraints. Finally, the viability of the devised control strategy is evaluated using stability analysis and simulation results. The main contributions of this article include the following aspects.

(1) New fractional differential inequalities concerning the Caputo-type fractional derivative of the product and the composition of continuously differentiable functions are developed to address the challenge posed by the fact that the traditional Leibniz and Chain Rules for the integer-order derivative are not simply applied to the fractional counterpart. These inequalities play an indispensable role in extending techniques involving the stability analysis and the controller design procedure of integer order systems to a more universal group of fractional-order plants subject to asymmetric time-varying pseudo-state constraints, unknown control directions, input nonlinearities, and nonaffine structures.
(2) Unlike the literature [1,9-12,18,22,27,38,42], the proposed adaptive control design does not require many conditions and assumptions concerning estimation errors, input-to-state stability (ISS), functions, dynamics, control directions, actuator nonlinearities, disturbances, constraints, and uncertainties.
(3) Incommensurate fractional-orders, time-varying asymmetric pseudo-state constraints, dynamical disturbances, immeasurable pseudo-states, triggering mechanisms, nonaffine nonstrict feedback forms, unknown control directions and actuator nonlinearities are considered simultaneously and Zeno behaviour is strictly excluded. Thus, the proposed adaptive event-triggered output-feedback neural control scheme is more advantageous to avoid the algebraic loop problem and is reasonable in practice to lower the burden of communication while ensures the convergence of tracking errors to zero in finite time and maintains the stability of the system without transgression of the constraints, compared with [2,15,34-37].

The remainder of this paper consists of the following sections. Some preliminaries and problem descriptions are introduced in Section 2. The main results of this article, which include the system transformation, the proposed control scheme, the stability analyses and their execution, are provided in Section 3. The simulation results are given in Section 4 to illustrate the effectiveness of the proposed scheme. Finally, the conclusions and future work are found in Section 5.

2. Preliminaries and problem statement

2.1. Preliminaries

For the process of the controller design and the proof of the main results, the subsequent Lemmas 1-5, Properties 1-2, and Definitions 1-3 are needed.

Definitions 1. [2,5,15,26,34-38,43,48,54-60]. The Riemann-Liouville fractional integral of a function $f(t)$ is expressed by the following equation:

$$D_t^{-\delta} f(t) = \frac{1}{\Gamma(\delta)} \int_0^t (t-\tau)^{\delta-1} f(\tau) d\tau \tag{D1.1}$$

with $\Gamma(\delta) = \int_0^{+\infty} \tau^{\delta-1} exp(-\tau) d\tau$ being the well-known Gamma function; $exp(.)$representing the natural exponential function and δ being a constant such that $0 < \delta < 1$.

Definitions 2. (Caputo derivative [34-38,43,48,54-60]). The δ -order Caputo fractional derivative of a function $f(t)$ is given as:

$$D_t^{\delta} f(t) = \frac{1}{\Gamma(1-\delta)} \int_0^t \frac{f^{(1)}(\tau)}{(t-\tau)^{\delta}} d\tau \tag{D2.1}$$

where $f^{(1)}(t) = \dot{f}(t) = \frac{\partial f(t)}{\partial t}$ is the first integer-order derivative of the function $f(t)$. δ is a constant satisfying $0 < \delta < 1$.

Definitions 3. [34,35,36] The properties of the continuous function $N(.)$ are as follows:

$$\begin{cases} \lim\limits_{s \to \pm\infty} \sup \dfrac{1}{s} \displaystyle\int_0^s N(\varsigma)\, d\varsigma = +\infty \\ \lim\limits_{s \to \pm\infty} \inf \dfrac{1}{s} \displaystyle\int_0^s N(\varsigma)\, d\varsigma = -\infty \end{cases} \tag{D3.1}$$

where $N(.)$ can be thought of as a Nussbaum-type function.

Property 1. *[2,4,34-37,54-60] The following expressions hold:*

$$\begin{cases} D_t^1 f(t) = f^{(1)}(t) = \dot{f}(t) = \dfrac{\partial f(t)}{\partial t} \\ D_t^{\delta}\left[D_t^{-\delta} f(t)\right] = f(t) \\ D_t^1 f(t) = D_t^{\delta}\left[D_t^{1-\delta} f(t)\right] = D_t^{1-\delta}\left[D_t^{\delta} f(t)\right] \\ D_t^{-\delta}\left[D_t^{\delta} f(t)\right] = f(t) - f(0) \\ D_t^{\delta}[\curlyvee_1 f(t)] = \curlyvee_1 D_t^{\delta}[f(t)] \\ D_t^{-\delta}[\curlyvee_1 f(t)] = \curlyvee_1 D_t^{-\delta}[f(t)] \\ D_t^{\delta}[\curlyvee_1 f(t) + \curlyvee_2 g(t)] = \curlyvee_1 D_t^{\delta}[f(t)] + \curlyvee_2 D_t^{\delta}[g(t)] \\ D_t^{-\delta}[\curlyvee_1 f(t) + \curlyvee_2 g(t)] = \curlyvee_1 D_t^{-\delta}[f(t)] + \curlyvee_2 D_t^{-\delta}[g(t)] \\ D_t^{\delta}[\curlyvee_1] = D_t^{\delta}[\curlyvee_2] = 0 \end{cases} \tag{P1.1}$$

with δ being a constant such that $0 < \delta < 1$. $\curlywedge_1$ and $\curlywedge_2$ being constants.

Property 2. *[34] The following inequalities hold*

$$\begin{cases} D_t^{-\delta} f(t) \geq 0, \quad \text{if } f(t) \geq 0 \\ g(t) \leq 0, \quad \text{if } D_t^{\delta} g(t) \leq 0 \text{ and } g(0) = 0 \end{cases} \tag{P2.1}$$

where δ is a constant satisfying $0 < \delta < 1$.

Lemma 1. *[2,11,23,28-30,32-39,42,44,49,61,62] For any arbitrary constant $\varepsilon^* > 0$ and a continuous function $f(.) : \Omega \to \mathbb{R}$, there exists a neural network $(W^*)^T \xi(x)$ such that :*

$$\begin{cases} \left|(W^*)^T \xi(x) - f(x)\right| \leq \varepsilon^* \\ f(x) = (W^*)^T \xi(x) + \varepsilon(x) \\ |\varepsilon(x)| \leq \varepsilon^* \end{cases} \tag{L1.1}$$

where $\boldsymbol{\Omega}$ is a compact set. $\mathbb{R}$ denotes the set of real numbers. $|.|$ represents the absolute value function.

$\boldsymbol{W}^* \in \mathbb{R}^{\boldsymbol{q}}$ is the ideal constant weight vector, $\boldsymbol{q}$ is the number of neural network nodes (the number of neurons in the hidden layer) and $\boldsymbol{\xi}(.) \in \mathbb{R}^{\boldsymbol{q}}$ is a vector of activation functions. $\mathbb{R}^{\boldsymbol{q}}$is the $\boldsymbol{q}$-dimensional real space.

According the Stone-Weierstrass theorem [61], $\| \boldsymbol{W}^* \|$ and $|\boldsymbol{\varepsilon}(\boldsymbol{x})|$ are bounded. The notation $\| . \|$ is employed to signify the Euclidean norm of a vector. $(\boldsymbol{W}^*)^{\boldsymbol{T}}$is the transpose of the vector $\boldsymbol{W}^*$.

Lemma 2. *[34-37] For any functions $\boldsymbol{\sigma}_1 \in \mathbb{R}$ and $\boldsymbol{\sigma}_2 \in \mathbb{R}_+^*$, the following inequality holds*

$$0 \leq |\boldsymbol{\sigma}_1| - \frac{(\boldsymbol{\sigma}_1)^2}{\sqrt{(\boldsymbol{\sigma}_1)^2 + (\boldsymbol{\sigma}_2)^2}} \leq \boldsymbol{\sigma}_2 \tag{L2.1}$$

where $\mathbb{R}_+^*$ stands for the set of strictly positive real numbers.

Lemma 3. *[34] The following inequalities are satisfied*

$$\begin{cases} \dfrac{1}{2} \boldsymbol{D}_t^{\delta} \log\left(\dfrac{(\boldsymbol{\kappa}_1(\boldsymbol{t}))^2}{(\boldsymbol{\kappa}_1(\boldsymbol{t}))^2 - (\boldsymbol{\kappa}_2(\boldsymbol{t}))^2}\right) \leq \dfrac{\boldsymbol{\kappa}_2(\boldsymbol{t})}{(\boldsymbol{\kappa}_1(\boldsymbol{t}))^2 - (\boldsymbol{\kappa}_2(\boldsymbol{t}))^2} \left(\boldsymbol{D}_t^{\delta} \boldsymbol{\kappa}_2(\boldsymbol{t}) - \boldsymbol{\kappa}_1(0) \left(\dfrac{\boldsymbol{\kappa}_2(\boldsymbol{t})}{(\boldsymbol{\kappa}_1(\boldsymbol{t}))^2}\right) \boldsymbol{D}_t^{\delta} \boldsymbol{\kappa}_1(\boldsymbol{t})\right) \\ \log\left(\dfrac{(\boldsymbol{\kappa}_1(\boldsymbol{t}))^2}{(\boldsymbol{\kappa}_1(\boldsymbol{t}))^2 - (\boldsymbol{\kappa}_2(\boldsymbol{t}))^2}\right) \leq \dfrac{(\boldsymbol{\kappa}_2(\boldsymbol{t}))^2}{(\boldsymbol{\kappa}_1(\boldsymbol{t}))^2 - (\boldsymbol{\kappa}_2(\boldsymbol{t}))^2} \\ \text{if } 0 \leq \left(\dfrac{\boldsymbol{\kappa}_2(\boldsymbol{t})}{\boldsymbol{\kappa}_1(\boldsymbol{t})}\right)^2 < 1, \quad \boldsymbol{\kappa}_2(\boldsymbol{t}) \in R \text{ and } \boldsymbol{\kappa}_1(\boldsymbol{t}) \in \mathbb{R}^* \end{cases} \tag{L3.1}$$

where $\boldsymbol{\delta}$ is a constant such that $0 < \boldsymbol{\delta} < 1$. $\mathbb{R}^* = \mathbb{R} \setminus \{0\}$ is the set of non-zero real numbers.

$\mathbf{log}(.)$ is the natural logarithm of $(.)$.

Lemma 4. *[28,54-56] Thanks to continuous frequency distributed model of the fractional integrator, $\boldsymbol{D}_t^{\delta} \boldsymbol{x} = \boldsymbol{f}(\boldsymbol{x})$ can be rewritten in the following form*

$$\begin{cases} \dfrac{\partial \beth(\boldsymbol{\omega}, \boldsymbol{t})}{\partial \boldsymbol{t}} = -\omega \beth(\boldsymbol{\omega}, \boldsymbol{t}) + f(\boldsymbol{x}) \\ x = \displaystyle\int_0^{+\infty} \curlyvee(\boldsymbol{\omega}) \beth(\boldsymbol{\omega}, \boldsymbol{t}) \, d\omega \\ \curlyvee(\boldsymbol{\omega}) = \dfrac{\mathbf{sin}(\boldsymbol{\delta\pi})}{\boldsymbol{\pi}} \boldsymbol{\omega}^{-\delta} \end{cases} \tag{L4.1}$$

where $\boldsymbol{\delta}$ is a constant satisfying $0 < \boldsymbol{\delta} < 1$.

Lemma 5. *[11,34-37,40] Let $\boldsymbol{V}(\boldsymbol{t}) \geq 0$, $\boldsymbol{g}(.)$ be a nonzero bounded function, $\curlywedge$ be a constant, $\boldsymbol{\varsigma}$ be a continuously differentiable function and $\boldsymbol{N}(.)$ be a Nussbaum-type function. If the following inequality holds:*

$$\boldsymbol{V}(\boldsymbol{t}) \leq \ell + \int_0^t (1 + \boldsymbol{g}(\boldsymbol{\tau})\boldsymbol{N}(\boldsymbol{\varsigma}(\boldsymbol{\tau})))\dot{\boldsymbol{\varsigma}}(\boldsymbol{\tau})\boldsymbol{d}\boldsymbol{\tau} \tag{L5.1}$$

Then, $\boldsymbol{V}(\boldsymbol{t})$, $\boldsymbol{\varsigma}(\boldsymbol{t})$ and $\int_0^t (\boldsymbol{1} + \boldsymbol{g}(\boldsymbol{\tau})\boldsymbol{N}(\boldsymbol{\varsigma}(\boldsymbol{\tau})))\dot{\boldsymbol{\varsigma}}(\boldsymbol{\tau})\boldsymbol{d}\boldsymbol{\tau}$ should be bounded $\forall\ \boldsymbol{t} \geq 0$.

Remark 1. The following statements are investigated.

- Because of a scarcity of suitable mathematical tools, it is challenging to apply stability analysis and controller design approaches made for integer-order plants to non-integer-order ones.
- Corollary 2 in [34], Lemma 1 in [35], Lemma 6 in [48] and Theorem 1 in [60] are more logical and reasonable than Eq. (13) in [2] ($\frac{1}{2}\boldsymbol{D}_t^{\boldsymbol{q}}\boldsymbol{\log}\left(\frac{(\kappa_{b_1})^2}{(\kappa_{b_1})^2-(z_1)^2}\right) = \frac{z_1 D_t^q z_1}{(\kappa_{b_1})^2-(z_1)^2}$) and Property 1 ($\boldsymbol{D}_t^{\boldsymbol{q}}\left(\frac{\boldsymbol{f}(\boldsymbol{t})}{\boldsymbol{g}(\boldsymbol{t})}\right) \leq \frac{D_t^q f(t)g(t) - D_t^q f(t) g(t)}{(g(t))^2}$) in [5] , if $0 < \boldsymbol{q} < 1$.
- If a function is concave or convex, in that case, its fractional-order derivatives can become more practical and be further simplified (see [34,35,48,60] and the references therein).

2.2. Problem statement

Consider a wide group of non-integer order non-strict feedback systems with asymmetric time-varying Pseudo-state constraints and input nonlinearities described by

$$\begin{cases} \boldsymbol{D}_t^{\delta_{i,j_i}}\boldsymbol{x}_{i,j_i} = \boldsymbol{f}_{i,j_i}(\boldsymbol{x}, \boldsymbol{d}),\ \textit{for}\ \boldsymbol{j_i} = 1,\ldots,\boldsymbol{n_i} - 1 \\ \boldsymbol{D}_t^{\delta_{i,n_i}}\boldsymbol{x}_{i,n_i} = \boldsymbol{f}_{i,n_i}(\boldsymbol{x}, \boldsymbol{\nu}_i, \boldsymbol{d}) \\ \boldsymbol{\nu_i} = \Delta_{1,i}\boldsymbol{\eta_i}(\boldsymbol{u_i}) + \Delta_{2,i} \\ \boldsymbol{y_i} = \boldsymbol{x}_{i,1},\quad \textit{for}\ i = 1,\ldots,p \end{cases} \tag{1}$$

where:

- $\boldsymbol{D}_t^{\delta_{i,j_i}} = \frac{\boldsymbol{d}^{\delta_{i,j_i}}}{\boldsymbol{dt}^{\delta_{i,j_i}}}$ denotes the symbol of the Caputo fractional-order calculus **for** $\boldsymbol{j_i} = 1,\ldots,\boldsymbol{n_i}$, $\boldsymbol{i} = 1,\ldots,\boldsymbol{p}$.
- $\boldsymbol{y} = \left[\boldsymbol{y}_1,\ldots,\boldsymbol{y}_p\right]^T \in \mathbb{R}^p$ and $\boldsymbol{u} = \left[\boldsymbol{u}_1,\ldots,\boldsymbol{u}_p\right]^T \in \mathbb{R}^p$ are the vectors of system outputs and control inputs, respectively.
- $\boldsymbol{x} = \left[\boldsymbol{x}_1{}^T,\ldots,\boldsymbol{x}_p{}^T\right]^T \in \mathbb{R}^n$ represents the vector of pseudo-states with $\sum_{i=1}^p \boldsymbol{n_i} = \boldsymbol{n}$ and $\boldsymbol{x_i} = \left[\boldsymbol{x}_{i,1}\ldots,\boldsymbol{x}_{i,n_i}\right]^T \in \mathbb{R}^{n_i}$, **for** $\boldsymbol{i} = 1,\ldots,\boldsymbol{p}$.
- The full pseudo-states are unmeasured, but the output $\boldsymbol{y} \in \mathbb{R}^p$ can be measured.
- The known constant $0 < \boldsymbol{\delta}_{i,j_i} < 1$, is the order of the Caputo fractional-order calculus **for** $\boldsymbol{j_i} = 1,\ldots,\boldsymbol{n_i}$, $\boldsymbol{i} = 1,\ldots,\boldsymbol{p}$.
- The unknown functions $\boldsymbol{f}_{i,j_i}(.)$ and $\boldsymbol{\eta_i}(.)$ are continuously differentiable, for $\boldsymbol{j_i} = 1,\ldots,\boldsymbol{n_i}$, $\boldsymbol{i} = 1,\ldots,\boldsymbol{p}$.
- $\Delta_{1,i}$ is an unknown nonzero bounded function, for $\boldsymbol{i} = 1,\ldots,\boldsymbol{p}$.
- $\Delta_{2,i}$ is an unknown bounded function, for $\boldsymbol{i} = 1,\ldots,\boldsymbol{p}$.
- The vector of bounded and unknown functions $\boldsymbol{d} \in \mathbb{R}^n$ denotes the external disturbance.
- The vector of unknown continuous functions $\boldsymbol{\nu} = \left[\nu_1,\ldots,\boldsymbol{\nu_p}\right]^T \in \mathbb{R}^p$ is the output of actuator nonlinearities.
- $\boldsymbol{x}_{i,j_i} \in \mathbb{R}$ is restricted to a time-varying region $\underline{\boldsymbol{\kappa}}_{1,i,j_i} < \boldsymbol{x}_{i,j_i} < \overline{\boldsymbol{\kappa}}_{1,i,j_i}$ **for** $\boldsymbol{j_i} = 1,\ldots,\boldsymbol{n_i}$, $\boldsymbol{i} = 1,\ldots,\boldsymbol{p}$. (Time-varying pseudo-state Constraints)
- The time-varying barrier functions $\underline{\boldsymbol{\kappa}}_{1,i,j_i}$ and $\overline{\boldsymbol{\kappa}}_{1,i,j_i}$ are known, bounded and smooth with $\underline{\boldsymbol{\kappa}}_{1,i,j_i} < \overline{\boldsymbol{\kappa}}_{1,i,j_i}$. Furthermore, the non-integer (fractional) order derivatives of the functions ($\underline{\boldsymbol{\kappa}}_{1,i,j_i}$ and $\overline{\boldsymbol{\kappa}}_{1,i,j_i}$) are bounded, **for** $\boldsymbol{j_i} = 1,\ldots,\boldsymbol{n_i}$, $\boldsymbol{i} = 1,\ldots,\boldsymbol{p}$.

Remark 2. In alignment with research on barrier Lyapunov functions [2,3,34-36,41,47,48], the initial condition of the considered system should be within the constrained region.

Remark 3. It is emphasized in [2,5,15,26,34-38,43,48,54-60,63-65] that, a variety of real-world phenomena and plants in inter-disciplinary domains of sciences, mathematics, engineering and physics (such as computer systems, electric vehicles, acoustics, mechanics, electromagnetism, viscoelastic system, electrode-electrolyte polarization, electromagnetic waves, signal processing, system identification, economy and finance, control and robotics, chemistry, biology, boundary layer effects in ducts, and so on) may be elegantly and successfully described by means of fractional calculus. The real purposes of the non-Integer Order plants are that there are more degrees of freedom in the model and that a memory is incorporated in these plants [34-38,43,48,54-60,63-65]. Researchers, scientists and engineers have confirmed that the integrals and derivatives of fractional orders are defined in the time domain by a convolution operation and that the traditional and classical definitions of the derivative and integral of a function in fractional calculus are generalized from integer orders to real orders [34-38,43,48,60,63-65]. Numerous definitions exist on the subject of the fractional order derivatives namely the Riemann-Liouville, the Caputo, Caputo-Fabrizio, the Erdelyi–Kober, the Coimbra, Atangana-Baleanu, the

Grunwald-Letnikov, the Weyl, the Marchaud, the Riesz, and the Miller and Ross [5,15,26,34-38,43,63-65]. Generally, the fractional derivatives are used for accurate modeling and controlling of systems and phenomena in the real world [5,15,26,34-38,43,48,63-65]. The primary reasons behind the popularity of the Caputo's fractional derivative in the midst of engineers and applied scientists are that [34-38,43,48,54-57,63-65]:

- Its Laplace transform merely needs the integer-order derivatives of the initial conditions.
- Its initial conditions take on the same form as for integer-order differential equations , which have more applications in engineering and have well-understood physical meanings.
- The hyper-singular improper integrals, the mass balance error, the non-zero derivative of constant are avoided when the fractional derivative is described in the Caputo sense.
- In various branches of sciences mathematics and engineering, the Caputo definition is more suitable, effective, concise, and convenient than the abovementioned definitions.

For these reasons, the Caputo definition is used throughout this research.

Remark 4. Fractional differential systems have an unusual characteristic known as infinite-horizon memory, which allows them to store the whole history of a system's dynamics [2,5,15,26,29,34-38,43,48,54-60,63-65]. In comparison, integer-order models rely entirely on initial conditions and subsequent external inputs to establish system states [29,34-38,43]. In fractional-order models, initialization requires knowledge of the system's whole previous behavior, resulting in the idea of pseudo states, which represent system states at any given moment [5,15,26,29,34-38,43]. These pseudo states provide the whole historical information necessary to obtain a singular solution [9,34-38,43,48,54-60]. To tackle the problem of initializing simulations at precise time points in fractional-order systems, researchers used additional correction terms in explicit models to help account to accommodate previous pseudo-state evolution [29,34-38,43,48,54-60]. Moreover, techniques for simulation have been devised, utilizing a (pseudo) state observer concept, to further enhance these corrections after resetting fractional integrators [34-38,43,48,54-60,63-65]. These methods leverage a formula introduced by Podlubny to modify the time reference point linked with fractional differentiation operators [68]. The incorporation of pseudo-states in fractional-order plants offers a more comprehensive insight into plant behaviors compared to traditional states in integer-order plants [2,5,15,26,29,34-38,43]. In contrast to traditional states associated with integer-order derivatives, pseudo-states in fractional-order systems are more complicated and adaptive, dynamically capturing behaviors resulting from fractional-order derivatives [26,29,34-38,43,48,54-60,63]. This flexibility enables pseudo-states to appear in a variety of ways, transcending locality and showing non-local effects and memory-dependent behaviors [15,26,29,34-38,43,48,54-60,63-65]. Understanding and acknowledging pseudo-states is critical for properly modeling, analyzing, and regulating fractional-order systems, and the pseudo-state space model is widely used to create Luenberger-like observers for estimating system variables [15,26,29,34-38,43,48,54-60,63-67]. This comparison emphasizes the importance of pseudo-states beyond the standard notion of states in integer-order systems, underlining their critical role in navigating fractional dynamics' complexity [29,34-38,43,48,54-60,63-65]. Overall, the unique character of pseudo-states emphasizes their tremendous effect on system behavior, providing a more complex and realistic depiction of fractional-order systems [48,54-60,63-65].

Remark 5. Table 1 demonstrates that Caputo's fractional derivative surpasses other approaches in terms of correctness, efficiency, physical interpretation, initialization, memory, computing and mathematical basis [15,26,29,34-38,43,69]. These benefits make Caputo's definition the ideal choice for modeling and controlling complex, long-term systems [26,29,34-38,43,48,54-60,63-65,69,70].

Remark 6. It is worth noting that the fractional-order model outperforms the integer-order model for modeling systems with non-local behaviors or long-term memory effects [26,29,34-38,43,48,54-60,63-65,69,70]. Unlike integer-order models, which only include the most recent states, fractional-order models take into account the full history of the system's evolution, allowing them to capture non-local impacts and long-term dependencies [29,34-38,43,48]. For instance, when studying the reaction of a viscoelastic material to stress, an integer-order model may neglect the material's memory qualities, resulting in inaccurate predictions of its behavior over time [34-38,43,48,54-60,63-65]. A fractional-order model, on the other hand, more fully accounts for the material's viscoelastic character, resulting in more accurate mechanical response predictions [29,34-38,43,48,54-60]. This highlights fractional-order models' supremacy in capturing the complicated dynamics of real-world systems, particularly those with memory-dependent behaviors, making them indispensable tools in areas such as biology, physics, and engineering [54-60,63-65].

Remark 7. It is worth pointing out that there exist up to now techniques primarily employed to solve fractional-order systems:

- the Adomian decomposition method [57],
- the Adams-Bashforth-Moulton algorithm [58],
- the frequency-domain approximation method [59],
- the Grünwald Letnikov (GL) approximation [65],

Similar to [34-37], the improved version of Adams-Bash-forth-Moulton algorithm is used in this study to numerically find an approximate solution of fractional differential equations by reason of its fast convergence, high accuracy and straightforward implementation as compared to other approaches.

Remark 8. It is worth noting that quite a number of plants found in the real world could be described as or converted into the system

Table 1
Comparison of Caputo's Fractional Derivative definition with other definitions [26,29,34-38,43].

Aspect	Caputo's Fractional Derivative	Other definitions
Initial Conditions	Initial values are required for all fractional orders to provide a comprehensive history of system dynamics.	In the absence of a complete system history, just initial values for integer orders may be required.
Mathematical Formulation	Founded on solid fractional calculus concepts, providing a clear physical explanation.	Formulation may differ, possibly lacking theoretical support.
Physical Interpretation	Provides a clear physical interpretation based on the mathematical foundation.	Interpretations may differ and may be less theoretically founded.
Memory	Retains memory of complete previous evolution, capturing long-term dependencies and historical behavior.	May have limited memory and emphasis on short-term dynamics.
Accuracy	Provides a more realistic portrayal of system dynamics, particularly with long-term interdependence.	Accuracy may differ based on the approach and system parameters.
Computational Efficiency	May entail more difficult computations, particularly with non-linear or multidimensional systems.	Some approaches may provide simplified computing procedures.

(1) more concisely and precisely, such as communication systems, flexible crane systems, thruster assisted position mooring systems, levitated ball systems, multiagent systems, cancer immunotherapy systems, electromechanical systems, flexible crane systems, viscoelastic structures, and so on [34-38]. Nonstrict feedback structures, unknown control directions, non-integer incommensurate orders, asymmetric time-varying Pseudo-state constraints and input nonlinearities are said to exist in the plant (1). Resulting from the absence of suitable mathematical methodologies, it is challenging to basically adapt the traditional tools of stability analysis and controller design employed for integer-order plants to fractional-order ones [2,5,15,26,34-38,43,48,54-60]. The fractional-order derivatives of composite functions, for instance, are the sums of an infinite number of terms, as opposed to the simple closed-form expressions of their integer-order derivatives, which are readily produced by applying the chain rule [34-38,43,48,54-60,63,64].

Remark 9. It is noteworthy in the unified frameworks [8,10,12,18,19,26,28,34-39,54,66] that the input (actuator) nonlinearities may be dead zone, saturation, backlash, and hysteresis with unknown parameters. A lot of industrial plants suffer from the presence of actuator nonlinearities, which can create the instability or degrade the performance of the control system [12,18,19,26,28,34-39,66]. This work's actuator nonlinearities ν_i , $i = 1,\ldots,p$ are more general than those presented in [8,10,12,18,19,26,28]. For a long time, the studies of actuator nonlinearities have been challenging and potential subjects in the control community because their exact parameters are unknown and there are no analytic characteristics [8,10,12,18,19,26,28,54].

In this paper, the control signal transmitted to the actuator is subject to some event-triggered mechanism, namely

$$\begin{cases} u_i = \varpi_i(t_k) \ \forall \ \ t_k \le t < t_{k+1} \\ t_{k+1} = inf\ \{t > t_k |\ |\zeta_i(t)| > \beta_i|u_i(t)| + r_i\} \\ \zeta_i(t) = \varpi_i(t) - u_i(t) \end{cases} \tag{2}$$

where:

- $\zeta_i(t)$ is the measurement error between the intermediate control $\varpi_i(t)$ and the control input $u_i(t)$, **for** $i = 1,\ldots,p$.
- $0 < \beta_i < 1$ and $r_i > 0$ are known design parameters, **for** $i = 1,\ldots,p$.
- t_k ($k \in \mathbb{Z}^+$) denotes the controller update time (the sequence of monotonically increasing triggering instant), that is, $t_{k+1} > t_k$ and $t_k \to +\infty$ as $k \to +\infty$), Without loss of generality, the initial sampling instant $t_0 = 0$.
- **inf** $\{.\}$ denotes the infimum (or greatest lower bound) of a set $\{.\}$.

Remark 10. It is worth mentioning that the event-triggered technique (or triggering mechanism) has recently attracted a great deal of attention inside the control systems society especially in network control field because it is an efficient means to minimize the computation cost of the controller, the communication burden, the release times of the sensor, and the actuator and sensor occupancy [2,3,15,22-25,27,38,39,42,43,52,56,62]. The relative threshold approach becomes the fixed threshold strategy if $\beta_i = 0$ [15,22-25,27,38,39]. Moreover, the relative threshold approach ensures longer event inter execution intervals and has less event-triggered times in comparison to the fixed threshold approach [42,43,52,56]. Akin to [42,43,52,56], for the aforementioned event-triggered technique, the smaller the parameters β_i and r_i, the higher the trigger frequency, and the larger the β_i and r_i, the lower the trigger frequency. Accordingly, better control performance may be ensured by the smaller threshold and the larger threshold generates longer release intervals of control input such that unnecessary communication may be avoided [15,22-25,27,38,39]. Mostly, the control inputs are near zero whenever the plant states are next to zero, and the reduced threshold provides the control more precise, resulting in greater system performance [42,43,52,56].

Inspired by the research works in [2,3,15,22-25,27,38], the control inputs can be expressed as follows:

$$u_i(t) = \frac{\varpi_i(t)}{1 + \varphi_{1,i}(t)\beta_i} - \frac{\varphi_{2,i}(t)r_i}{1 + \varphi_{1,i}(t)\beta_i} \tag{3}$$

where $\varphi_{m,i}(t)$ is a nonzero function such that $|\varphi_{m,i}(t)| \leq 1$ for $m = 1, 2$, $i = 1, \ldots, p$.

Remark 11. In view of the fact that uncertain disturbances, time-varying Pseudo-state constraints, input nonlinearities, unknown control directions, non-affine forms, non-strict feedback structures and triggering mechanisms are simultaneously allowed within each subsystem, the plant (1) is more general than that in [4,8,11-13,17-19,21,22,26,28,29,51,61,62].This emphasizes an important distinction between this work and the related research on command filter-based adaptive control schemes [22,43].

Remark 12. It is worth mentioning that one uses time-varying factors, $\varphi_{1,i}(t)$ and $\varphi_{2,i}(t)$, $i = 1, \ldots, p$ in the formula (3), to build the correlation between the intermediate control $\varpi_i(t)$ and the control input $u_i(t)$. Furthermore, the expression (3) will be found to play a crucial part in the control design and the stability analysis later on.

As mentioned above, the primary interest of this paper is to design an observer-Based output Feedback Event-Triggered Adaptive Control scheme for system (1) such that:

- the full pseudo-state constraints are not violated,
- the Zeno behavior does not happen, i.e., the events cannot be triggered an infinite number of times in any finite period.
- the system output y_i tracks in finite time a given bounded desired trajectory $y_{d_i} \in \mathbb{R}$, **for** $i = 1, \ldots, p$
- and all signals in the closed-loop system are bounded.

Remark 13. It should be underlined that numerous academic and practical plants require reaching the control purpose in finite time, such as guided missile plants, uncertain switched port-controlled Hamiltonian systems [7], networked nonaffine nonlinear systems [45], and so on. The advantages of finite time control consist of the better robustness and transient performance of the resulting closed loop control plant [7,45].

Remark 14. For the reason that the event-triggered control system might be modeled as a hybrid system, the analysis of sampling behavior is critical [2,3,15,22-25,27,38,39,42,43,52,56,62]. In reality, at what time a positive lower constraint on inter-event intervals cannot be guaranteed, a specific phenomenon of hybrid dynamical systems (Zeno behavior) may emerge [2,3,15,22-25,27,38]. Inside a given time span, Zeno behavior causes an endless number of discrete transitions (events) [27,38,39,42,43,52,56]. As a result, in event-triggered control, Zeno behavior is particularly uninvited [15,22-25,27,38,39,42,43,52,56,62].

Remark 15. It is assumed in a lot of outstanding research results that the disturbances, the target trajectories and their non integer-order derivatives are bounded [34-37].

To move on, the following assumptions are needed.

Assumption 1. The functions $\frac{\partial f_{i,j_i}(\bar{x},\bar{d})}{\partial x_{i,j_i+1}}$, $\frac{\partial f_{i,n_i}(\bar{x},\nu_i,\bar{d})}{\partial \nu_i}$ and $\frac{\partial \eta_i(u_i)}{\partial u_i}$ are unknown, nonzero, bounded and piecewise continuous, **for** $j_i = 1, \ldots, n_i - 1$, $i = 1, \ldots, p$.

Assumption 2. The desired trajectory y_{d_i} and its Caputo fractional derivatives are piecewise continuous, available and bounded satisfying the conditions $\underline{\kappa}_{1,i,1} < \underline{\kappa}_{2,i,1} < y_{d_i} < \overline{\kappa}_{2,i,1} < \overline{\kappa}_{1,i,1}$, with $\underline{\kappa}_{2,i,1}$ and $\overline{\kappa}_{2,i,1}$ being bounded functions, **for** $i = 1, \ldots, p$.

Remark 16. Note that Assumptions 1–2 are two standard, logical and familiar assumptions for achieving the control objective of uncertain systems involving dynamical disturbances, event-triggered mechanism, asymmetric time-varying constraints, unmeasured pseudo-states, unknown control directions, and non-affine characteristics [3,34-37]. Such assumptions have formerly surfaced in real applications connected to various disciplines of science and engineering, such as wind turbines, robot manipulators, unmanned surface vehicles, rigid spacecraft, and so on [34-37]. Assumption 1 concerns the plant's controllability and the boundedness of control directions, which is not only necessary and reasonable but also well justified for a wide range of substantial beneficial plants such as aerial vehicles, high-speed trains, robotic systems, and so on [15,43,56]. Furthermore, Assumption 2 is a basic assumption about the virtual control signals and the desired trajectories commonly used in the backstepping-based robust adaptive control design of non-integer order systems with asymmetric time-varying Pseudo-state constraints [2,15,43,56].

3. Main results

For achieving the aims of this research study under Assumptions 1–2, the succeeding techniques and tools will be employed in the system controller design and stability analysis:

- Caputo fractional derivative definitions, novel continuous functions and the mean-value theorem to approximate the input nonlinearities.
- Auxiliary non-integer order integrators to transform the original non-affine system into an augmented affine system and to make explicit control design possible.
- Artificial Neural networks to address the unknown nonlinear functions and internal dynamics.

- A high-gain observer to estimate the immeasurable pseudo-states and to relax the requirement of the Lipschitz continuity about the nonlinear dynamics.
- An auxiliary time and frequency domain function to transform the incommensurate fractional-order nonlinear systems into a continuous frequency distributed model.
- Nussbaum-type functions to avoid the need for any knowledge of the control directions.
- An event-triggered scheme to save network resources and to trim down some unnecessary transmissions from controller to actuator so as to get better resource efficiency.
- The computation of minimal triggering intervals to exclude the undesired Zeno behavior.
- A new dynamic surface control technique based on fractional order filters to overcome the 'explosion of complexity' problem exists in the traditional backstepping design process and to appropriately select the parameter update laws and the control signals.
- The combination of Young's inequality, elementary monochromatic Lyapunov functions of internal state variables and Asymmetric Barrier Lyapunov functions with error variables to guarantee the stability of the transformed system and that the full pseudo-state constraints are not violated.

3.1. System transformation

Similar to [34-37], by employing novel continuous functions, auxiliary non-integer order integrators, the mean value theorem, and the Eq. (3), the system (1) can be rewritten as follows:

$$\begin{cases} \boldsymbol{D}_t^{\delta_{i,j_i}} \boldsymbol{x}_{i,j_i} = \boldsymbol{x}_{i,j_i+1} - \boldsymbol{b}_i \boldsymbol{x}_{i,j_i} + \boldsymbol{g}_{i,j_i}(\chi, \boldsymbol{d}), \ \textit{for } \boldsymbol{j_i} = 1, \ldots, \boldsymbol{n_i}+1 \\ \boldsymbol{D}_t^{\delta_{i,n_i+2}} \boldsymbol{x}_{i,n_i+2} = \vartheta_i - \boldsymbol{b}_i \boldsymbol{x}_{i,n_i+2} + \boldsymbol{g}_{i,n_i+2}(\chi, \boldsymbol{d}) \\ \boldsymbol{y_i} = \boldsymbol{x}_{i,1}, \ \ \textit{for } i = 1, \ldots, p \end{cases} \tag{4}$$

where:

- $\chi = \left[{\chi_1}^T, \ \cdots, \ {\chi_p}^T \right]^T \in \mathbb{R}^{n+2p}$ is the pseudo-state vector of new augmented affine system with ${\chi_i}^T = \left[{\boldsymbol{x}_i}^T, \ \boldsymbol{x}_{i,n_i+1}, \ \boldsymbol{x}_{i,n_i+2} \right]^T \in \mathbb{R}^{n_i+2}$ and $\boldsymbol{x}_{i,n_i+1} = \varpi_i$, **for** $\boldsymbol{i} = 1, \ldots, \boldsymbol{p}$.
- $\boldsymbol{g}_{i,j_i}(\chi, \boldsymbol{d}) = \boldsymbol{f}_{i,j_i}(\boldsymbol{x}, \boldsymbol{d}) + \boldsymbol{b}_i \boldsymbol{x}_{i,j_i} - \boldsymbol{x}_{i,j_i+1}$, **for** $\boldsymbol{j_i} = 1, \ldots, \boldsymbol{n_i} - 1, \ \boldsymbol{i} = 1, \ldots, \boldsymbol{p}$.
- $\boldsymbol{g}_{i,n_i}(\chi, \boldsymbol{d}) = \boldsymbol{f}_{i,n_i}(\boldsymbol{x}, \nu_i, \boldsymbol{d}) - \varpi_i + \boldsymbol{b}_i \boldsymbol{x}_{i,n_i}$, **for** $\boldsymbol{i} = 1, \ldots, \boldsymbol{p}$.
- $\boldsymbol{g}_{i,j_i}(\chi, \boldsymbol{d}) = (\boldsymbol{b}_i - \boldsymbol{b}_{1,ij}) \boldsymbol{x}_{i,j_i}$, **for** $\boldsymbol{j_i} = \boldsymbol{n_i} + 1, \ \boldsymbol{n_i} + 2, \ \boldsymbol{i} = 1, \ldots, \boldsymbol{p}$.
- $\boldsymbol{b}_{1,ij_i}$ and $\boldsymbol{b_i}$ are known strictly positive constants, for $\boldsymbol{j_i} = \boldsymbol{n_i} + 1, \ \boldsymbol{n_i} + 2, \ \boldsymbol{i} = 1, \ldots, \boldsymbol{p}$.
- The known strictly positive constants $\boldsymbol{\delta}_{i,n_i+1}$ and $\boldsymbol{\delta}_{i,n_i+2}$ satisfy the conditions $\boldsymbol{\delta}_{i,n_i+1} + \boldsymbol{\delta}_{i,n_i+2} = 1, \ \ 0 < \boldsymbol{\delta}_{i,n_i+1} < 1$ and $0 < \boldsymbol{\delta}_{i,n_i+2} < 1$, **for** $\boldsymbol{i} = 1, \ldots, \boldsymbol{p}$.
- $\vartheta_i \in \mathbb{R}$ is an auxiliary control input, **for** $\boldsymbol{i} = 1, \ldots, \boldsymbol{p}$.
- The vector of full pseudo-states $\chi \in \mathbb{R}^{n+2p}$ is unmeasured , but the output $\boldsymbol{y} \in \mathbb{R}^p$ can be measured.
- The pseudo-state $\boldsymbol{x}_{i,}$ is required to remain at the constraint condition $\underline{\boldsymbol{\kappa}}_{1,ij_i} < \boldsymbol{x}_{i,j_i} < \bar{\boldsymbol{\kappa}}_{1,ij_i}$ but $\boldsymbol{x}_{i,n_i+1}$ and $\boldsymbol{x}_{i,n_i+2}$ are free from the constraints. for $\boldsymbol{j_i} = 1, \ldots, \boldsymbol{n_i}$, $\boldsymbol{i} = 1, \ldots, \boldsymbol{p}$.

Remark 17. It is noticed that to cope with the controller design complexity from the unknown nonaffine term $\boldsymbol{f}_{i,n_i}(\boldsymbol{x}, \nu_i, \boldsymbol{d})$ in (1), auxiliary filters and the mean value theorem are used. Consequently, the non-affine nonlinear system (1) is obviously converted into an affine-in-control system (4) by means of newly specified pseudo-states and auxiliary control inputs. Because of the use of fractional-order filters (auxiliary filters), the augmented system (4) is one order higher than the original system (1). The intermediate control ϖ_i defined in Eqs. (2)-(3) may be considered as one pseudo-state in this augmented system, while ϑ_i can be seen as the new control input, **for** $\boldsymbol{i} = 1, \ldots, \boldsymbol{p}$. As a result, our key objective in the following is to determine ϑ_i that can force the output $\boldsymbol{y_i} \in \mathbb{R}$ of the augmented system to track a specified reference signal $\boldsymbol{y}_{d_i} \in \mathbb{R}$. It is directly concluded that by controlling plant (4), the control purpose of system (1) can be preserved.

3.2. Neural networks for unknown dynamic system identification

Because of their good capability of modeling nonlinear functions [2,11,23,28-30,32-39,42,44,49,61], Artificial Neural networks are applied over compact sets (regions) $\boldsymbol{\Omega}_{\bar{\chi}} \subset \mathbb{R}^{n+2p}$ and $\boldsymbol{\Omega}_{\chi} \subset \mathbb{R}^{n+2p}$ to identify those unknown nonlinear functions $\boldsymbol{g}_{i,j_i}(\chi, \boldsymbol{d})$ and $\triangle \boldsymbol{g}_{i,j_i}$ in this research work as follows:

$$\begin{cases} g_{ij_i}(\chi,d) = \left(W^*_{ij_i}\right)^T \xi_{ij_i}(\hat{\chi}) + \triangle g_{ij_i} + \varepsilon_{1,ij_i} \\ \qquad\qquad\qquad\qquad \text{for } j_i = 1,\cdots,n_i+2, \quad i=1,\cdots,p \\ \left|\triangle g_{ij_i}\right| \le \ l_{ij_i} \parallel \overline{\chi}_{ij_i} - \widehat{\overline{\chi}}_{ij_i} \parallel + \varepsilon^*_{2,ij_i} \end{cases} \tag{5}$$

where

- $\hat{\chi} = \left[\hat{\chi}_1{}^T, \ \cdots, \ \hat{\chi}_p{}^T\right]^T \in \Omega_{\hat{\chi}} \subset \mathbb{R}^{n+2p}$ is the estimation of χ and also denotes the neural input vector with $\hat{\chi}_i{}^T = [\hat{x}_{i,1}, \ \cdots, \ \hat{x}_{i,n_{i+2}}]^T \in \mathbb{R}^{n_i+2}$, $i = 1,\cdots,p$.
- $\chi \in \ \Omega_\chi \subset \mathbb{R}^{n+2p}$ and $\hat{\chi} \in \Omega_{\hat{\chi}} \subset \mathbb{R}^{n+2p}$.
- $\Omega_{\hat{\chi}}$ and Ω_χ also stand for bounded compacts.
- $\triangle g_{ij_i} = g_{ij_i}(\chi,d) - g_{ij_i}(\hat{\chi},d) = \left(W^*_{ij_i}\right)^T \left[\xi_{ij_i}(\chi) - \xi_{ij_i}(\hat{\chi})\right]$, *for* $j_i = 1,\cdots,n_i+2, \quad i=1,\cdots,p$
- The optimal parameter vector (the ideal neural weight vector) $W^*_{ij_i} \in \mathbb{R}^{q_{ij_i}}$ is an uncertain constant vectors presented as follows

$$W^*_{ij_i} = \underset{W_{ij_i}\in\mathbb{R}^{q_{ij_i}}}{arg\ min} \left[\sup_{\substack{\hat{\chi}\in\Omega_{\hat{\chi}} \\ \chi\in\Omega_\chi}} \left| \left(W_{ij_i}\right)^T \xi_{ij_i}(\chi) - g_{ij_i}(\chi,d) \right| \right], \ for\ j_i = 1,\cdots,n_i+2, \quad i=1,\cdots,p$$

- $\widehat{W}_{ij_i}$ is the estimate of the uncertain constant vector $W^*_{ij_i}$, *for* $j_i = 1,\cdots,n_i+2, \quad i=1,\cdots,p$.
- The neural approximation error (corresponding reconstruction error) $\varepsilon_{1,ij_i} \in \mathbb{R}$ satisfies the inequality $|\varepsilon_{1,ij_i}| < \varepsilon^*_{1,ij_i}$, *for* $j_i = 1,\cdots,n_i+2, \quad i=1,\cdots,p$,
- The unknown strictly positive constant ε^*_{1,ij_i} is arbitrarily small, for $j_i = 1,\cdots,n_i+2, \quad i=1,\cdots,p$.
- $q_{ij_i} \in \mathbb{N}^*$ is the neural node number, for $j_i = 1,\cdots,n_i+2, \quad i=1,\cdots,p$ with $\mathbb{N}^*$ being the set of non-zero integer numbers.
- $\xi_{ij_i}(\hat{\chi}) \in \mathbb{R}^{q_{ij_i}}$ represents the hidden-layer activation function of the neural network (the activation function vector) and satisfies Lipschitz condition, for $j_i = 1,\cdots,n_i+2, \quad i=1,\ldots,p$.
- $\parallel . \parallel$ denotes the 2-norm.
- l_{ij_i} is a known strictly positive constant, for $j_i = 1,\ldots,n_i+2, \quad i=1,\ldots,p$.
- ε^*_{2,ij_i} is an unknown strictly positive constant.
- $\widehat{\overline{\chi}}_{ij_i} = \left[\hat{x}_{i,1}, \ \ldots, \ \ \hat{x}_{ij_i}\right]^T \in \mathbb{R}^{j_i}$ and $\overline{\chi}_{ij_i} = \left[x_{i,1}, \ \ \cdots, \ \ x_{ij_i}\right]^T \in \mathbb{R}^{j_i}$, *for* $j_i = 1,\cdots,n_i+2$, $i=1,\cdots,p$.
- $0 < \left(\xi_{ij_i}(.)\right)^T \left(\xi_{ij_i}(.)\right) \le q_{ij_i}$, *for* $j_i = 1,\cdots,n_i+2$, $i=1,\cdots,p$.

Remark 18. It is widely recognized that:

- There are three Artificial Neural Network groups: Spiking Neural Networks, Recurrent (FeedBack) Neural Networks and Feed-Forward Networks [32-39,42,44,49,61,62].
- Artificial Neural Networks must be trained and have the ability to learn [2,11,23,28–30,32–37,39,42,44,49,61,71].
- Supervised Learning, unsupervised Learning and reinforcement Learning are types of machine learning [6,62,71].
- Deep learning is an artificial neural network-based machine learning technique [6,34-37,62].
- Feedforward neural networks are the most basic and widely used network structure, and they serve as the foundation for the majority of deep learning models [6,32-39,62].
- Linearly parameterized neural networks, Multi-Layer Perceptron Neural networks, Radial-Basis Function Neural Networks, Autoencoder neural networks and Convolutional Neural Networks are the major types of Feedforward neural networks employed to design control schemas and to represent the unknown dynamics of nonlinear plants [2,11,23,28-30,32-39,42,44,49,61,62].
- The artificial neural network utilized in this research, $\left(W^*_{ij_i}\right)^T \xi_{ij_i}(\hat{\chi})$ is a single weight tuning layer or linearly parameterized neural network with three layers: a hidden layer, an input layer, and an output layer.
- The input vector's coordinates are broadcasted to every unit in the hidden layer by the input layer [23,28-30,32-39].
- Every hidden layer unit subsequently generates an activation based on the related non-linear functions [32-39,42,44,49,61].
- All units in the output layer compute linear combinations of the hidden units' activations [11,23,28-30,32-39].
- Linearly parameterized neural networks or single hidden-layer tunable neural networks such as Radial-Basis Function Neural Networks are more potent than other typical neural networks because they successfully manage the compromise between accuracy and computation [32-39,42].
- Logistic functions, hyperbolic tangent functions, sigmoid functions, and Radial basis functions (RBF), are frequently used as non-linear activation functions of the hidden layer neurons while the output layer neurons habitually exploit linear functions as activation functions [2,11,23,28-30,32-39,42,44,49,61,62].
- The hidden-layer activation function $\xi_{ij_i}(\hat{\chi})$ selected in this research, like those in [34-37], meets generalized Lipschitz criteria

- Any continuously differentiable function is locally Lipschitz [1–70].
- Akin to [2,11,23,28-30,32-39,42,44,49,61], the output layer weight vectors $\boldsymbol{W}_{i,j_i}^{*}$, $\boldsymbol{j_i} = 1,\ldots,\boldsymbol{n_i}+2,\ \ \boldsymbol{i} = 1,\ldots,\boldsymbol{p}$, are only calculated and updated online, However, the input layer weights and the bias parameters are primarily selected at random and held constant throughout the control system design in this research.
- The neural networks necessitate several computation and learning operations, which consume an inordinate amount of time.
- The decrease in approximation errors is achieved by increasing the number of nodes in the neural network [34].
- Similar to [32-39,42,44,49,61], the properties of the hidden-layer activation functions of the neural network $0 < \left(\boldsymbol{\xi}_{i,j_i}(.)\right)^{T}\left(\boldsymbol{\xi}_{i,j_i}(.)\right) \leq \boldsymbol{q}_{i,j_i}$ will be employed in the control design to address the algebraic loop issue.

Remark 19. It is noticed that Radial-Basis Function Neural Networks are three-layered neural networks (linearly parameterized neural networks) in particular [2,11,23,28-30,32-39,42,44,49,61,62]. The input neurons (nodes) send the input data to the inner neurons, which create the hidden layer [23,28-30,32-39]. Inside the output (third) layer, the hidden neurons' nonlinear responses are weighted to determine the neural network's final outputs [28-30,32-39,42,44,49]. The Radial-Basis Function Neural Networks are created by introducing radial basis functions into the neural networks [11,23,28-30,32-39,42]. There are several types of radial basis functions, including inverse multiple quadratic functions, reflection Sigmoid functions, and Gaussian functions [32-39,42,44,49]. The essential features of radial basis function neural networks over other neural networks are their better pattern recognition and their ability to identify all unknown continuous functions with arbitrary precisions under compact sets [32-39,42,44,49,61].

3.3. Neural adaptive pseudo-state observer design

Since the pseudo-states of the augmented system$\boldsymbol{x}_{i,2},\ldots,\boldsymbol{x}_{i,\boldsymbol{n}_{i}+2}, \boldsymbol{i} = 1,\ldots,\boldsymbol{p}$ cannot be directly measured, a high-gain observer with an input-driven filter is designed by means of the previous Eqs. (4) and (5) to estimate the immeasurable pseudo-states as follows:

$$
\begin{aligned}
&\boldsymbol{D}_{t}^{\delta_{i,j_i}}\widehat{\boldsymbol{x}}_{i,1} = \widehat{\boldsymbol{x}}_{i,2} - \boldsymbol{b}_{i}\widehat{\boldsymbol{x}}_{i,1} + \left(\widehat{\boldsymbol{W}}_{i,1}\right)^{T}\boldsymbol{\xi}_{i,1}(\widehat{\chi}) + \frac{(3+\boldsymbol{\sigma})\left(\boldsymbol{y}_{i}-\widehat{\boldsymbol{x}}_{i,1}\right)\hbar_{i}}{2\left(\boldsymbol{y}_{i}-\widehat{\boldsymbol{x}}_{i,1}\right)^{2}\left(\boldsymbol{B}_{i,1}\right)^{T}\boldsymbol{P}_{i}\boldsymbol{B}_{i,1} + \left(\hbar_{i}\boldsymbol{\sigma}\right)^{2}}\widehat{\Theta} + \left(\boldsymbol{y}_{i}-\widehat{\boldsymbol{x}}_{i,1}\right)\hbar_{i}\mathrm{K}_{i,1}\\
&\boldsymbol{D}_{t}^{\delta_{i,j_i}}\widehat{\boldsymbol{x}}_{i,j_i} = \widehat{\boldsymbol{x}}_{i,j_i+1} - \boldsymbol{b}_{i}\widehat{\boldsymbol{x}}_{i,j_i} + \left(\widehat{\boldsymbol{W}}_{i,j_i}\right)^{T}\boldsymbol{\xi}_{i,j_i}(\widehat{\chi}) + \left(\boldsymbol{y}_{i}-\widehat{\boldsymbol{x}}_{i,1}\right)\mathrm{K}_{i,j_i}(\hbar_{i})^{j_i},\quad \textbf{for } \boldsymbol{j_i} = 2,\ldots,\boldsymbol{n_i}+1\\
&\boldsymbol{D}_{t}^{\delta_{i,n_i+2}}\widehat{\boldsymbol{x}}_{i,\boldsymbol{n}_{i}+2} = \vartheta_{i} - \boldsymbol{b}_{i}\widehat{\boldsymbol{x}}_{i,\boldsymbol{n}_{i}+2} + \left(\widehat{\boldsymbol{W}}_{i,\boldsymbol{n}_{i}+2}\right)^{T}\boldsymbol{\xi}_{i,\boldsymbol{n}_{i}+2}(\widehat{\chi}) + \left(\boldsymbol{y}_{i}-\widehat{\boldsymbol{x}}_{i,1}\right)\mathrm{K}_{i,\boldsymbol{n}_{i}+2}(\hbar_{i})^{\boldsymbol{n}_{i}+2}\\
&\boldsymbol{y}_{i} = \boldsymbol{x}_{i,1},\quad \textbf{for } \boldsymbol{i} = 1,\ldots,\boldsymbol{p}
\end{aligned}
\tag{6}
$$

where:

- The strictly positive constants $\mathrm{K}_{i,j_i} \in \mathbb{R}_{+}^{*}$, $\boldsymbol{j_i} = 1,\ldots,\boldsymbol{n_i}+2$, are the fixed feedback gains for observer design chosen such that $\boldsymbol{A_i} = \begin{pmatrix} -\mathrm{K}_{i,1} & 1 & 0 & \cdots & 0\\ -\mathrm{K}_{i,2} & 0 & 1 & \ddots & \vdots\\ -\mathrm{K}_{i,3} & 0 & 0 & \ddots & 0\\ \vdots & \vdots & \vdots & \ddots & 1\\ -\mathrm{K}_{i,\boldsymbol{n}_{i}+2} & 0 & 0 & \cdots & 0 \end{pmatrix} \in \mathbb{R}^{(\boldsymbol{n}_{i}+2)\times(\boldsymbol{n}_{i}+2)}$ is a Hurwitz matrix, for $\boldsymbol{i} = 1,\cdots,\boldsymbol{p}$.
- $\mathbb{R}^{(\boldsymbol{n}_{i}+2)\times(\boldsymbol{n}_{i}+2)}$ is the set of $(\boldsymbol{n}_{i}+2)\times(\boldsymbol{n}_{i}+2)$ real matrices.
- The strictly positive constant $\hbar_{i}$ is an adaptive high-gain verifying the condition $\hbar_{i} > \max\left(1, \frac{5+\|\boldsymbol{P}_{i}\|^{2}\sum_{j_i=1}^{\boldsymbol{n}_{i}+2}\left(\mathrm{l}_{i,j_i}\right)^{2}+\lambda_{\min}(\boldsymbol{P}_{i})-2\boldsymbol{b}_{i}\lambda_{\min}(\boldsymbol{P}_{i})}{\lambda_{\min}(\boldsymbol{Q}_{i})}\right)$, for $\boldsymbol{i} = 1,\ldots,\boldsymbol{p}$.
- $\boldsymbol{Q}_{i} = \boldsymbol{Q}_{i}^{T} > 0$ and $\boldsymbol{P}_{i} = \boldsymbol{P}_{i}^{T} > 0$ are symmetric definite positive matrices satisfying $\boldsymbol{A}_{i}^{T}\boldsymbol{P}_{i} + \boldsymbol{P}_{i}\boldsymbol{A}_{i} = -\boldsymbol{Q}_{i}$, for $\boldsymbol{i} = 1,\ldots,\boldsymbol{p}$.
- $\boldsymbol{\lambda_{min}}(.)$ denotes the minimum (smallest) eigenvalue of the matrix $(.)$.
- $\boldsymbol{\lambda_{max}}(.)$ represents the maximum (largest) eigenvalue of the matrix $(.)$,
- $\boldsymbol{max}()$ represents the function of maximum.
- $\|\boldsymbol{P}_{i}\| = \sqrt{\boldsymbol{\lambda_{max}}(\boldsymbol{P}_{i}\boldsymbol{P}_{i})} = \boldsymbol{\lambda_{max}}(\boldsymbol{P}_{i})$.
- $\widehat{\Theta}$ is the estimate of the unknown constant $\boldsymbol{\Theta}^{*}$that will be defined later.
- The known function $\boldsymbol{\sigma}$ is strictly positive and continuously differentiable, such that $\boldsymbol{\sigma}^{2}$, $\boldsymbol{\sigma}$,$\dot{\boldsymbol{\sigma}}$ and $\int_{0}^{t}\boldsymbol{\sigma}(\boldsymbol{\tau})\boldsymbol{d\tau}$ are bounded, $\forall\ t \geq 0$. ($\lim_{\boldsymbol{t}\to+\infty}\boldsymbol{\sigma}(\boldsymbol{t}) = 0$).
- $\boldsymbol{B}_{i,1} = \begin{bmatrix} 1\\ 0\\ \vdots\\ 0 \end{bmatrix} \in \mathbb{R}^{\boldsymbol{n}_{i}+2},\ \textbf{for}\ \ \boldsymbol{i} = 1,\ldots,\boldsymbol{p}.$

Remark 20. It is worthy to point out that the high-gain observer may be viewed as a general case of the classical Luenberger observer

[9,51,53,67]. Besides, the Lipschitz constant of nonlinear dynamics is no longer mandatory in the high-gain observer design compared to some existing observer design for nonlinear systems [9,53,67]. If one supposes that the plant states develop inside a known compact set, the global Lipschitz property can be relaxed to the local Lipschitz, as typically done in the literature [51,53,67]. The main advantages of the so-called high-gain observer are the robustness in the attendance of uncertainties and external disturbances, the acceleration of the convergence speed and the rapid exponential decay of the estimation error (exponential observers) by increasing the observer's gain and acting on design parameters [53]. On the other hand, the main disadvantages of high-gain observers are obviously connected to their sensitivities to noises, as well as, the rising power of the high-gain parameters which might make the practical numerical implementation difficult [51,53]. As a result, as previously observed, these observers' sensitivity to high-frequency measurement noise is often unsatisfactory [9]. In this paper, the terms $-\boldsymbol{b_i}\widehat{\boldsymbol{x}}_{\boldsymbol{i}\boldsymbol{j_i}}$, $\boldsymbol{j_i} = 1,\ldots,\boldsymbol{n_i}+2$, $\boldsymbol{i}=1,\ldots,\boldsymbol{p}$ are used to enhance the high-gain observer's sensitivity properties concerning the high-frequency measurement noise, without sacrificing its advantageous characteristics such as arbitrarily and asymptotic rapid convergence rates and input-to-state stability.

Remark 21. It is worth to mention that:

- $\frac{(\boldsymbol{y_i}-\widehat{\boldsymbol{x}}_{\boldsymbol{i},1})\hbar_i}{2(\boldsymbol{y_i}-\widehat{\boldsymbol{x}}_{\boldsymbol{i},1})^2(\boldsymbol{B}_{\boldsymbol{i},1})^T\boldsymbol{P_i}\boldsymbol{B}_{\boldsymbol{i},1}+(\hbar_i\sigma)^2}$ replaces the term $\frac{\hbar_i}{2(\boldsymbol{y_i}-\widehat{\boldsymbol{x}}_{\boldsymbol{i},1})(\boldsymbol{B}_{\boldsymbol{i},1})^T\boldsymbol{P_i}\boldsymbol{B}_{\boldsymbol{i},1}}$ to force the neural adaptive pseudo-state observer term to be well-defined even when $(\boldsymbol{y_i}-\widehat{\boldsymbol{x}}_{\boldsymbol{i},1})$ converges to zero, which may be thought of as the Levenberg-Marquard regularised inverse utilized in a scalar function.
- $\frac{(3+\sigma)(\boldsymbol{y_i}-\widehat{\boldsymbol{x}}_{\boldsymbol{i},1})\hbar_i}{2(\boldsymbol{y_i}-\widehat{\boldsymbol{x}}_{\boldsymbol{i},1})^2(\boldsymbol{B}_{\boldsymbol{i},1})^T\boldsymbol{P_i}\boldsymbol{B}_{\boldsymbol{i},1}+(\hbar_i\sigma)^2}\widehat{\Theta}$ is incorporated in the adaptive pseudo-state observer in order to compensate the uncertainties, the disturbances and the neural network approximation errors.

Based on the aforesaid Eqs. (4)-(6), the dynamics of the observer errors can be rewritten by the following continuous frequency distributed model (see Lemma 4)

$$\begin{cases} \dfrac{\partial \boldsymbol{\beth}_i(\omega,t)}{\partial t} = -\omega\boldsymbol{\beth}_i(\omega,t) - \boldsymbol{b_i}\boldsymbol{e_i} + \hbar_i\boldsymbol{A_i}\boldsymbol{e_i} - \boldsymbol{B}_{\boldsymbol{i},1}\dfrac{(3+\sigma)\boldsymbol{e}_{\boldsymbol{i},1}}{2(\boldsymbol{e}_{\boldsymbol{i},1})^2(\boldsymbol{B}_{\boldsymbol{i},1})^T\boldsymbol{P_i}\boldsymbol{B}_{\boldsymbol{i},1}+(\sigma)^2}\widehat{\Theta} \\ \qquad\qquad + \displaystyle\sum_{\boldsymbol{j_i}=1}^{\boldsymbol{n_i}+2} \beth_i\boldsymbol{B}_{\boldsymbol{i}\boldsymbol{j_i}}\Big[(\widetilde{\boldsymbol{W}}_{\boldsymbol{i}\boldsymbol{j_i}})^T\boldsymbol{\xi}_{\boldsymbol{i}\boldsymbol{j_i}}(\widehat{\chi}) + \triangle\boldsymbol{g}_{\boldsymbol{i}\boldsymbol{j_i}} + \boldsymbol{\varepsilon}_{\boldsymbol{1},\boldsymbol{i}\boldsymbol{j_i}}\Big] \\ \boldsymbol{e}_{\boldsymbol{i}\boldsymbol{j_i}} = \dfrac{\boldsymbol{x}_{\boldsymbol{i}\boldsymbol{j_i}}-\widehat{\boldsymbol{x}}_{\boldsymbol{i}\boldsymbol{j_i}}}{(\hbar_{\boldsymbol{i}})^{\boldsymbol{j_i}}} = \dfrac{\widetilde{\boldsymbol{x}}_{\boldsymbol{i}\boldsymbol{j_i}}}{(\hbar_{\boldsymbol{i}})^{\boldsymbol{j_i}}} = \displaystyle\int_0^{+\infty} \curlyvee_{\boldsymbol{i}\boldsymbol{j_i}}(\boldsymbol{\omega})\boldsymbol{\beth}_{\boldsymbol{i}\boldsymbol{j_i}}(\omega,t)d\omega \qquad \textit{for } \boldsymbol{j_i}=1,\cdots,\boldsymbol{n_i}+2,\quad \boldsymbol{i}=1,\cdots,\boldsymbol{p} \\ \curlyvee_{\boldsymbol{i}\boldsymbol{j_i}}(\boldsymbol{\omega}) = \dfrac{\sin(\boldsymbol{\delta}_{\boldsymbol{i}\boldsymbol{j_i}}\pi)}{\pi}\omega^{-\delta_{ij_i}} \\ \boldsymbol{\beth}_{\boldsymbol{i}\boldsymbol{j_i}}(\omega,0) = 0 \end{cases} \tag{7}$$

where

- $\mathbf{o}_{\boldsymbol{i}\boldsymbol{j_i}}(\boldsymbol{\omega})$is the frequency weighting function (Auxiliary function) defined in both the time and frequency domains, for $\boldsymbol{j_i}=1,\ldots,\boldsymbol{n_i}+2$, $\boldsymbol{i}=1,\ldots,\boldsymbol{p}$.
- $\boldsymbol{\beth_i}(\boldsymbol{\omega},\boldsymbol{t}) = [\,\boldsymbol{\beth}_{\boldsymbol{i},1}(\boldsymbol{\omega},\boldsymbol{t}),\quad \ldots,\quad \boldsymbol{\beth}_{\boldsymbol{i},\boldsymbol{n_i}+2}(\boldsymbol{\omega},\boldsymbol{t})\,]^{\boldsymbol{T}} \in \mathbb{R}^{\boldsymbol{n_i}+2}$ denotes the frequency distributed state variable.
- $\boldsymbol{\omega}$ is the elementary frequency.
- $\beth_{\boldsymbol{i}} = \mathbf{diag}\left(\dfrac{1}{\hbar_{\boldsymbol{i}}},\quad \ldots,\quad \dfrac{1}{(\hbar_{\boldsymbol{i}})^{\boldsymbol{n_i}+2}}\right) = \begin{bmatrix} \frac{1}{\hbar_i} & 0 & & 0 \\ 0 & \frac{1}{(\hbar_i)^2} & \cdots & \vdots \\ \vdots & \ddots & \ddots & 0 \\ 0 & \cdots & 0 & \frac{1}{(\hbar_i)^{n_i+2}} \end{bmatrix} \in \mathbb{R}^{(\boldsymbol{n_i}+2)\times(\boldsymbol{n_i}+2)}$, *for* $\boldsymbol{i}=1,\ldots,\boldsymbol{p}$.
- $\boldsymbol{e_i} = [\,\boldsymbol{e}_{\boldsymbol{i},1},\quad \ldots,\quad \boldsymbol{e}_{\boldsymbol{i},\boldsymbol{n_i}+2}\,]^{\boldsymbol{T}} \in \mathbb{R}^{\boldsymbol{n_i}+2}$, *for* $\boldsymbol{i}=1,\ldots,\boldsymbol{p}$.
- $\boldsymbol{B}_{\boldsymbol{i},1} = \begin{bmatrix} 1 \\ 0_{(\boldsymbol{n_i}+1)} \end{bmatrix} \in \mathbb{R}^{\boldsymbol{n_i}+2}$, *for* $\boldsymbol{i}=1,\ldots,\boldsymbol{p}$.

- $\boldsymbol{B_{i,j_i}} = \begin{bmatrix} 0_{(j_i-1)} \\ 1 \\ 0_{(n_i+2-j_i)} \end{bmatrix} \in \mathbb{R}^{n_i+2}$, **for** $\boldsymbol{j_i = 2,\ldots,n_i+2,\ i = 1,\ldots,p}$.
- $0_{(j_i-1)} = [0, \quad \cdots, \quad 0]^T \in \mathbb{R}^{j_i-1}$ stands for the zero vector of size $(j_i - 1)$, **for** $\boldsymbol{j_i = 2,\ldots,n_i+2,\ i = 1,\ldots,p}$.
- $0_{(n_i+2-j_i)} = [0, \quad \cdots, \quad 0]^T \in \mathbb{R}^{n_i+2-j_i}$ represents the zero vector of size $(n_i + 2 - j_i)$, **for** $\boldsymbol{j_i = 1,\ldots,n_i,\ i = 1,\ldots,p}$.
- $\widetilde{W}_{i,j_i} = W^*_{i,j_i} - \widehat{W}_{i,j_i}$, **for** $\boldsymbol{j_i = 1,\ldots,n_i+2,\ i = 1,\ldots,p}$.
- $\widetilde{x}_{i,j_i} = x_{i,j_i} - \widehat{x}_{i,j_i}$, **for** $\boldsymbol{j_i = 1,\ldots,n_i+2,\ i = 1,\ldots,p}$.

Remark 22. It should be noted that models with infinite dimensions known as "diffusive representations" can represent fractional-order systems [2,5,15,26,33-38,43,48,54-61,63,64]. As well, the fractional order system can be described as an infinite dimensional integral order system using the continuous frequency distributed model of the fractional integrator [15,26,33-38,43,48,54-61,63,64]. Consequently, the continuous frequency distributed model with properly chosen initial states is a general case of the fractional order system when utilizing Caputo's or Riemann-Liouville's derivative definition [26,33-38,43,48,54-61,63,64]. The non-local in time fractional-order integrator can be exactly converted into a first-order equation on an infinite-dimensional state space by the diffusive realization [33-38,43,48,54-60]. Because a fractional order system is usually implemented in its discrete form, the results for the continuous frequency distributed model can be expanded to the discrete frequency version [33-38,43,48,54-58,63,64].

Let us define the following signals, variables and parameters to be used during the Controller design process and the System stability analysis:

$$\begin{cases} \alpha_{i,0} = y_{d_i} \\ z_{i,1} = y_i - y_{d_i} \\ z_{i,j_i} = \widehat{x}_{i,j_i} - \alpha_{i,j_i-1} \\ D_t^{\delta_{i,j_i}} \alpha^c_{i,j_i-1} = b_{2,i,j_i-1}\left[\alpha_{i,j_i-1} - \alpha^c_{i,j_i-1}\right] \text{ for } \ j_i = 2,\ldots,n_i+2, \quad i = 1,\ldots,p \\ D_t^{\delta_{i,j_i}} \alpha_{i,j_i-1} = D_t^{\delta_{i,j_i}} \alpha^c_{i,j_i-1} + \varepsilon_{3,i,j_i-1} \\ \alpha^c_{i,j_i-1}(0) = \alpha_{i,j_i-1}(0) \end{cases} \tag{8}$$

where :

- z_{i,j_i} is referred to as an error surface, **for** $\boldsymbol{j_i = 1,\ldots,n_i+2\ ,\ i = 1,\ldots,p}$.
- $\alpha_{i,j_i-1} \in \mathbb{R}$ is the virtual control signal recursively designed later and may furthermore be viewed as the input of the fractional order low pass Butterworth filter **for** $\boldsymbol{j_i = 2,\ldots,n_i+2\ ,\ i = 1,\ldots,p}$.
- α^c_{i,j_i-1} represents the output of the fractional order low pass Butterworth filter, **for** $\boldsymbol{j_i = 2,\ldots,n_i+2\ ,\ i = 1,\ldots,p}$.
- b_{2,i,j_i-1} is a known strictly positive design constant, **for** $\boldsymbol{j_i = 2,\ldots,n_i+2\ ,\ i = 1,\ldots,p}$.
- ε_{3,i,j_i-1} is an unknown bounded function satisfying the condition $|\varepsilon_{3,i,j_i-1}| \leq \varepsilon^*_{3,i,j_i-1}$, with $\varepsilon^*_{3,i,j_i-1}$ being an unknown strictly positive constant, **for** $\boldsymbol{j_i = 2,\ldots,n_i+2\ ,\ i = 1,\ldots,p}$.
- $b_{i,0} = \varepsilon^*_{3,i,0} = 0$, **for** $\boldsymbol{i = 1,\cdots,p}$.

Remark 23. As discussed in [29,34], it is well documented that:

- To avoid the algebraic loop issue, filtered signals travelling through fractional order low pass Butterworth filters are used.
- To address the explosion of complexity issues inherent in the traditional backstepping design, the command filters are created.
- $\left[\alpha_{i,j_i-1} - \alpha^c_{i,j_i-1}\right]$, $D_t^{\delta_{i,j_i}}\left[\alpha_{i,j_i-1} - \alpha^c_{i,j_i-1}\right]$ and $D_t^{2\delta_{i,j_i}}\left[\alpha_{i,j_i-1} - \alpha^c_{i,j_i-1}\right]$ are bounded over compact sets, **for** $\boldsymbol{j_i = 2,\cdots,n_i+2\ ,\ i = 1,\cdots,p}$
- The employ of the fractional order filters unavoidably provokes the filtering errors, which will insert to the complexity of obtaining small steady-state errors.

Then, from (4), (6) and (8), the dynamics of error surface can be expressed as

$$
\begin{cases}
D_t^{\delta_{i,1}} z_{i,1} = \alpha_{i,1} + \gamma_{i,1} + \left(\widehat{W}_{i,1}\right)^T \xi_{i,1}\left(\widehat{x}_{i,1}\right) + \left(\widetilde{W}_{i,1}\right)^T \xi_{i,1}\left(\widehat{x}_{i,1}\right) + z_{i,2} \\
+\dfrac{\mu_{i,1}\overline{\kappa}_{3,i,1}(0) z_{i,1} D_t^{\delta_{i,1}} \overline{\kappa}_{3,i,1}}{\left(\overline{\kappa}_{3,i,1}\right)^2} + \dfrac{(1-\mu_{i,1})\overline{\kappa}_{3,i,1}(0) z_{i,1} D_t^{\delta_{i,1}} \overline{\kappa}_{3,i,1}}{\left(\overline{\kappa}_{3,i,1}\right)^2} \\
D_t^{\delta_{i,j_i}} z_{i,j_i} = \alpha_{i,j_i} + \gamma_{i,j_i} + \left(\widehat{W}_{i,j_i}\right)^T \xi_{i,j_i}\left(\widehat{\widehat{\chi}}_{i,j_i}\right) + \left(\widetilde{W}_{i,j_i}\right)^T \xi_{i,j_i}\left(\widehat{\widehat{\chi}}_{i,j_i}\right) + z_{i,j_i+1} \\
+\dfrac{\mu_{i,j_i}\overline{\kappa}_{3,i,j_i}(0) z_{i,j_i} D_t^{\delta_{i,j_i}} \overline{\kappa}_{3,i,j_i}}{\left(\overline{\kappa}_{3,i,j_i}\right)^2} + \dfrac{\left(1-\mu_{i,j_i}\right)\overline{\kappa}_{3,i,j_i}(0) z_{i,j_i} D_t^{\delta_{i,j_i}} \overline{\kappa}_{3,i,j_i}}{\left(\overline{\kappa}_{3,i,j_i}\right)^2} \\
-\dfrac{\left(\left(\overline{\kappa}_{3,i,j_i}\right)^2 - \left(z_{i,j_i}\right)^2\right)\left(\left(\overline{\kappa}_{3,i,j_i}\right)^2 - \left(z_{i,j_i}\right)^2\right)}{\mu_{i,j_i}\left(\overline{\kappa}_{3,i,j_i}\right)^2 + \left(1-\mu_{i,j_i}\right)\left(\overline{\kappa}_{3,i,j_i}\right)^2 - \left(z_{i,j_i}\right)^2} E_{i,j_i-1} \\
\text{for } j_i = 2, \cdots, n_i \\
D_t^{\delta_{i,j_i}} z_{i,j_i} = \alpha_{i,j_i} + \gamma_{i,j_i} + \left(\widehat{W}_{i,j_i}\right)^T \xi_{i,j_i}\left(\widehat{\widehat{\chi}}_{i,j_i}\right) + \left(\widetilde{W}_{i,j_i}\right)^T \xi_{i,j_i}\left(\widehat{\widehat{\chi}}_{i,j_i}\right) + z_{i,j_i+1} - E_{i,j_i-1}, \quad \text{for} \quad j_i = n_i+1,\ n_i+2 \\
\alpha_{i,n_i+2} = \vartheta_i, \quad \text{for} \quad i = 1, \cdots, p
\end{cases}
\tag{9}
$$

where:

■ $E_{i,j_i} = \{ \left[\dfrac{\mu_{i,j_i}}{\left(\left(\underline{\kappa}_{3,i,j_i}\right)^2 - \left(z_{i,j_i}\right)^2\right)} + \dfrac{1-\mu_{i,j_i}}{\left(\left(\overline{\kappa}_{3,i,j_i}\right)^2 - \left(z_{i,j_i}\right)^2\right)} \right] z_{i,j_i},\ for\ j_i = 1, \ldots, n_i$

$$z_{i,j_i},\ \ for\ j_i = n_i+1, n_i+2\ ,\ i = 1, \ldots, p$$

■ $\mu_{i,j_i} = \{ \begin{matrix} 1, & \text{if } z_{i,j_i} \le 0 \\ 0, & \text{if } z_{i,j_i} > 0 \end{matrix}$, for $j_i = 1, \ldots, n_i$, $i = 1, \ldots, p$.

■ The known bounded functions $\overline{\kappa}_{3,i,j_i}$, $\overline{\kappa}_{3,i,j_i}$, $D_t^{\delta_{i,j_i}} \overline{\kappa}_{3,i,1}$ and $D_t^{\delta_{i,j_i}} \overline{\kappa}_{3,i,j_i}$ will be defined later, for $j_i = 1, \ldots, n_i$, $i = 1, \ldots, p$.

■ $z_{i,n_i+3} = E_{i,0} = 0$, for $i = 1, \ldots, p$.

■ $\dfrac{\left(\left(\underline{\kappa}_{3,i,j_i}\right)^2 - \left(z_{i,j_i}\right)^2\right)\left(\left(\overline{\kappa}_{3,i,j_i}\right)^2 - \left(z_{i,j_i}\right)^2\right)}{\mu_{i,j_i}\left(\overline{\kappa}_{3,i,j_i}\right)^2 + \left(1-\mu_{i,j_i}\right)\left(\underline{\kappa}_{3,i,j_i}\right)^2 - \left(z_{i,j_i}\right)^2} E_{i,j_i} = z_{i,j_i}$, for $j_i = 1, \ldots, n_i$, $i = 1, \ldots, p$.

■ $\widehat{\widehat{\chi}}_{i,j_i} = \left[\ \widehat{x}_{i,1},\ \ \ldots,\ \ \widehat{x}_{i,j_i}\ \right]^T \in \mathbb{R}^{j_i}$ and $\overline{\chi}_{i,j_i} = \left[\ x_{i,1},\ \ \cdots,\ \ x_{i,j_i}\ \right]^T \in \mathbb{R}^{j_i}$, for $j_i = 1, \cdots, n_i+2$, $i = 1, \cdots, p$.

■
$$
\begin{cases}
\gamma_{i,1} = -\dfrac{\mu_{i,1}\overline{\kappa}_{3,i,1}(0) z_{i,1} D_t^{\delta_{i,1}} \overline{\kappa}_{3,i,1}}{\left(\overline{\kappa}_{3,i,1}\right)^2} - \dfrac{(1-\mu_{i,1})\overline{\kappa}_{3,i,1}(0) z_{i,1} D_t^{\delta_{i,1}} \overline{\kappa}_{3,i,1}}{\left(\overline{\kappa}_{3,i,1}\right)^2} - D_t^{\delta_{i,1}} y_{d_i} + \left(W_{i,1}^*\right)^T \xi_{i,j_i}(\widehat{\chi}) \\
-\left(W_{i,1}^*\right)^T \xi_{i,j_i}\left(\widehat{x}_{i,1}\right) + \triangle g_{i,1} + (\hbar_i)^2 e_{i,2} + \varepsilon_{1,i,1} \\
\gamma_{i,j_i} = -\dfrac{\mu_{i,j_i}\overline{\kappa}_{3,i,j_i}(0) z_{i,j_i} D_t^{\delta_{i,j_i}} \overline{\kappa}_{3,i,j_i}}{\left(\overline{\kappa}_{3,i,j_i}\right)^2} - \dfrac{\left(1-\mu_{i,j_i}\right)\overline{\kappa}_{3,i,j_i}(0) z_{i,j_i} D_t^{\delta_{i,j_i}} \overline{\kappa}_{3,i,j_i}}{\left(\overline{\kappa}_{3,i,j_i}\right)^2} - b_{2,i,j_i-1}\left[\alpha_{i,j_i-1} - \alpha_{i,j_i-1}^c\right] \\
-\varepsilon_{3,i,j_i-1} + \left(y_i - \widehat{x}_{i,1}\right) \mathrm{K}_{i,j_i} (\hbar_i)^{j_i} + \left(W_{i,j_i}^*\right)^T \xi_{i,j_i}(\widehat{\chi}) - \left(W_{i,j_i}^*\right)^T \xi_{i,j_i}\left(\widehat{\widehat{\chi}}_{i,j_i}\right) \\
-\left(\widetilde{W}_{i,j_i}\right)^T \xi_{i,j_i}(\widehat{\chi}) + \dfrac{\left(\left(\overline{\kappa}_{3,i,j_i}\right)^2 - \left(z_{i,j_i}\right)^2\right)\left(\left(\overline{\kappa}_{3,i,j_i}\right)^2 - \left(z_{i,j_i}\right)^2\right)}{\mu_{i,j_i}\left(\overline{\kappa}_{3,i,j_i}\right)^2 + \left(1-\mu_{i,j_i}\right)\left(\overline{\kappa}_{3,i,j_i}\right)^2 - \left(z_{i,j_i}\right)^2} E_{i,j_i-1} - b_i \alpha_{i,j_i-1} - b_i z_{i,j_i}, \\
\text{for} \quad j_i = 2, \cdots, n_i \\
\gamma_{i,j_i} = -b_{2,i,j_i-1}\left[\alpha_{i,j_i-1} - \alpha_{i,j_i-1}^c\right] - \varepsilon_{3,i,j_i-1} + \left(y_i - \widehat{x}_{i,1}\right) \mathrm{K}_{i,j_i} (\hbar_i)^{j_i} + \left(W_{i,j_i}^*\right)^T \xi_{i,j_i}(\widehat{\chi}) \\
-\left(W_{i,j_i}^*\right)^T \xi_{i,j_i}\left(\widehat{\widehat{\chi}}_{i,j_i}\right) - \left(\widetilde{W}_{i,j_i}\right)^T \xi_{i,j_i}(\widehat{\chi}) + E_{i,j_i-1} - b_i \alpha_{i,j_i-1} - b_i z_{i,j_i} \\
\text{for} \quad j_i = n_i+1,\ n_i+2
\end{cases}
$$

Based on the Eqs. (5) and (9), the following inequality holds over compact sets $\boldsymbol{\Omega}_{\bar{\chi}}$ and $\boldsymbol{\Omega}_{\chi}$

$$\sum_{i=1}^{p}\sum_{j_i=1}^{n_i+2}\left(\gimel_{i,j_i}\boldsymbol{E}_{i,j_i}\right)+\sum_{i=1}^{p}\sum_{j_i=1}^{n_i+2}\left(\frac{\|\boldsymbol{W}_{i,j_i}^{*}-\widehat{\boldsymbol{W}}_{i,j_i}(0)\|^{2}}{2\phi_{2,i,j_i}}\boldsymbol{E}_{i,j_i}\boldsymbol{z}_{i,j_i}\right)$$
$$\leq$$
$$\boldsymbol{\Theta}^{*}\sum_{i=1}^{p}\sum_{j_i=1}^{n_i+2}\left(\|\Im_{i,j_i}\|\,|\boldsymbol{E}_{i,j_i}|\right)+\sum_{i=1}^{p}\|\,\boldsymbol{e}_i\|^{2}+\boldsymbol{\Theta}^{*}-\sum_{i=1}^{p}\sum_{j_i=1}^{n_i+2}\left(2\boldsymbol{q}_{i,j_i}\left(\widetilde{\boldsymbol{W}}_{i,j_i}\right)^{T}\widehat{\boldsymbol{W}}_{i,j_i}\right)$$

$$\textbf{for } \boldsymbol{j_i}=1,\ldots,\boldsymbol{n_i}+2,\boldsymbol{i}=1,\ldots,\boldsymbol{p} \tag{10}$$

with

- $$\Im_{i,j_i}=\left[1,\boldsymbol{E}_{i,j_i}\boldsymbol{z}_{i,j_i},\ \boldsymbol{z}_{i,j_i}\ ,\ \boldsymbol{y}_{d_i},\ \frac{\left(\left(\underline{k}_{3,i,j_i}\right)^{2}-\left(\boldsymbol{z}_{i,j_i}\right)^{2}\right)\left(\left(\overline{k}_{3,i,j_i}\right)^{2}-\left(\boldsymbol{z}_{i,j_i}\right)^{2}\right)}{\boldsymbol{\mu}_{i,j_i}\left(\overline{k}_{3,i,j_i}\right)^{2}+\left(1-\boldsymbol{\mu}_{i,j_i}\right)\left(\overline{\boldsymbol{\kappa}}_{3,i,j_i}\right)^{2}-\left(\boldsymbol{z}_{i,j_i}\right)^{2}}\boldsymbol{E}_{i,j_i-1},\boldsymbol{y}_{i},\widehat{\boldsymbol{x}}_{i,1},\right.$$

  $\left.\alpha_{i,j_i-1}^{c},\ \alpha_{i,j_i-1},\ E_{i,j_i},\ E_{i,j_i-1}\ \right]^{T}\in\mathbb{R}^{11}$ *being a vector of know functions* $\quad\textbf{for } \boldsymbol{j_i}=1,\cdots,\boldsymbol{n_i},\quad \boldsymbol{i}=1,\cdots,\boldsymbol{p}$
- $\Im_{i,j_i}=\left[1,\boldsymbol{z}_{i,j_i}\ ,\boldsymbol{y}_{i}\ ,\widehat{\boldsymbol{x}}_{i,1},\ \boldsymbol{E}_{i,j_i}\boldsymbol{z}_{i,j_i},\ \ \boldsymbol{\alpha}_{i,j_i-1}^{c},\boldsymbol{\alpha}_{i,j_i-1}\ ,\ \boldsymbol{E}_{i,j_i},\boldsymbol{E}_{i,j_i-1}\right]^{T}\in\mathbb{R}^{9}$ being a vector of know functions $\textbf{for } \boldsymbol{j_i}=\boldsymbol{n_i}+1\ ,\ \boldsymbol{n_i}+2\ ,\ \boldsymbol{i}=1,\ldots,\boldsymbol{p}.$
- $\boldsymbol{\Theta}^{*}$ is an unknown constant that fulfills the given condition

$$\sum_{i=1}^{p}\sum_{j_i=1}^{n_i+2}\left(\sqrt{\left(\frac{\overline{\boldsymbol{\kappa}}_{3,i,j_i}(0)\boldsymbol{D}_{t}^{\delta_{i,j_i}}\overline{\boldsymbol{\kappa}}_{3,i,j_i}}{\left(\overline{\boldsymbol{\kappa}}_{3,i,j_i}\right)^{2}}\right)^{2}+\left(\frac{\overline{\boldsymbol{\kappa}}_{3,i,j_i}(0)\boldsymbol{D}_{t}^{\delta_{i,j_i}}\overline{\boldsymbol{\kappa}}_{3,i,j_i}}{\left(\overline{\boldsymbol{\kappa}}_{3,i,j_i}\right)^{2}}\right)^{2}+\left(\boldsymbol{D}_{t}^{\delta_{i,1}}\boldsymbol{y}_{d_i}\right)^{2}+1}+2\boldsymbol{b}_{2,i,j_i-1}\right)$$
$$+\sum_{i=1}^{p}\left(6+2\boldsymbol{b}_{i}\ +4(\boldsymbol{n_i}+2)\|\boldsymbol{P}_i\|^{2}\right)\sum_{j_i=1}^{n_i+2}\left(1+10\boldsymbol{q}_{i,j_i}\|\boldsymbol{W}_{i,j_i}^{*}\|^{2}+\left(\boldsymbol{\varepsilon}_{3,i,j_i-1}^{*}\right)^{2}+\left(\boldsymbol{\varepsilon}_{1,i,j_i}^{*}\right)^{2}+\left(\boldsymbol{\varepsilon}_{2,i,j_i}^{*}\right)^{2}+(\hbar_i)^{j_i}\mathrm{K}_{i,j_i}\right)$$
$$+2\sum_{i=1}^{p}\sum_{j_i=1}^{n_i+2}\left(\left(1+\left(\boldsymbol{l}_{i,j_i}\right)^{2}\right)\left((\hbar_i)^{4}+2\right)\ +\frac{\|\boldsymbol{W}_{i,j_i}^{*}-\widehat{\boldsymbol{W}}_{i,j_i}(0)\|^{2}}{2\phi_{2,i,j_i}}\right)$$
$$\leq$$
$$\boldsymbol{\Theta}^{*}$$

- $\boldsymbol{E}_{i,0}=0,\ \textbf{for } \boldsymbol{i}=1,\ldots,\boldsymbol{p}$

3.4. Adaptive neural network control design

Based on Eqs. (4), (5), (8)-(10) and by combining with a pseudo-state observer (6), an adaptive Backstepping technique and a dynamic surface control method, the adaptive law of parameters, the virtual controller and the auxiliary control inputs are designed as follows:

$$\boldsymbol{\alpha}_{i,j_i}=\boldsymbol{N}\left(\boldsymbol{\varsigma}_{i,j_i}\right)\left[\left(\widehat{\boldsymbol{W}}_{i,j_i}\right)^{T}\boldsymbol{\xi}_{i,j_i}\left(\widehat{\bar{\chi}}_{i,j_i}\right)+\boldsymbol{\Phi}_{i,j_i}\widehat{\theta}\boldsymbol{E}_{i,j_i}+\phi_{1,i,j_i}\int_{0}^{t}\boldsymbol{E}_{i,j_i}(\tau)\ d\tau\right]$$

$$\dot{\boldsymbol{\varsigma}}_{i,j_i}=\left[\left(\widehat{\boldsymbol{W}}_{i,j_i}\right)^{T}\boldsymbol{\xi}_{i,j_i}\left(\widehat{\bar{\chi}}_{i,j_i}\right)+\boldsymbol{\Phi}_{i,j_i}\widehat{\theta}\boldsymbol{E}_{i,j_i}+\phi_{1,i,j_i}\int_{0}^{t}\boldsymbol{E}_{i,j_i}(\tau)\ d\tau\right]\boldsymbol{E}_{i,j_i}$$

$$\dot{\widehat{\boldsymbol{W}}}_{i,j_i}=\phi_{2,i,j_i}\boldsymbol{E}_{i,j_i}\boldsymbol{\xi}_{i,j_i}\left(\widehat{\bar{\chi}}_{i,j_i}\right)-\left((\boldsymbol{n_i}+2)\|\ \boldsymbol{P}_i\|^{2}+1\right)2\phi_{2,i,j_i}\boldsymbol{q}_{i,j_i}\widehat{\boldsymbol{W}}_{i,j_i}-\left(\boldsymbol{E}_{i,j_i}\boldsymbol{z}_{i,j_i}+\boldsymbol{\sigma}\right)\left[\widehat{\boldsymbol{W}}_{i,j_i}-\widehat{\boldsymbol{W}}_{i,j_i}(0)\right] \tag{11}$$

$$\dot{\widehat{\theta}}=\sum_{i=1}^{p}\left(\frac{2(3+\boldsymbol{\sigma})\left(\boldsymbol{e}_{i,1}\right)^{2}\left(\boldsymbol{B}_{i,1}\right)^{T}\boldsymbol{P}_i\boldsymbol{B}_{i,1}}{2\left(\boldsymbol{e}_{i,1}\right)^{2}\left(\boldsymbol{B}_{i,1}\right)^{T}\boldsymbol{P}_i\boldsymbol{B}_{i,1}+(\hbar_i\boldsymbol{\sigma})^{2}}+\sum_{j_i=1}^{n_i+2}\left(\boldsymbol{E}_{i,j_i}\right)^{2}\boldsymbol{\Phi}_{i,j_i}\right)\phi_3-[\widehat{\Theta}-\widehat{\Theta}(0)]\boldsymbol{\sigma},$$

$$\vartheta_i=\boldsymbol{\alpha}_{i,\boldsymbol{n_i}+2},$$
$$\dot{\varpi}_i=-\boldsymbol{b}_{1,i,\boldsymbol{n_i}+2}\boldsymbol{b}_{1,i,\boldsymbol{n_i}+1}\varpi_i-\boldsymbol{b}_{1,i,\boldsymbol{n_i}+1}\boldsymbol{D}_{t}^{\delta_{i,\boldsymbol{n_i}+2}}\varpi_i-\boldsymbol{b}_{1,i,\boldsymbol{n_i}+2}\boldsymbol{D}_{t}^{\delta_{i,\boldsymbol{n_i}+1}}\varpi_i+\vartheta_i\ ,\quad \textbf{for } \boldsymbol{i}=1,\ldots,\boldsymbol{p}$$

with :

- $\boldsymbol{N}(\boldsymbol{\varsigma}_{i,j_i}) = ((\boldsymbol{\varsigma}_{i,j_i})^2 + 2)\exp\left(\frac{(\boldsymbol{\varsigma}_{i,j_i})^2}{2}\right)\sin(\boldsymbol{\varsigma}_{i,j_i})$ being a Nussbaum-type function. for $\boldsymbol{j_i} = 1,\ldots,\boldsymbol{n_i}+2,\ \boldsymbol{i} = 1,\ldots,\boldsymbol{p}$.
- $\boldsymbol{\Phi}_{i,j_i} = \left[\frac{(\rho_{i,j_i})^2}{\sqrt{(\rho_{i,j_i}E_{i,j_i})^2+(\sigma)^2}} + \frac{(z_{i,j_i}\varsigma_{i,j_i}\rho_{i,j_i})^2}{\sqrt{(\rho_{i,j_i}z_{i,j_i}\varsigma_{i,j_i}E_{i,j_i})^2+(\sigma)^2}} + \frac{(3+\sigma)\ (z_{i,j_i})^2}{(z_{i,j_i}E_{i,j_i})^2+(\sigma)^2} + (\rho_{i,j_i}z_{i,j_i}\varsigma_{i,j_i})^2\right]$ being a known strictly positive function **for** $j_i = 1,\ldots,\boldsymbol{n_i}+2,\ \boldsymbol{i} = 1,\ldots,\boldsymbol{p}$.
- $\boldsymbol{\rho}_{i,j_i} = 1 + \|\ \Im_{i,j_i}\ \|$ being a known strictly positive function, **for** $j_i = 1,\ldots,\ \boldsymbol{n_i}+2,\ \boldsymbol{i} = 1,\ldots,\boldsymbol{p}$.
- ϕ_{k,i,j_i} and $\phi_3$being known strictly positive constants, for $\boldsymbol{k} = 1,2\ \boldsymbol{j_i} = 1,\ldots,\boldsymbol{n_i}+2,\ \boldsymbol{i} = 1,\ldots,\boldsymbol{p}$.
- $\widehat{\Theta}$ being the estimate of the unknown constant $\boldsymbol{\Theta}^*$.

Remark 24. It is necessary to point out that:

- $\boldsymbol{\varsigma}^2\mathbf{sin}(\boldsymbol{\varsigma})$, $\mathbf{cosh}\ (\boldsymbol{\varsigma})\ \mathbf{sin}(\boldsymbol{\varsigma})$, $(\boldsymbol{\varsigma}^2+2)\mathbf{exp}\left(\frac{\boldsymbol{\varsigma}^2}{2}\right)\mathbf{sin}(\boldsymbol{\varsigma})$, $\mathbf{exp}(\boldsymbol{\varsigma}^2)\mathbf{sin}(\boldsymbol{\varsigma})$, $\boldsymbol{\varsigma}\ \mathbf{cos}\left(\sqrt{|\boldsymbol{\varsigma}|}\right)$, $\mathbf{cos}\left(\frac{\pi}{2}\boldsymbol{\varsigma}\right)\mathbf{exp}(\boldsymbol{\varsigma}^2)$, $\mathbf{cos}(\boldsymbol{\varsigma})\mathbf{exp}(\boldsymbol{\varsigma}^2)$, $\boldsymbol{\varsigma}^2\mathbf{cos}(\boldsymbol{\varsigma})$, $\mathbf{sin}(\boldsymbol{\varsigma})\mathbf{exp}(|\boldsymbol{\varsigma}|)$ and $\mathbf{cos}\left(\frac{\pi}{2}\boldsymbol{\varsigma}\right)\mathbf{exp}(\boldsymbol{\varsigma}^2)$ have been widely incorporated as Nussbaum-type functions into several control design research works to restrain the harmful effects caused by uncertain control directions and unknown multiple actuator nonlinearities (These functions are formed through a process called as amplitude elongation) [11,34-37,40,66].
- Under certain situations, new families of Nussbaum functions are represented by Mittag-Leffler functions [34-37].
- There exist also new groups of Nussbaum Functions developed by the means of time-elongation (These functions successfully restrain potential control shocks with the help of their predefined and saturated amplitude characteristics.) [34].
- In this research, the more general Nussbaum-type function $(\boldsymbol{\varsigma}^2+2)\mathbf{exp}\left(\frac{\boldsymbol{\varsigma}^2}{2}\right)\mathbf{sin}(\boldsymbol{\varsigma})$ is applied to settle the issues resulting from the event-triggered strategy, the actuator nonlinearities and the unknown control direction because of their many motivating properties.

Remark 25. It is obvious that:

- The term $(\widehat{\boldsymbol{W}}_{i,j_i})^T\boldsymbol{\xi}_{i,j_i}\left(\widehat{\bar{\chi}}_{i,j_i}\right)$ is applied to approximate the unknown nonlinear functions and the uncertain dynamics.
- The Integral term $\phi_{1,i,j_i}\int_0^t \boldsymbol{E}_{i,j_i}(\boldsymbol{\tau})\ \boldsymbol{d\tau}$ is added to the neural adaptive controller, to reduce the steady-state errors.
- The term $\boldsymbol{\Phi}_{i,j_i}\widehat{\Theta}\boldsymbol{E}_{i,j_i}$ is incorporated to guarantee the finite-time stability of the closed-loop system and to achieve robustness to observer errors, disturbances, event errors, neural network approximation errors, uncertainties and command filter errors.
- The e-modification term $[\widehat{\boldsymbol{W}}_{i,j_i} - \widehat{\boldsymbol{W}}_{i,j_i}(0)]\boldsymbol{E}_{i,j_i}\boldsymbol{z}_{i,j_i}$ and the sigma-modification terms $[\widehat{\Theta} - \widehat{\Theta}(0)]\boldsymbol{\sigma}$ and $[\widehat{\boldsymbol{W}}_{i,j_i} - \widehat{\boldsymbol{W}}_{i,j_i}(0)]\boldsymbol{\sigma}$ make the parameter updates robust to every bounded approximation error (ensure robustness by merely restraining parameter growth).
- The initial parameter $\widehat{\Theta}(0)$ must be strictly positive for the conditions $\widehat{\Theta} > 0$ to be valid.$\forall\ \boldsymbol{t} \geq 0$.
- The integration of Nussbaum gain and dynamic surface control techniques poses substantial hurdles to closed-loop stability analysis [34-37]. For this reason, the auxiliary variables $\frac{(\rho_{i,j_i})^2}{\sqrt{(\rho_{i,j_i}E_{i,j_i})^2+(\sigma)^2}}\boldsymbol{E}_{i,j_i}$, $\frac{(z_{i,j_i}\varsigma_{i,j_i}\rho_{i,j_i})^2}{\sqrt{(\rho_{i,j_i}z_{i,j_i}\varsigma_{i,j_i}E_{i,j_i})^2+(\sigma)^2}}\boldsymbol{E}_{i,j_i}$, $\frac{(3+\sigma)\ (z_{i,j_i})^2}{(z_{i,j_i}E_{i,j_i})^2+(\sigma)^2}\boldsymbol{E}_{i,j_i}$ and $(\rho_{i,j_i}z_{i,j_i}\varsigma_{i,j_i})^2\boldsymbol{E}_{i,j_i}$ are added to make the ensuing stability analysis easier and to offset the effect of the filtering errors and event errors.
- The auxiliary control input ϑ_i, the virtual control signal $\boldsymbol{\alpha}_{i,j_i}$ and the controller parameters ($\boldsymbol{\varsigma}_{i,j_i}$, $\widehat{\boldsymbol{W}}_{i,j_i}$, $\widehat{\Theta}$) are adjusted online, with no pre-training step (or plain offline training step).
- Since the parameter adaptation laws, the virtual control signals, the auxiliary control input and the control inputs are continuous, potential control design problems such as chattering and control singularity are avoided [34].

Remark 26. It should be noted that:

- The event-triggered control condition (2) has been recently supplied in [2,3,23,38,42,43,56] to aid in deciding at what time the controller must be updated.
- The crucial point in [2,3,38,39,42,43,56] is that the developed adaptive law incorporates a preset resilient term with Hyperbolic tangent function tanh (.) to mitigate constant errors,
- The use of restricted information with constant measurement errors which is impractical in some situations, is the limitations of previous research works on the event-triggering conditions [2,3,38,39,42,43,56],
- A strategy based on a new adaptive control scheme (11) is proposed in this paper to adaptively compensate for constant measurement errors.

Remark 27. As mentioned in [28,29,34-37], the choice to build the controller as an integer-order controller, despite the fact that the system is fractional-order, is taken to simplify the controller design process. In contrast to fractional-order controllers, integer-order controllers are more widely utilized and have well-established design approaches [26,29,34]. Furthermore, integer-order controllers can provide great performance for a wide range of systems, particularly when fractional-order effects are minor or can be managed effectively via stability analysis [35-37]. This technique addresses the system's fractional-order characteristics largely during the stability analysis phase [28,34,37]. By examining the stability of a closed-loop system with an integer-order controller, the influence of fractional-order dynamics on system stability may be understood and compensated for [28,29,36]. This enables the discovery of tuning techniques and crucial parameters that provide good performance and stability in the attendance of fractional-order dynamics [28,29, 35]. In general, building the controller in integer order at the same time as addressing the fractional-order issues in stability analysis strikes a balance between system performance and controller complexity, integrating the benefits of both approaches [28,34-37].

3.5. Stability analysis

In this section, stability analysis of the closed-loop system is presented for the proposed Observer-Based Output Feedback Event-Triggered Adaptive Neural Control scheme, which extends the dynamic surface control technique to systems with asymmetric time-varying Pseudo-state constraints and input nonlinearities in non-integer order non-strict feedback form.

In what follows, using the above control design, the principal outcomes of this study can be stated as Theorem 1.

Theorem 1. *Consider the nonlinear nonaffine non-integer order non-strict feedback systems (1) subject to input nonlinearities, asymmetric time-varying Pseudo-state constraints and dynamic uncertainties. Under Assumptions 1–2, the neural adaptive pseudo-state observer (6) and the adaptive control laws (11) with the event-triggered condition (2) ensure that:*

- All of the closed-loop systems signals are bounded.
- the full pseudo-state constraints are not violated,
- no Zeno behavior occurs in the execution times.
- The tracking error signals, the observer errors and the error surfaces converge to zero in finite-time.

Proof. of Theorem 1.

Choose a positive definite Lyapunov function as

$$\boldsymbol{V}=\sum_{i=1}^{p}\boldsymbol{V}_{1,i}+\boldsymbol{V}_{2}+\sum_{i=1}^{p}\sum_{j_i=1}^{n_i+2}\boldsymbol{V}_{3,ij_i}+\sum_{i=1}^{p}\sum_{j_i=1}^{n_i+2}\boldsymbol{V}_{4,ij_i}+\sum_{i=1}^{p}\sum_{j_i=1}^{n_i+2}\boldsymbol{V}_{5,ij_i} \tag{12}$$

with :

- $\boldsymbol{V}_{1,i}=\int_{0}^{+\infty}\mathbf{o}_i(\boldsymbol{\omega})(\beth_i(\boldsymbol{\omega},\boldsymbol{t}))^{T}\boldsymbol{P}_i(\beth_i(\boldsymbol{\omega},\boldsymbol{t}))\,\boldsymbol{d\omega},\ \boldsymbol{for\ i}=1,\ldots,\boldsymbol{p}.$
- $\mathscr{o}_i(\boldsymbol{\omega})=\boldsymbol{diag}(\mathscr{o}_{i,1}(\boldsymbol{\omega}),\quad\cdots,\quad\mathscr{o}_{i,n_i+2}(\boldsymbol{\omega}))=\begin{bmatrix}\mathscr{o}_{i,1}(\boldsymbol{\omega}) & 0 & \cdots & 0\\ 0 & \mathscr{o}_{i,2}(\boldsymbol{\omega}) & \ddots & \vdots\\ \vdots & \ddots & \ddots & 0\\ 0 & \cdots & 0 & \mathscr{o}_{i,n_i+2}(\boldsymbol{\omega})\end{bmatrix}\in\mathbb{R}^{(n_i+2)\times(n_i+2)},\ \boldsymbol{for\ i}=1,\cdots,\boldsymbol{p}.$
- $(\beth_i(\boldsymbol{\omega},\boldsymbol{t}))^{T}\boldsymbol{P}_i(\beth_i(\boldsymbol{\omega},\boldsymbol{t}))$ being an elementary monochromatic Lyapunov function of the internal state variable $\beth_i(\boldsymbol{\omega},\boldsymbol{t}),\ \boldsymbol{for\ i}=1,\ldots,\boldsymbol{p}.$

- $\boldsymbol{V}_2 = \frac{(\widetilde{\Theta})^2}{2\phi_3}$
- $\widetilde{\Theta} = \boldsymbol{\Theta}^* - \widehat{\Theta}$
- $\boldsymbol{V}_{3,i,j_i} = \frac{\|\widetilde{\boldsymbol{W}}_{i,j_i}\|^2}{2\phi_{2,i,j_i}} = \frac{(\widetilde{\boldsymbol{W}}_{i,j_i})^T(\widetilde{\boldsymbol{W}}_{i,j_i})}{2\phi_{2,i,j_i}}$, *for* $\boldsymbol{j_i} = 1,\cdots,\boldsymbol{n_i}+2,\ \boldsymbol{i} = 1,\cdots,\boldsymbol{p}$.
- $\boldsymbol{V}_{4,i,j_i} = \frac{\phi_{1,i,j_i}}{2}\left[\int_0^t \boldsymbol{E}_{i,j_i}(\tau)\, d\tau\right]^2$, *for* $\boldsymbol{j_i} = 1,\ldots,\boldsymbol{n_i}+2,\ \boldsymbol{i} = 1,\ldots,\boldsymbol{p}$.
- $\boldsymbol{V}_{5,i,j_i} = \frac{1}{2}\boldsymbol{D}_t^{-1+\delta_{i,j_i}}\left[\boldsymbol{V}_{6,i,j_i}\right]$, **for** $\boldsymbol{j_i} = 1,\ \cdots,\boldsymbol{n_i}+2,\quad \boldsymbol{i} = 1,\ldots,\boldsymbol{p}$
- $\boldsymbol{V}_{6,i,j_i} = \{$ $\boldsymbol{\mu}_{i,j_i} log\left(\frac{\left(\underline{\boldsymbol{\kappa}}_{3,i,j_i}\right)^2}{\left(\left(\underline{\boldsymbol{\kappa}}_{3,i,j_i}\right)^2 - \left(\boldsymbol{z}_{i,j_i}\right)^2\right)}\right) + \left(1-\boldsymbol{\mu}_{i,j_i}\right) log\left(\frac{\left(\overline{\boldsymbol{\kappa}}_{3,i,j_i}\right)^2}{\left(\left(\overline{\boldsymbol{\kappa}}_{3,i,j_i}\right)^2 - \left(\boldsymbol{z}_{i,j_i}\right)^2\right)}\right)$, *for* $\boldsymbol{j_i} = 1,\ldots,\boldsymbol{n_i}$

  $\left(\boldsymbol{z}_{i,j_i}\right)^2$, *for* $\boldsymbol{j_i} = \boldsymbol{n_i}+1,\ \ \boldsymbol{n_i}+2,\quad i = 1,\ldots,p$

Remark 28. It is worth noting that:

- $\boldsymbol{D}_t^{-1+\delta_{i,j_i}}$ denotes the fractional integer of order $1-\boldsymbol{\delta}_{i,j_i}$, for $\boldsymbol{j_i} = 1,\ldots,\boldsymbol{n_i}+2,\ \boldsymbol{i} = 1,\ldots,\boldsymbol{p}$.
- The Lyapunov function $\boldsymbol{V}$ is convex with respect to the variables $\boldsymbol{z}_{i,j_i}$, $\widetilde{\Theta}$, $\widetilde{\boldsymbol{W}}_{i,j_i}$, $\boldsymbol{E}_{i,j_i}$ and $\beth_{i,i,j_i}$, for $\boldsymbol{j_i} = 1,\ldots,\boldsymbol{n_i}+2,\ \boldsymbol{i} = 1,\ldots,\boldsymbol{p}$.
- $\boldsymbol{V}$escapes to infinity if $\boldsymbol{z}_{i,j_i} \to -\underline{\boldsymbol{\kappa}}_{3,i,j_i}$, $\boldsymbol{z}_{i,j_i} \to \overline{\boldsymbol{\kappa}}_{3,i,j_i}$, $\widetilde{\Theta} \to +\infty$, $\|\widetilde{\boldsymbol{W}}_{i,j_i}\| \to +\infty$, $\boldsymbol{E}_{i,j_i} \to +\infty$ *or* $\beth_{i,i,j_i} \to +\infty$, for $\boldsymbol{j_i} = 1,\ldots,\boldsymbol{n_i}+2,\ \boldsymbol{i} = 1,\ldots,\boldsymbol{p}$.
- $\boldsymbol{V} = 0$ when $\boldsymbol{z}_{i,j_i} = 0,\ \|\widetilde{\boldsymbol{W}}_{i,j_i}\| = 0,\ \widetilde{\Theta} = 0,\ \boldsymbol{E}_{i,j_i} = 0$ and $\beth_{i,j_i} = 0$, for $\boldsymbol{j_i} = 1,\ldots,\boldsymbol{n_i}+2,\ \boldsymbol{i} = 1,\ldots,\boldsymbol{p}$.
- The Lyapunov function V is positive definite and continuously derivable with regard to the error variables, counting the observer errors, the tracking errors and the parameter estimation errors, $\forall -\underline{\boldsymbol{\kappa}}_{3,i,j_i} < \boldsymbol{z}_{i,j_i} < \overline{\boldsymbol{\kappa}}_{3,i,j_i}$, for $\boldsymbol{j_i} = 1,\ldots,\boldsymbol{n_i},\ \boldsymbol{i} = 1,\ldots,\boldsymbol{p}$.

Remark 29. It is important to mention that Lyapunov functions related to Grünwald-Letnikov, Riemann–Liouville, and Caputo definitions, vector Lyapunov functions, Time-varying Lyapunov functions, Finite Energy Lyapunov Functions, Lyapunov-like barrier functions, exponential-type Lyapunov functions, Convex Lyapunov functions, Volterra-type Lyapunov functions, quadratic Lyapunov functions, polynomial Lyapunov functions, piecewise Lyapunov functions as well as several others have been effectively employed in the literature for the stability analysis of non integer order systems that are incommensurate and commensurate [2,5,15,26,34-38,43,48,54-61].

Remark 30. In the literature, there are several kinds of symmetric and asymmetric barrier Lyapunov functions, such as tangent Lyapunov barrier functions, prescribed performance-barrier Lyapunov functions, composite barrier Lyapunov functions, high-order barrier Lyapunov functions, time-varying barrier Lyapunov functions, exponent-dependent barrier Lyapunov functions, integral Lyapunov barrier functions, and so on [2,3,34-36,41,47,48]. The primary distinction between Lyapunov barrier functions and classical Lyapunov functions is that Lyapunov barrier functions approach infinity when their arguments reach specified limitations [2,3,34-36,

48].

Using Young's inequality [1-3,10-13,18,34], Lemmas 2-3 and Eqs. (6), (7), (11)-(12), one obtains

$$
\begin{cases}
-2\int_0^{+\infty}\boldsymbol{\omega\Gamma}_i(\boldsymbol{\omega})\left(\beth_i(\boldsymbol{\omega},\boldsymbol{t})\right)^T\boldsymbol{P}_i\left(\beth_i(\boldsymbol{\omega},\boldsymbol{t})\right)d\boldsymbol{\omega}\le 0\\
\hbar_i\boldsymbol{e}_i^T\left(\boldsymbol{A}_i^T\boldsymbol{P}_i+\boldsymbol{P}_i\boldsymbol{A}_i\right)\boldsymbol{e}_i\le-\hbar_i\boldsymbol{\lambda}_{min}(\boldsymbol{Q}_i)\|\boldsymbol{e}_i\|^2\\
2\boldsymbol{e}_i^T\boldsymbol{P}_i\sum_{j_i=1}^{n_i+2}\daleth_i\boldsymbol{B}_{j_i}\left[\Delta\,\boldsymbol{g}_{i,j_i}\right]\le\left(1+\|\boldsymbol{P}_i\|^2\sum_{j_i=1}^{n_i+2}\left(\boldsymbol{l}_{i,j_i}\right)^2\right)\|\boldsymbol{e}_i\|^2+(\boldsymbol{n}_i+2)\|\boldsymbol{P}_i\|^2\sum_{j_i=1}^{n_i+2}\left(\boldsymbol{\varepsilon}^*_{2,i,j_i}\right)^2\\
-2\boldsymbol{e}_i^T\boldsymbol{P}_i\boldsymbol{b}_i\boldsymbol{e}_i\le-2\boldsymbol{\lambda}_{min}(\boldsymbol{P}_i)\boldsymbol{b}_i\|\boldsymbol{e}_i\|^2\\
2\boldsymbol{e}_i^T\boldsymbol{P}_i\sum_{j_i=1}^{n_i+2}\daleth_i\boldsymbol{B}_{j_i}\left[\boldsymbol{\varepsilon}_{1,i,j_i}\right]\le\|\boldsymbol{e}_i\|^2+(\boldsymbol{n}_i+2)\|\boldsymbol{P}_i\|^2\sum_{j_i=1}^{n_i+2}\left(\boldsymbol{\varepsilon}^*_{1,i,j_i}\right)^2\\
2\boldsymbol{e}_i^T\boldsymbol{P}_i\sum_{j_i=1}^{n_i+2}\daleth_i\boldsymbol{B}_{j_i}\left[\left(\widetilde{\boldsymbol{W}}_{i,j_i}\right)^T\boldsymbol{\xi}_{i,j_i}(\widehat{\boldsymbol{\chi}})\right]\le\|\boldsymbol{e}_i\|^2+(\boldsymbol{n}_i+2)\|\boldsymbol{P}_i\|^2\sum_{j_i=1}^{n_i+2}\boldsymbol{q}_{i,j_i}\left\|\widetilde{\boldsymbol{W}}_{i,j_i}\right\|^2\\
\left\|\widetilde{\boldsymbol{W}}_{i,j_i}\right\|^2\le\left\|\boldsymbol{W}^*_{i,j_i}\right\|^2-2\left(\widetilde{\boldsymbol{W}}_{i,j_i}\right)^T\widehat{\boldsymbol{W}}_{i,j_i}\\
\left[\left(\boldsymbol{W}^*_{i,j_i}\right)^T\boldsymbol{\xi}_{i,j_i}(\widehat{\boldsymbol{\chi}})-\left(\boldsymbol{W}^*_{i,j_i}\right)^T\boldsymbol{\xi}_{i,j_i}(\widehat{\widehat{\boldsymbol{\chi}}}_{i,j_i})\right]\boldsymbol{E}_{i,j_i}\le 2\left(\boldsymbol{E}_{i,j_i}\right)^2+2\boldsymbol{q}_{i,j_i}\left\|\boldsymbol{W}^*_{i,j_i}\right\|^2\\
-\left[\left(\widetilde{\boldsymbol{W}}_{i,j_i}\right)^T\boldsymbol{\xi}_{i,j_i}(\widehat{\boldsymbol{\chi}})\right]\boldsymbol{E}_{i,j_i}\le\left(\boldsymbol{E}_{i,j_i}\right)^2+\boldsymbol{q}_{i,j_i}\left\|\widetilde{\boldsymbol{W}}_{i,j_i}\right\|^2\\
\left[\Delta\,\boldsymbol{g}_{i,1}+\boldsymbol{\varepsilon}_{1,i,1}+(\hbar_i)^2\boldsymbol{e}_{i,2}\right]\boldsymbol{E}_{i,1}\le\|\boldsymbol{e}_i\|^2+\left[1+\sum_{j_i=1}^{n_i+2}\left(\boldsymbol{l}_{i,j_i}\right)^2\right]\left[(\hbar_i)^4+2\right]\left(\boldsymbol{E}_{i,1}\right)^2\\
\qquad+\sum_{j_i=1}^{n_i+2}\left(\boldsymbol{\varepsilon}^*_{2,i,j_i}\right)^2+\sum_{j_i=1}^{n_i+2}\left(\boldsymbol{\varepsilon}^*_{1,i,j_i}\right)^2\\
\left(\widetilde{\boldsymbol{W}}_{i,j_i}\right)^T\left[\widehat{\boldsymbol{W}}_{i,j_i}-\widehat{\boldsymbol{W}}_{i,j_i}(\boldsymbol{0})\right]\le\frac{1}{2}\left[\left\|\boldsymbol{W}^*_{i,j_i}-\widehat{\boldsymbol{W}}_{i,j_i}(\boldsymbol{0})\right\|^2-\left\|\widetilde{\boldsymbol{W}}_{i,j_i}\right\|^2\right]\\
\widetilde{\boldsymbol{\theta}}\ \left[\widehat{\boldsymbol{\theta}}\ -\widehat{\boldsymbol{\theta}}\ (\boldsymbol{0})\right]\le\frac{1}{2}\left[\left(\boldsymbol{\theta}^*\ -\widehat{\boldsymbol{\theta}}\ (\boldsymbol{0})\right)^2-\left(\widetilde{\boldsymbol{\theta}}\ \right)^2\right]\\
\left[-\hbar_i\boldsymbol{\lambda}_{min}(\boldsymbol{Q}_i)+5+\|\boldsymbol{P}_i\|^2\sum_{j_i=1}^{n_i+2}\left(\boldsymbol{l}_{i,j_i}\right)^2-2\boldsymbol{b}_i\boldsymbol{\lambda}_{min}(\boldsymbol{P}_i)\right]\|\boldsymbol{e}_i\|^2\le-\boldsymbol{\lambda}_{min}(\boldsymbol{P}_i)\|\boldsymbol{e}_i\|^2\\
\sum_{i=1}^{p}\sum_{j_i=1}^{n_i-1}\boldsymbol{z}_{i,j_i+1}\boldsymbol{E}_{i,j_i}-\sum_{i=1}^{p}\sum_{j_i=2}^{n_i}\frac{\left(\left(\underline{\boldsymbol{\kappa}}_{3,i,j_i}\right)^2-\left(\boldsymbol{z}_{i,j_i}\right)^2\right)\left(\left(\overline{\boldsymbol{\kappa}}_{3,i,j_i}\right)^2-\left(\boldsymbol{z}_{i,j_i}\right)^2\right)}{\boldsymbol{\mu}_{i,j_i}\left(\overline{\boldsymbol{\kappa}}_{3,i,j_i}\right)^2+\left(1-\boldsymbol{\mu}_{i,j_i}\right)\left(\underline{\boldsymbol{\kappa}}_{3,i,j_i}\right)^2-\left(\boldsymbol{z}_{i,j_i}\right)^2}\boldsymbol{E}_{i,j_i}\boldsymbol{E}_{i,j_i-1}=\boldsymbol{0}\\
\sum_{i=1}^{p}\sum_{j_i=\boldsymbol{n}_i}^{n_i+1}\boldsymbol{z}_{i,j_i+1}\boldsymbol{E}_{i,j_i}-\sum_{i=1}^{p}\sum_{j_i=\boldsymbol{n}_i+1}^{n_i+2}\boldsymbol{E}_{i,j_i-1}\boldsymbol{E}_{i,j_i}=\boldsymbol{0}\\
\left(\boldsymbol{V}_{6,i,j_i}\right)^2\le\left(\boldsymbol{z}_{i,j_i}\boldsymbol{E}_{i,j_i}\right)^2\\
-\boldsymbol{\Theta}^*\sum_{i=1}^{p}\frac{2(3+\sigma)(e_{i,1})^2(B_{i,1})^TP_iB_{i,1}}{2(e_{i,1})^2(B_{i,1})^TP_iB_{i,1}+(\sigma)^2}\le-\frac{\boldsymbol{\Theta}^*\sum_{i=1}^{p}2(3+\sigma)(e_{i,1})^2(B_{i,1})^TP_iB_{i,1}}{\sum_{i=1}^{p}2(e_{i,1})^2(B_{i,1})^TP_iB_{i,1}+\sum_{i=1}^{p}\sum_{j_i=1}^{n_i+2}\left(V_{6,i,j_i}\right)^2+(\sigma)^2}\\
-\boldsymbol{\Theta}^*\sum_{i=1}^{p}\sum_{j_i=1}^{n_i+2}\frac{(3+\sigma)\sum_{i=1}^{p}\sum_{j_i=1}^{n_i+2}\left(z_{i,j_i}E_{i,j_i}\right)^2}{\left(z_{i,j_i}E_{i,j_i}\right)^2+(\sigma)^2}\le-\frac{(3+\sigma)\boldsymbol{\Theta}^*\sum_{i=1}^{p}\sum_{j_i=1}^{n_i+2}\left(V_{6,i,j_i}\right)^2}{\sum_{i=1}^{p}2(e_{i,1})^2(B_{i,1})^TP_iB_{i,1}+\sum_{i=1}^{p}\sum_{j_i=1}^{n_i+2}\left(V_{6,i,j_i}\right)^2+(\sigma)^2}
\end{cases}
\tag{13}
$$

By taking the time derivative of $\sum_{i=1}^{p}\boldsymbol{V}_{1,i}$, $\boldsymbol{V}_2$, $\sum_{i=1}^{p}\sum_{j_i=1}^{n_i+2}\boldsymbol{V}_{3,i,j_i}$, $\sum_{i=1}^{p}\sum_{j_i=1}^{n_i+2}\boldsymbol{V}_{4,i,j_i}$ and $\sum_{i=1}^{p}\sum_{j_i=1}^{n_i+2}\boldsymbol{V}_{5,i,j_i}$ and based on Properties 1-2, Lemmas 1-5, and Eqs. (6)-(13), one has

$$
\begin{cases}
\sum_{i=1}^{p}\dot{V}_{1,i} = \sum_{i=1}^{p}\left[\int_0^{+\infty} -2\omega\Gamma_i(\omega)\left(\beth_i(\omega,t)\right)^T P_i\left(\beth_i(\omega,t)\right)d\omega + e_i{}^T\left(\left(A_i{}^T P_i + P_i A_i\right)\hbar_i - 2P_i b_i\right)e_i\right] \\
\quad + \sum_{i=1}^{p} 2e_i{}^T P_i \sum_{j_i=1}^{n_i+2} \beth_i B_{j_i}\left[\left(\widetilde{W}_{i,j_i}\right)^T \xi_{i,j_i}(\widehat{\chi}) + \triangle\, g_{i,j_i} + \varepsilon_{1,i,j_i}\right] - \widehat{\Theta}\ \ \sum_{i=1}^{p}\frac{2(3+\sigma)\left(e_{i,1}\right)^2\left(B_{i,1}\right)^T P_i B_{i,1}}{2\left(e_{i,1}\right)^2\left(B_{i,1}\right)^T P_i B_{i,1}+(\sigma)^2} \\
\quad \le -\sum_{i=1}^{p}\left(1+\lambda_{min}(P_i)\right)\|e_i\|^2 + \widetilde{\Theta}\ \ \sum_{i=1}^{p}\frac{2(3+\sigma)\left(e_{i,1}\right)^2\left(B_{i,1}\right)^T P_i B_{i,1}}{2\left(e_{i,1}\right)^2\left(B_{i,1}\right)^T P_i B_{i,1}+(\sigma)^2} - \Theta^*\ \sum_{i=1}^{p}\frac{2(3+\sigma)\left(e_{i,1}\right)^2\left(B_{i,1}\right)^T P_i B_{i,1}}{2\left(e_{i,1}\right)^2\left(B_{i,1}\right)^T P_i B_{i,1}+(\sigma)^2} \\
\qquad - \sum_{i=1}^{p} 2\left((n_i+2)\|P_i\|^2\right)\sum_{j_i=1}^{n_i+2} q_{i,j_i}\left(\widetilde{W}_{i,j_i}\right)^T\widehat{W}_{i,j_i} \\
\qquad + \sum_{i=1}^{p}\left((n_i+2)\|P_i\|^2\right)\sum_{j_i=1}^{n_i+2}\left[4q_{i,j_i}\left\|W^*_{i,j_i}\right\|^2 + \left(\varepsilon^*_{1,i,j_i}\right)^2 + \left(\varepsilon^*_{2,i,j_i}\right)^2\right] \\
\dot{V}_2 = \frac{\tilde{\Theta}\ \dot{\tilde{\Theta}}}{\phi_3} \le -\widetilde{\Theta}\ \ \sum_{i=1}^{p}\left[\frac{2(3+\sigma)\left(e_{i,1}\right)^2\left(B_{i,1}\right)^T P_i B_{i,1}}{2\left(e_{i,1}\right)^2\left(B_{i,1}\right)^T P_i B_{i,1}+(\sigma)^2} + \left(E_{i,j_i}\right)^2\Phi_{i,j_i}\right] + \frac{\left[\left(\theta^* - \widehat{\theta}\ \ (0)\right)^2 - \left(\tilde{\theta}\ \ \right)^2\right]\sigma}{2\phi_3} \\
\sum_{i=1}^{p}\sum_{j_i=1}^{n_i+2}\dot{V}_{3,i,j_i} = \sum_{i=1}^{p}\sum_{j_i=1}^{n_i+2}\frac{\left(\widetilde{W}_{i,j_i}\right)^T\left(\dot{\widetilde{W}}_{i,j_i}\right)}{\phi_{2,i,j_i}} \\
\qquad \le \sum_{i=1}^{p}\sum_{j_i=1}^{n_i+2}\left[\frac{\left[\left\|W^*_{i,j_i} - \widetilde{W}_{i,j_i}(0)\right\|^2 - \left\|\widetilde{W}_{i,j_i}\right\|^2\right]}{2\phi_{2,i,j_i}}\right]\left(E_{i,j_i}z_{i,j_i} + \sigma\right) \\
\qquad + \sum_{i=1}^{p}\sum_{j_i=1}^{n_i+2}\left(\widetilde{W}_{i,j_i}\right)^T\left[-E_{i,j_i}\xi_{i,j_i}\left(\widehat{\chi}_{i,j_i}\right) + 2\left((n_i+2)\|P_i\|^2+1\right)q_{i,j_i}\widehat{W}_{i,j_i}\right] \\
\sum_{i=1}^{p}\sum_{j_i=1}^{n_i+2}\dot{V}_{4,i,j_i} = \sum_{i=1}^{p}\sum_{j_i=1}^{n_i+2}\phi_{1,i,j_i}E_{i,j_i}\int_0^t E_{i,j_i}(\tau)\,d\tau \\
\sum_{i=1}^{p}\sum_{j_i=1}^{n_i+2}\dot{V}_{5,i,j_i} \le \sum_{i=1}^{p}\sum_{j_i=n_i+1}^{n_i+2} z_{i,j_i}D_t^{\delta_{i,j_i}}z_{i,j_i} + \sum_{i=1}^{p}\sum_{j_i=1}^{n_i}\left[D_t^{\delta_{i,j_i}}z_{i,j_i} - \mu_{i,j_i}\underline{\kappa}_{3,i,j_i}(0)\left(\frac{z_{i,j_i}}{\left(\underline{\kappa}_{3,i,j_i}\right)^2}\right)D_t^{\delta_{i,j_i}}\underline{\kappa}_{3,i,j_i}\right. \\
\qquad \left. -\left(1-\mu_{i,j_i}\right)\overline{\kappa}_{3,i,j_i}(0)\left(\frac{z_{i,j_i}}{\left(\overline{\kappa}_{3,i,j_i}\right)^2}\right)D_t^{\delta_{i,j_i}}\overline{\kappa}_{3,i,j_i}\right]E_{i,j_i} \\
\qquad \le \sum_{i=1}^{p}\sum_{j_i=1}^{n_i+2}\left[\alpha_{i,j_i} + \left(\widetilde{W}_{i,j_i}\right)^T\xi_{i,j_i}\left(\widehat{\chi}_{i,j_i}\right) + \left(\widetilde{W}_{i,j_i}\right)^T\xi_{i,j_i}\left(\widehat{\chi}_{i,j_i}\right)\right]E_{i,j_i} \\
\qquad + \Theta^*\ + \sum_{i=1}^{p}\|e_i\|^2 + \Theta^*\ \sum_{i=1}^{p}\sum_{j_i=1}^{n_i+2}\left(\left\|\Im_{i,j_i}\right\|\left|E_{i,j_i}\right|\right) \\
\qquad - \sum_{i=1}^{p}\sum_{j_i=1}^{n_i+2}\left[2q_{i,j_i}\left(\widetilde{W}_{i,j_i}\right)^T\widehat{W}_{i,j_i} - \frac{\left\|W^*_{i,j_i} - \widetilde{W}_{i,j_i}(0)\right\|^2}{2\phi_{2,i,j_i}}E_{i,j_i}z_{i,j_i}\right] \\
\qquad\qquad \theta^*\ \rho_{i,j_i}\left|E_{i,j_i}\right| - \theta^*\ \frac{\left(\rho_{i,j_i}E_{i,j_i}\right)^2}{\sqrt{\left(\rho_{i,j_i}E_{i,j_i}\right)^2+(\sigma)^2}} \le \theta^*\ \sigma \\
\qquad\qquad \theta^*\ \left\|\Im_{i,j_i}\right\|\left|E_{i,j_i}\right| - \theta^*\ \rho_{i,j_i}\left|E_{i,j_i}\right| \le 0
\end{cases}
\tag{14}
$$

From the above Eqs. (8)-(12) and inequalities (13)-(14), it can be known that

$$\dot{V} = \sum_{i=1}^{p}\dot{V}_{1,i} + \dot{V}_2 + \sum_{i=1}^{p}\sum_{j_i=1}^{n_i+2}\dot{V}_{3,i,j_i} + \sum_{i=1}^{p}\sum_{j_i=1}^{n_i+2}\dot{V}_{4,i,j_i} + \sum_{i=1}^{p}\sum_{j_i=1}^{n_i+2}\dot{V}_{5,i,j_i}$$

$$\begin{aligned}
&\leq \\
&-\sum_{i=1}^{p}\lambda_{min}(P_i)\|e_i\|^2 + \sum_{i=1}^{p}\sum_{j_i=1}^{n_i+2}\left[\alpha_{i,j_i} + \left(\widehat{W}_{i,j_i}\right)^T\xi_{i,j_i}\left(\widehat{\chi}_{i,j_i}\right)\right]E_{i,j_i} - \left[\frac{\left(\tilde{\theta}\right)^2}{2\phi_3}\right]\sigma \\
&+\Theta^* + \sum_{i=1}^{p}\sum_{j_i=1}^{n_i+2}\phi_{1,i,j_i}E_{i,j_i}\int_0^t E_{i,j_i}(\tau)\,d\tau - \sum_{i=1}^{p}\sum_{j_i=1}^{n_i+2}\left[\frac{\left\|\widetilde{W}_{i,j_i}\right\|^2}{2\phi_{2,i,j_i}}\right]\left(\sigma + E_{i,j_i}z_{i,j_i}\right) \\
&+\sum_{i=1}^{p}\sum_{j_i=1}^{n_i+2}\left[\frac{\left[\left\|W^*_{i,j_i}-\widehat{W}_{i,j_i}(0)\right\|^2\right]}{2\phi_{2,i,j_i}}\right]\sigma + \frac{\left[\left(\theta^* - \hat{\theta}\ (0)\right)^2\right]}{2\phi_3}\sigma \ + \Theta^*\ \sum_{i=1}^{p}\sum_{j_i=1}^{n_i+2}\left\|\Im_{i,j_i}\right\|\left|E_{i,j_i}\right| \\
&-\Theta^*\ \sum_{i=1}^{p}\frac{2(3+\sigma)(e_{i,1})^2(B_{i,1})^T P_i B_{i,1}}{2(e_{i,1})^2(B_{i,1})^T P_i B_{i,1}+(\sigma)^2} \\
&+\sum_{i=1}^{p}\left((n_i+2)\|P_i\|^2\right)\sum_{j_i=1}^{n_i+2}\left[4q_{i,j_i}\left\|W^*_{i,j_i}\right\|^2 + \left(\varepsilon^*_{1,i,j_i}\right)^2 + \left(\varepsilon^*_{2,i,j_i}\right)^2\right] \\
&\leq \\
&-\sum_{i=1}^{p}\lambda_{min}(P_i)\|e_i\|^2 - \Theta^*\ \sum_{i=1}^{p}\sum_{j_i=1}^{n_i+2}\rho_{i,j_i}\left|\varsigma_{i,j_i}\right|V_{6,i,j_i} - \sum_{i=1}^{p}\sum_{j_i=1}^{n_i+2}(\sigma + V_{6,i,j_i})V_{3,i,j_i} \\
&-\sigma V_2 - \sigma\sum_{i=1}^{p}\sum_{j_i=1}^{n_i+2}V_{4,i,j_i} - \Theta^*\ \sum_{i=1}^{p}\sum_{j_i=1}^{n_i+2}\left(\rho_{i,j_i}\varsigma_{i,j_i}V_{6,i,j_i}\right)^2 + (5+n+2p)\sigma\Theta^* \\
&-\Theta^*\ + \left[\frac{\left[\left(\theta^* - \hat{\theta}\ (0)\right)^2\right]}{2\phi_3}\right]\sigma + \sum_{i=1}^{p}\sum_{j_i=1}^{n_i+2}\left[1+N\left(\varsigma_{i,j_i}\right)\right]\dot{\varsigma}_{i,j_i} \ + \sum_{i=1}^{p}\sum_{j_i=1}^{n_i+2}\left[\frac{\left[\left\|W^*_{i,j_i}-\widehat{W}_{i,j_i}(0)\right\|^2\right]}{2\phi_{2,i,j_i}}\right]\sigma \\
&+\frac{(\sigma)^2-(1+\sigma)\left(\sum_{i=1}^{p}2(e_{i,1})^2(B_{i,1})^T P_i B_{i,1}+\sum_{i=1}^{p}\sum_{j_i=1}^{n_i+2}\left(V_{6,i,j_i}\right)^2\right)}{2\sum_{i=1}^{p}(e_{i,1})^2(B_{i,1})^T P_i B_{i,1}+\sum_{i=1}^{p}\sum_{j_i=1}^{n_i+2}\left(V_{6,i,j_i}\right)^2+(\sigma)^2}\Theta^*
\end{aligned} \tag{15}$$

Then, integrating (15) from 0 to t, we arrive at

$$\begin{aligned}
&V(t) + \sum_{i=1}^{p}\lambda_{min}(P_i)\int_0^t \|\ e_i(\tau)\|^2 d\tau + \Theta^*\sum_{i=1}^{p}\sum_{j_i=1}^{n_i+2}\int_0^t V_{6,i,j_i}(\tau)\rho_{i,j_i}(\tau)\left|\varsigma_{i,j_i}(\tau)\right|d\tau \\
&+\int_0^t \sigma(\tau)V_2(\tau)d\tau + \sum_{i=1}^{p}\sum_{j_i=1}^{n_i+2}\int_0^t\left(\sigma(\tau)+V_{6,i,j_i}(\tau)\right)V_{3,i,j_i}(\tau)d\tau \\
&+\Theta^*\sum_{i=1}^{p}\sum_{j_i=1}^{n_i+2}\int_0^t\left(V_{6,i,j_i}(\tau)\varsigma_{i,j_i}(\tau)\rho_{i,j_i}(\tau)\right)^2 d\tau + \sum_{i=1}^{p}\sum_{j_i=1}^{n_i+2}\int_0^t\sigma(\tau)V_{4,i,j_i}(\tau)d\tau \\
&\leq \\
&-\Theta^* t + V(0) + \left[\frac{\left[(\Theta^* - \widehat{\Theta}(0))^2\right]}{2\phi_3}\right]\int_0^t\sigma(\tau)d\tau + \sum_{i=1}^{p}\sum_{j_i=1}^{n_i+2}\left[\frac{\left[\|\ W^*_{i,j_i} - \widehat{W}_{i,j_i}(0)\|^2\right]}{2\phi_{2,i,j_i}}\right]\int_0^t\sigma(\tau)d\tau \\
&+(5+n+2p)\int_0^t\sigma(\tau)d\tau \ + \sum_{i=1}^{p}\sum_{j_i=1}^{n_i+2}\int_0^t\left[1+N\left(\varsigma_{i,j_i}(\tau)\right)\right]\dot{\varsigma}_{i,j_i}(\tau)d\tau \\
&+\Theta^*\int_0^t\frac{(\sigma(\tau))^2 - (1+\sigma(\tau))\left(\sum_{i=1}^{p}2\left(e_{i,1}(\tau)\right)^2(B_{i,1})^T P_i B_{i,1} + \sum_{i=1}^{p}\sum_{j_i=1}^{n_i+2}\left(V_{6,i,j_i}(\tau)\right)^2\right)}{2\sum_{i=1}^{p}\left(e_{i,1}(\tau)\right)^2(B_{i,1})^T P_i B_{i,1} + \sum_{i=1}^{p}\sum_{j_i=1}^{n_i+2}\left(V_{6,i,j_i}(\tau)\right)^2 + (\sigma(\tau))^2}d\tau
\end{aligned} \tag{16}$$

Based on lemmas 1-5 and the previous Eq. (16), it is worth mentioning that $V(t)$, $\sum_{i=1}^{p}\int_0^t\|\ \mathbf{e}_i(\tau)\|^2 d\tau$, $\int_0^t V_2(\tau)d\tau$, $\sum_{i=1}^{p}\sum_{j_i=1}^{n_i+2}\int_0^t V_{6,i,j_i}(\tau)d\tau$, $\sum_{i=1}^{p}\sum_{j_i=1}^{n_i+2}\int_0^t V_{3,i,j_i}(\tau)d\tau$, $\sum_{i=1}^{p}\sum_{j_i=1}^{n_i+2}\int_0^t V_{4,i,j_i}(\tau)d\tau$, $\sum_{i=1}^{p}\sum_{j_i=1}^{n_i+2}\int_0^t\left[1+N\left(\varsigma_{i,j_i}(\tau)\right)\right]\dot{\varsigma}_{i,j_i}(\tau)d\tau$, $\int_0^t\sigma(\tau)d\tau$,

$$\frac{\left[(\Theta^* - \widehat{\Theta}(0))^2\right]}{2\phi_3}\int_0^t\sigma(\tau)d\tau, \sum_{i=1}^{p}\sum_{j_i=1}^{n_i+2}\left[\frac{\left[\|W^*_{i,j_i} - \widehat{W}_{i,j_i}(0)\|^2\right]}{2\phi_{2,i,j_i}}\right]\int_0^t\sigma(\tau)d\tau$$

$$\Theta^*\int_0^t\frac{(\sigma(\tau))^2 - (1+\sigma(\tau))\left(\sum_{i=1}^{p}2\left(e_{i,1}(\tau)\right)^2(B_{i,1})^T P_i B_{i,1} + \sum_{i=1}^{p}\sum_{j_i=1}^{n_i+2}\left(V_{6,i,j_i}(\tau)\right)^2\right)}{2\sum_{i=1}^{p}\left(e_{i,1}(\tau)\right)^2(B_{i,1})^T P_i B_{i,1} + \sum_{i=1}^{p}\sum_{j_i=1}^{n_i+2}\left(V_{6,i,j_i}(\tau)\right)^2 + (\sigma(\tau))^2}d\tau$$

and $\sum_{i=1}^{p}\sum_{j_i=1}^{n_i+2}\int_0^t\left(\rho_{i,j_i}(\tau)\varsigma_{i,j_i}(\tau)V_{6,i,j_i}(\tau)\right)^2 d\tau$ are bounded.

From (16), we have $D_t^{\delta_{i,j_i}} e_{i,j}(t) \in L_\infty$ and $D_t^{\delta_{i,j_i}} z_{i,j}(t) \in L_\infty$. Also, $e_{i,j} \in L_2 \cap L_\infty$ and $z_{i,j} \in L_2 \cap L_\infty$ hold. According to Barbalat lemma [19,28,29,34-37], it is obtained $\lim_{t\to+\infty} e_{i,j} = 0$ and $\lim_{t\to+\infty} z_{i,j} = 0$, for $j_i = 1,\ldots,n_i+2,\ i = 1,\ldots,p$.

Consequently, all of the closed-loop systems signals α_{i,j_i}, $\widehat{W}_{i,j_i}$, $\widehat{\Theta}$, E_{i,j_i}, z_{i,j_i} and e_{i,j_i} are bounded, for $j_i = 1,\ldots,n_i+2,\ i = 1,\ldots,p$. Also, there exist an unknown strictly positive constant ℓ and a known function $\mathscr{L}$ such that

$$\begin{cases} V(0) + \sum_{i=1}^{p}\sum_{j_i=1}^{n_i+2}\int_0^t \left[1 + N\left(\varsigma_{i,j_i}(\tau)\right)\right]\dot{\varsigma}_{i,j_i}(\tau)d\tau + (5+n+2p)\Theta^*\int_0^t \sigma(\tau)d\tau \\ \quad + \left[\frac{\left[(\Theta^* - \widehat{\Theta}(0))^2\right]}{2\phi_3}\right]\int_0^t \sigma(\tau)d\tau + \sum_{i=1}^{p}\sum_{j_i=1}^{n_i+2}\left[\frac{\left[\| W_{i,j_i}^* - \widehat{W}_{i,j_i}(0)\|^2\right]}{2\phi_{2,i,j_i}}\right]\int_0^t \sigma(\tau)d\tau \\ +\Theta^*\int_0^t \mathscr{L}\dfrac{(\sigma(\tau))^2 - (1+\sigma(\tau))\left(\sum_{i=1}^{p} 2\left(e_{i,1}(\tau)\right)^2 \left(B_{i,1}\right)^T P_i B_{i,1} + \sum_{i=1}^{p}\sum_{j_i=1}^{n_i+2}\left(V_{6,i,j_i}(\tau)\right)^2\right)}{2\sum_{i=1}^{p}\left(e_{i,1}(\tau)\right)^2 \left(B_{i,1}\right)^T P_i B_{i,1} + \sum_{i=1}^{p}\sum_{j_i=1}^{n_i+2}\left(V_{6,i,j_i}(\tau)\right)^2 + (\sigma(\tau))^2} d\tau \\ \qquad \le \\ \qquad \ell \end{cases} \tag{17}$$

$$\begin{cases} \mathscr{L} = 1, \ \text{if} \left(\sum_{i=1}^{p} 2\left(e_{i,1}\right)^2 \left(B_{i,1}\right)^T P_i B_{i,1} + \sum_{i=1}^{p}\sum_{j_i=1}^{n_i+2}\left(V_{6,i,j_i}\right)^2\right) \neq 0 \\ \mathscr{L} = 0, \ \text{if} \left(\sum_{i=1}^{p} 2\left(e_{i,1}\right)^2 \left(B_{i,1}\right)^T P_i B_{i,1} + \sum_{i=1}^{p}\sum_{j_i=1}^{n_i+2}\left(V_{6,i,j_i}\right)^2\right) = 0 \end{cases}$$

More specific, from any initial condition $V(0)$, V will converge to zero in a finite time $T_r \le \frac{1}{\theta^*}$

Furthermore, from (7) and (16) - (17), it is obtained that

$$\begin{cases} \| e_i\| = 0, \\ \widetilde{x}_{i,j_i} = 0, \\ V_{5,i,j_i} = 0\ , \\ z_{i,j_i} = 0, \end{cases} \quad \forall t \ge T_r \tag{18}$$

$$\textit{for } j_i = 1,\cdots,n_i+2,\ i = 1,\cdots,p$$

From $x_{i,1} = z_{i,1} + y_{d_i}$ and $\underline{\kappa}_{1,i,1} < \underline{\kappa}_{2,i,1} < y_{d_i} < \overline{\kappa}_{2,i,1} < \overline{\kappa}_{1,i,1}$, we can know $-\underline{\kappa}_{3,i,1} < z_{i,1} < \overline{\kappa}_{3,i,1}$. Define $\underline{\kappa}_{3,i,1} = y_{d_i} - \underline{\kappa}_{1,i,1}$ and $\overline{\kappa}_{3,i,1} = \overline{\kappa}_{1,i,1} - y_{d_i}$ and then, it has $\underline{\kappa}_{1,i,1} < x_{i,1} < \overline{\kappa}_{1,i,1}$. By $z_{i,j_i} = \widehat{x}_{i,j_i} - \alpha_{i,j_i-1}$ and $-\underline{\kappa}_{3,i,j_i} < z_{i,j_i} < \overline{\kappa}_{3,i,j_i}$, if we choose $\underline{\kappa}_{3,i,j_i} = \alpha_{i,j_i-1} - \underline{\kappa}_{1,i,j_i}$ and $\overline{\kappa}_{3,i,j_i} = \overline{\kappa}_{1,i,j_i} - \alpha_{i,j_i-1}$, then we can prove $\underline{\kappa}_{1,i,j_i} < \widehat{x}_{i,j_i} < \overline{\kappa}_{1,i,j_i}$. Moreover, based on the above results and according to [47,48], we can infer that the pseudo-state satisfies $\underline{\kappa}_{1,i,j_i} < x_{i,j_i} < \overline{\kappa}_{1,i,j_i}$, **for** $j_i = 2,\ldots,n_i,\ i = 1,\ldots,p$.

Then, the state x_{i,j_i} is not violated, **for** $j_i = 1,\ldots,n_i,\ i = 1,\ldots,p$.

In addition, building on the description of Zeno phenomenon [2,3,15,22-25,27,38,39,42,43,52,56], we should demonstrate that the lower bound of the release interval $t_e = t_{k+1} - t_k$ verify $t_e > 0$ for the purpose of exemplifying that the Zeno behavior is effectively avoided. Based on (2) and motivated by the research [15,22-25,27,38,39,42,43], it has $\frac{d}{dt}|\zeta_i(t)| \le |\dot{\varpi}_i(t)|,\ \forall\ t_k \le t < t_{k+1}$.

Since $\dot{\varpi}_i(t) = -b_{1,i,n_i+2} b_{1,i,n_i+1} \varpi_i - b_{1,i,n_i+1} D_t^{\delta_{i,n_i+2}} \varpi_i - b_{1,i,n_i+2} D_t^{\delta_{i,n_i+1}} \varpi_i + \vartheta_i$ and all the signals are globally bounded, there exists a constant l_0 such that $|\dot{\varpi}_i(t)| < l_0$

According to (2), $\zeta_i(t_k) = 0$ and $\lim_{t\to t_{k+1}} \zeta_i(t) = \beta_i|u_i(t)| + r_i$ hold. Consequently, the lower bound of inter-execution intervals t^* has to satisfy $t^* > \frac{\beta_i|u_i(t)|+r_i}{l_0}$, which signifies that the event-triggered system cannot generate an infinite number of jumps in a finite amount of time. This implies that the Zeno behavior does not occur, ($\{t_{k+1} - t_k\} \ge t^*$, and $t^* > \frac{\beta_i|u_i(t)|+r_i}{l_0} > 0$).

Hence, the proof is complete.

Remark 31. Note that :

- The settling time T_r depends on the unknown functions, the initial conditions and the updating control and observer parameters.
- Inadmissible triggers and Zeno behaviors lead to the squandering of recourses and bandwidth, even the instability of the affected system. As a result, accurate triggers and no-Zeno behavior are needed in control process [27,38,39,42,43,52].

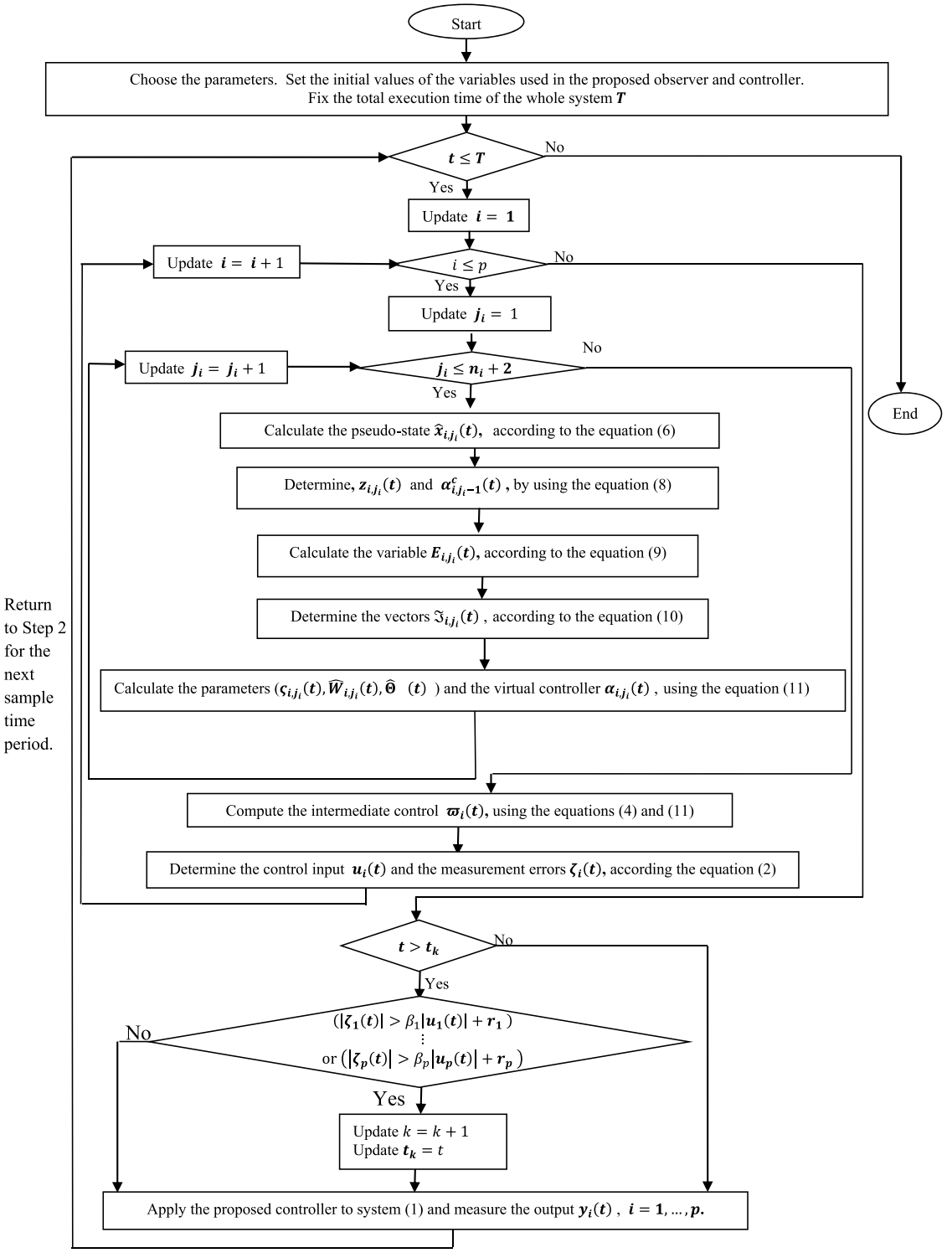

Fig.. 1. Flow chart of the proposed neural observer and adaptive control algorithm.

■ The inter-execution time intervals are influenced by the threshold $\beta_i|u_i(t)| + r_i$. In Theorem 1, the relationship between the lower bound of the inter-sampling interval t^* and the threshold $\beta_i|u_i(t)| + r_i$ is discovered. Furthermore, $\beta_i|u_i(t)| + r_i$cannot be made arbitrarily huge since it grows the control computation cost [3,15,22-25,27,38]. The lower the threshold, the more precise the control, which improves system performance [2,27,38,39,42,43,52,56].

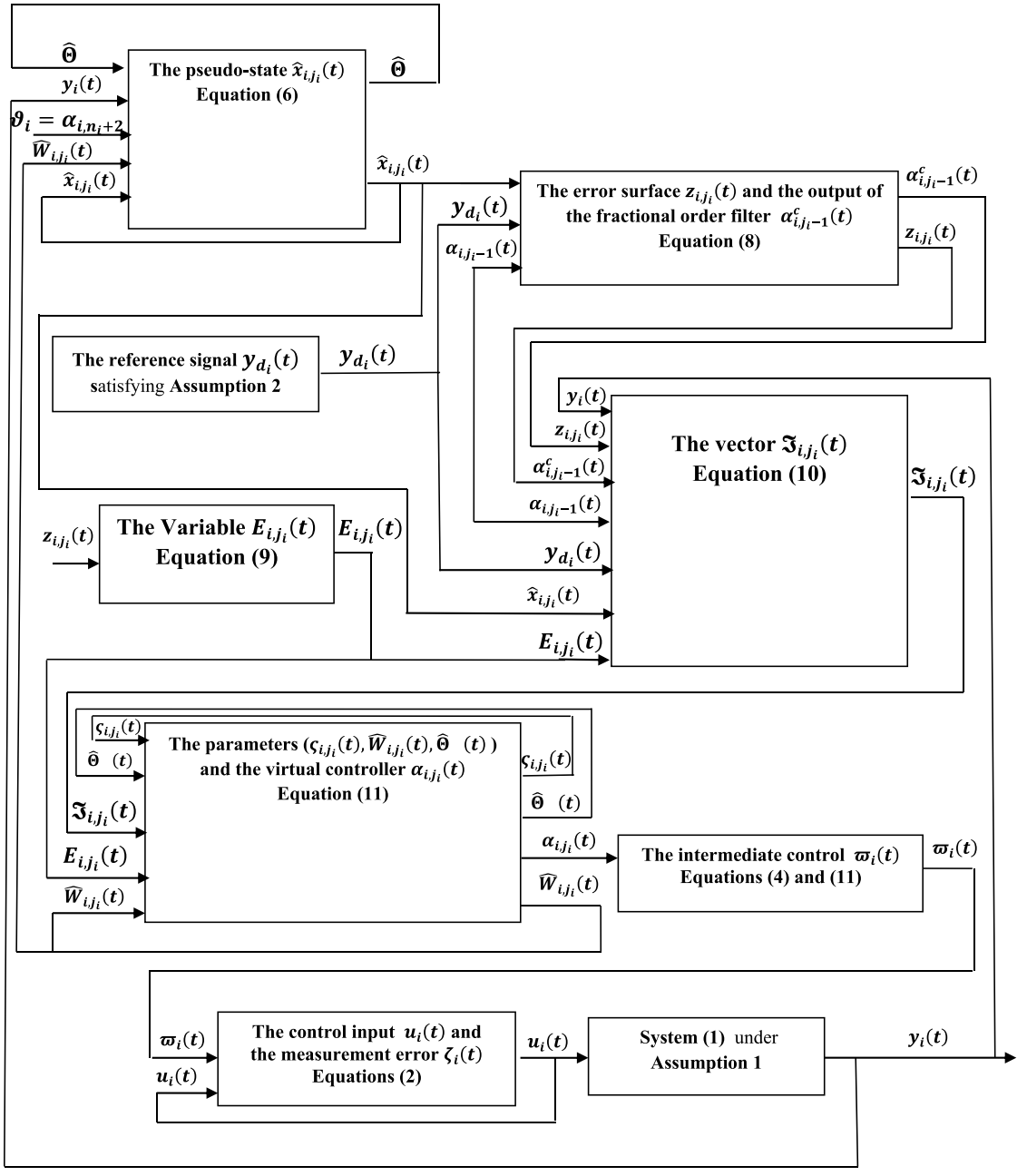

Fig.. 2. Block diagram of the proposed control scheme.

3.6. Proposed controller implementation and application

After the theoretical derivation, it is worth noting that the proposed finite-Time Observer-Based Output Feedback Adaptive Neural Control strategy can be implemented and applicable to a wide group of uncertain non-linear systems, which are described by mathematical expressions akin to (1) with an event-triggered mechanism (2) and Under Assumptions 1–2. The above analysis and results demonstrate that the proposed controller and observer include online-fitted variables with no offline learning. To recap the main points and findings mentioned above, Figs. 1 and 2 provide a flowchart and block diagram showing the practical implementation and execution of the proposed neural adaptive controller technique, respectively. The following algorithm displays the running procedure of the proposed Observer (7) and Controller (12) through a digital computer based on Theorem 1.

Remark 32. From a theoretical and practical point of view, it is obvious that;'

- Choosing adequately huge neural node numbers $\boldsymbol{q}_{i,j_i}$, a tolerably small function $\boldsymbol{\sigma}$ and large constants (K_{i,j_i}, $\boldsymbol{b}_i$, $\boldsymbol{b}_{1,i,n_i+1}$, $\boldsymbol{b}_{1,i,n_i+2}$, $\boldsymbol{b}_{2,i,j_i-1}$, $\hbar_i$, ϕ_{1,i,j_i}, ϕ_{2,i,j_i}, ϕ_3, $\boldsymbol{j_i} = 1,\ldots,\boldsymbol{n_i}+2$, $\boldsymbol{i} = 1,\ldots,\boldsymbol{p}$) during the design of neural adaptive observer and control schemes speed up the convergence to zero of the tracking error signals, the observer errors, and the error surfaces. On the other hand, this can result in massive amplitudes of the control input variables.
- For real-world applications and plants, the tradeoffs between convergence performances and control efforts have to be considered [34-37].

Remark 33. The literature has suggested a number of MATLAB and Simulink-based toolboxes, such as Fractional Order Modelling and Control (FOMCON), fractional-order transfer functions, Fractional State Space Tool (FSST), and Non-Integer Order Robust control (CRONE), for practical analog and digital realizations or implementations of fractional-order differentiator and integrator modeling and control applications [63,64]. As mentioned in [65], there are two popular techniques to numerically implement non-integer order systems. The first path consists of non-embedded implementations centered on parallel computing on reconfigurable hardware while the second path is made up of digital platforms based on ARM (Advanced RISC Machine) or embedded implementations oriented towards sequential computing in DSPs (Digital Signal Processors) [65]. In this manner, Field-Programmable Gate Arrays (FPGA) is a good choice for hardware implementation of sophisticated fractional order systems when conventional microprocessors cannot offer enough performance or design suppleness [63-65]. The implementation of the proposed controller in this work is inspired by previous related approaches.

3.7. Comparison with related works and discussion

The following are the primary advantages of this research work:

- To the best of the researchers' knowledge, there is so far no study on the problem of designing a finite-time adaptive neural network event-triggered control scheme for a general group of incommensurate fractional-order systems subject to immeasurable Pseudo-states, non-affine non-linear characteristics, actuator nonlinearities, unknown dynamics, non-strict feedback forms, asymmetric time-varying Pseudo-state constraints, unknown control directions and disturbances.
- Comparing with available works [1,9-12,18,22,27,38,42], numerous conditions and assumptions related to the estimation errors, the input-to-state stability (ISS), the functions, the dynamics, the control directions, the actuator nonlinearities, the measurement errors, the constraints, and the uncertainties are not absolutely necessary during the proposed adaptive control design.
- Approaches and techniques about the stability analysis and the control design of integer-order plants are extended to non integer-order ones by new proposed theorems, and lemmas based on Caputo's definitions.
- In comparison to the articles [1-14,34-38], the method in this article addresses a broad range of issues encountered in practical engineering applications and systems (issues provoked by incommensurate fractional-orders, asymmetric time-varying pseudo-State constraints, immeasurable Pseudo-states, dynamical disturbances, triggering mechanisms, measurement errors, zeno behavior, non-affine properties, unknown control directions, actuator nonlinearities, algebraic loops, steady-state errors and repeated calculation of virtual variables' derivatives).
- Different from the existing research [17,27,40], neither the chattering phenomena nor the singularity problems come into view in the system's response for the reason that the control inputs, the virtual control signals, and the parameter adaptive laws are continuous inside the set $\underline{\boldsymbol{\kappa}}_{1,i,j_i} < \boldsymbol{x}_{i,j_i} < \bar{\boldsymbol{\kappa}}_{1,i,j_i}$, $\boldsymbol{j_i} = 1,\ldots,\boldsymbol{n_i}$, $\boldsymbol{i} = 1,\ldots,\boldsymbol{p}$,
- In contrast to existing results [2,5,15,26,34-38,43,48], the strategy given in this study is based on an augmented nonlinear system technology, Caputo definitions and dynamic surface control method to reduce the times of controller update, and to further achieves better performance of the error system without violating the constraints,
- Preceding infinite-time tracking methods [3,42] are extended to finite-time tracking control methods for non-integer order non-strict feedback systems with asymmetric time-varying Pseudo-state constraints and nonsmooth input nonlinearities,

Remark 34. Our study's shortcomings are as follows:

- The approach suggested in this article is incapable of dealing with the difficulties caused by the Time-Delays and time-varying deferred constraints.
- In addition, our proposed controller cannot be applied directly to a class of a stochastic fractional-order system when the fractional-order value lies in the interval $[0,\ \boldsymbol{n}]$ (with $\boldsymbol{n} > 1$).

4. Simulation results

This section conducts two simulation examples to demonstrate the efficacy and superiority of our theoretical results. Similar to [34-37], all simulations are performed by applying an improved version of the Adams Bashforth-Moulton algorithm based on a predictor-corrector scheme in MATLAB R2020b environments running with the time step size10^{-4} $\boldsymbol{s}$.

Example 1. (An academic system)

Consider the following fractional-order non-strict feedback system subject to input saturation and pseudo-state constraints

$$\begin{cases} \boldsymbol{D}_t^{\delta_{1,j_1}} \boldsymbol{x}_{1,j_1} = \boldsymbol{f}_{1,j_1}(\boldsymbol{x},\ \boldsymbol{d}),\ \boldsymbol{j}_1 = 1,\cdots,3 \\ \boldsymbol{D}_t^{\delta_{1,4}} \boldsymbol{x}_{1,4} = \boldsymbol{f}_{1,4}(\boldsymbol{x},\ \boldsymbol{\nu}_1,\ \boldsymbol{d}) \\ \boldsymbol{y}_1 = \boldsymbol{x}_{1,1} \end{cases} \tag{19}$$

where

- $\boldsymbol{\delta}_{1,1} = 0.4,\ \boldsymbol{\delta}_{1,2} = 0.6,\ \boldsymbol{\delta}_{1,3} = 0.7$ and $\boldsymbol{\delta}_{1,4} = 0.3$ are the fractional orders of system (19).
- $\boldsymbol{d}_{1,1} = 0.01\ \mathbf{cos}\left(\frac{\pi t}{4}\right),\ \boldsymbol{d}_{1,2} = 0.02\ \mathbf{sin}\left(\frac{\pi t}{3}\right),\ \boldsymbol{d}_{1,3} = 0.03\ \mathbf{sin}\left(\frac{\pi t}{2}\right)$ and $\boldsymbol{d}_{1,4} = 0.2\mathbf{sin}(\pi t)$ denote external disturbances with $\boldsymbol{d} = \boldsymbol{d}_1 = \left[\boldsymbol{d}_{1,1},\ \boldsymbol{d}_{1,2},\ \boldsymbol{d}_{1,3},\ \boldsymbol{d}_{1,4}\right]^T \in \mathbb{R}^4$.
- $\boldsymbol{x} = \boldsymbol{x}_1 = \left[\boldsymbol{x}_{1,1},\ \boldsymbol{x}_{1,2},\ \boldsymbol{x}_{1,3},\ \boldsymbol{x}_{1,4}\right]^T \in \mathbb{R}^4$, $\boldsymbol{y} = \boldsymbol{y}_1 \in \mathbb{R}$, and $\boldsymbol{u} = \boldsymbol{u}_1 \in \mathbb{R}$ stand for the system pseudo-state, output, and input, respectively,
- $\boldsymbol{f}_{1,1}(\boldsymbol{x},\ \boldsymbol{d}) = \left[1 + \frac{\mathbf{sin}(\|\boldsymbol{x}\|)}{4+2\|\boldsymbol{x}\|}\right]\left[\boldsymbol{x}_{1,2} + \frac{\boldsymbol{d}_{1,1}}{1+2\|\boldsymbol{d}\|}\right]$, $\boldsymbol{f}_{1,2}(\boldsymbol{x},\ \boldsymbol{d}) = \left[1 + \frac{\mathbf{cos}(\|\boldsymbol{x}\|)}{4+2\|\boldsymbol{x}\|}\right]\left[\boldsymbol{x}_{1,3} + \frac{\boldsymbol{d}_{1,2}}{1+4\|\boldsymbol{d}\|}\right]$, $\boldsymbol{f}_{1,3}(\boldsymbol{x},\ \boldsymbol{d}) = \left[1 + \frac{\mathbf{cos}(\|\boldsymbol{x}\|)}{4+8\|\boldsymbol{x}\|}\right]\left[\boldsymbol{x}_{1,4} + \frac{\boldsymbol{d}_{1,3}}{1+4\|\boldsymbol{d}\|}\right]$ and $\boldsymbol{f}_{1,4}(\boldsymbol{x},\ \boldsymbol{\nu}_1,\ \boldsymbol{d}) = \left[\boldsymbol{\nu}_1 - 1.5\boldsymbol{x}_{1,3} - 2 + \boldsymbol{d}_{1,4}\right]\left[1 + \frac{\mathbf{sin}(\|\boldsymbol{x}_1\| + |\boldsymbol{u}_1|)}{5+8\|\boldsymbol{x}_1\|}\right]$ are continuously differentiable functions.
- $\boldsymbol{\nu} = \boldsymbol{\nu}_1 = \mathbf{sat}(\boldsymbol{u}_1) = \begin{cases} 20, & if\ \ \boldsymbol{u}_1 > 20 \\ \boldsymbol{u}_1, & if\ \ -15 \le \boldsymbol{u}_1 \le 20 \\ -15, & if\ \ \boldsymbol{u}_1 < -15 \end{cases}$ is the actuator saturation.
- The pseudo-state $\boldsymbol{x}_{1,j_1}$ is restricted to a time-varying region $\underline{\boldsymbol{\kappa}}_{1,1,j_1} < \boldsymbol{x}_{1,j_1} < \bar{\boldsymbol{\kappa}}_{1,1,j_1},\ \boldsymbol{j}_1 = 1,\cdots,4$

  with
  $\underline{\boldsymbol{\kappa}}_{1,1,1} = 0.05\mathbf{cos}(\pi t) - 0.6,\ \bar{\boldsymbol{\kappa}}_{1,1,1} = 0.1\mathbf{sin}(\pi t) + 0.5,\ \underline{\boldsymbol{\kappa}}_{1,1,2} = 0.05\mathbf{cos}(\pi t) - 1.2,\ \bar{\boldsymbol{\kappa}}_{1,1,2} = 0.1\mathbf{sin}(\pi t) + 1.2,\ -\underline{\boldsymbol{\kappa}}_{1,1,3} = 0.5\mathbf{cos}(\pi t) - 1.5,\ \bar{\boldsymbol{\kappa}}_{1,1,3} = 0.1\mathbf{sin}(\pi t) + 1.7,\ \underline{\boldsymbol{\kappa}}_{1,1,4} = 0.05\mathbf{cos}(\pi t) - 2.2$ and $\bar{\boldsymbol{\kappa}}_{1,1,4} = 0.1\mathbf{sin}(\pi t) + 2.3$.
- $\begin{cases} \boldsymbol{u}_1 = \varpi_1(\boldsymbol{t}_k)\ \forall\ \ \boldsymbol{t}_k \le t < \boldsymbol{t}_{k+1} \\ \boldsymbol{t}_{k+1} = inf\ \{t > \boldsymbol{t}_k |\ |\boldsymbol{\zeta}_1(t)| > \boldsymbol{\beta}_1|\boldsymbol{u}_1(t)| + \boldsymbol{r}_1\} \\ \boldsymbol{\zeta}_1(t) = \varpi_1(t) - \boldsymbol{u}_1(t) \end{cases}$ is the event-triggered condition with $\boldsymbol{\beta}_1 = 0.9$ and $\boldsymbol{r}_1 = 1$ being event-triggered parameters.
- The pseudo-states $\boldsymbol{x}_{1,2},\ \boldsymbol{x}_{1,3},\ \boldsymbol{x}_{1,4}$ are unmeasured, but the output $\boldsymbol{y}_1$ is measured.
- The initial conditions of the system pseudo-states are defined as $\boldsymbol{x}_{1,1}(0) = -0.2,\ \boldsymbol{x}_{1,2}(0) = 0,\ \boldsymbol{x}_{1,3}(0) = 0$ and $\boldsymbol{x}_{1,4}(0) = 0$.

According to [28,34-37], the actuator saturation can be expressed as follows

$$\boldsymbol{\nu}_1 = \Delta_{1,1}\boldsymbol{\eta}_1(\boldsymbol{u}_1) + \Delta_{2,1} \tag{20}$$

where $\Delta_{1,1} = \frac{5}{2} + \frac{35}{2}\mathbf{sign}(\boldsymbol{u}_1)$ is a bounded function with $\mathbf{sign}(.)$ being the standard sign function. $\boldsymbol{\eta}_1(\boldsymbol{u}_1) = \boldsymbol{erf}\left(\frac{\sqrt{\pi}}{2\Delta_{1,1}}\boldsymbol{u}_1\right)$ is a continuously differentiable function with $\boldsymbol{erf}(t) = \frac{2}{\sqrt{\pi}}\int_0^t \boldsymbol{exp}(-\tau^2)d\tau$ being the gauss error function. $\Delta_{2,1} = \mathbf{sat}(\boldsymbol{u}_1) - \Delta_{1,1}\boldsymbol{\eta}_1(\boldsymbol{u}_1)$ is a bounded function.

The main purpose of this example is to have the system output $\boldsymbol{y}_1$ track the reference signal $\boldsymbol{y}_{d_1} = 0.5\mathbf{sin}(\pi t)\left[1 - \mathbf{exp}\left(-0.01\mathbf{t}^3\right)\right]$ with no transgressing the constraints and Zeno behavior excluded thanks to the controller described in Section 3.

The suggested controller design algorithm is described in SubSection 3.6.

It is clear from this example that Assumptions 1–2 are met.

Akin to [34-37], Radial basis function neural networks are put into use throughout the simulation for approximating the unknown functions.

Following that, the suggested observer (6) and controller (11) are applied to the system (19) with the event-triggered mechanism (2), and design parameters are given as follows:

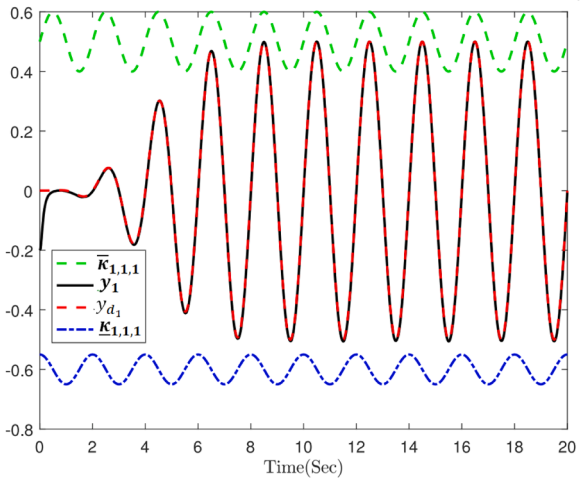

Fig. 3. System output y_1 , Reference signaly_{d_1} and constraints.

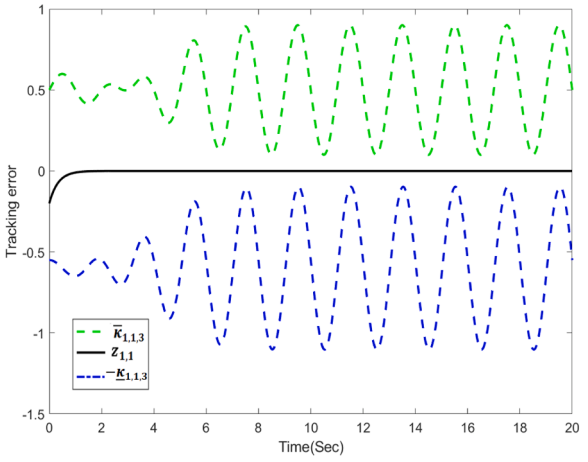

Fig. 4. Tracking error $z_{1,1}$.

■ The symmetric definite positive matrices $P_1 = \begin{bmatrix} 12.2 & -0.5 & -4.6 & 0.5 & 3.5 & -0.5 \\ -0.5 & 4.6 & -0.5 & -3.5 & 0.5 & 4.6 \\ -4.6 & -0.5 & 3.5 & -0.5 & -4.6 & 0.5 \\ 0.5 & -3.5 & -0.5 & 4.6 & -0.5 & -12.2 \\ 3.5 & 0.5 & -4.6 & -0.5 & 12.2 & -0.5 \\ -0.5 & 4.6 & 0.5 & -12.2 & -0.5 & 113.1 \end{bmatrix}$ and $Q_1 = \begin{bmatrix} 1 & 0 & 0 & 0 & 0 & 0 \\ 0 & 1 & 0 & 0 & 0 & 0 \\ 0 & 0 & 1 & 0 & 0 & 0 \\ 0 & 0 & 0 & 1 & 0 & 0 \\ 0 & 0 & 0 & 0 & 1 & 0 \\ 0 & 0 & 0 & 0 & 0 & 1 \end{bmatrix}$

■ $\boldsymbol{\delta}_{1,5} = 0.3$, $\boldsymbol{\delta}_{1,6} = 0.7$, $\boldsymbol{l}_{1j_1} = 0.001$, $\boldsymbol{b}_{1,1,5} = 8$, $\boldsymbol{b}_{1,1,6} = 7$, $\boldsymbol{b}_{2,1j_1-1} = 4$, $\boldsymbol{\phi}_{1,1j_1} = 11$, $\boldsymbol{\phi}_{2,1j_1} = 6.5$, $\boldsymbol{\phi}_3 = 7$, $\mathrm{K}_{1j_1} = \frac{6!}{(6-j_1)!\, j_1!}$, $\boldsymbol{b}_1 = 100$, $\hbar_1 = 1.1$, ***for*** $\boldsymbol{j}_1 = 1, \cdots, 6$.

■ the appropriate function $\boldsymbol{\sigma} = 0.01\boldsymbol{exp}(-5\boldsymbol{t})$,

■ The neural node number $\boldsymbol{q}_{1j_1} = 6$, for $\boldsymbol{j}_1 = 1, \cdots, 6$.

■ The hidden-layer activation function of the neural network $\boldsymbol{\xi}_{ij_i}(.)$ is a Radial basis function, $\boldsymbol{j}_1 = 1, \cdots, 6$.

■ The Radial basis function centers are uniformly distributed over the region of $[-0.5, \quad 0.5\,] \times \cdots \times [-0.5, \quad 0.5\,] \subset \mathbb{R}^6$ and the widths are all equal to 10.

■ The total execution time of the whole system $\boldsymbol{T} = 20$.

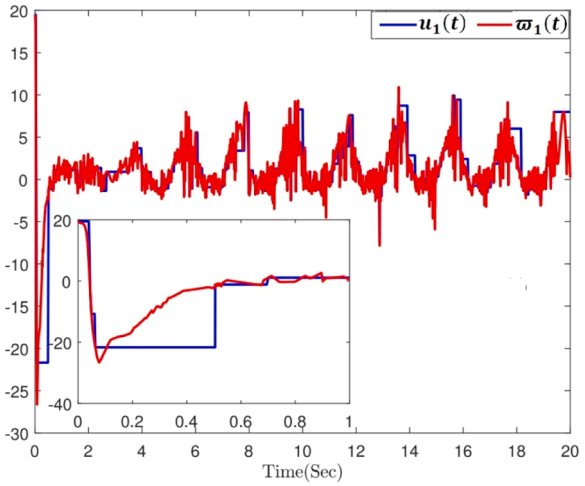

Fig. 5. Intermediate control signal $\varpi_1(t)$ and Event-triggered control signal $u_1(t)$.

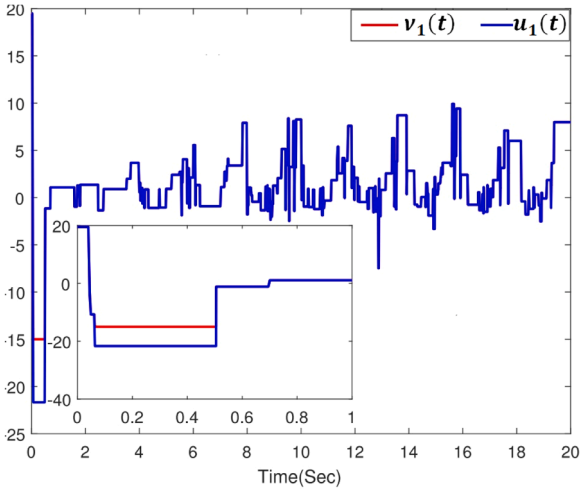

Fig. 6. Control input $\boldsymbol{u_1(t)}$ and Output of nonsmooth input nonlinearities $\boldsymbol{\nu_1(t)}$.

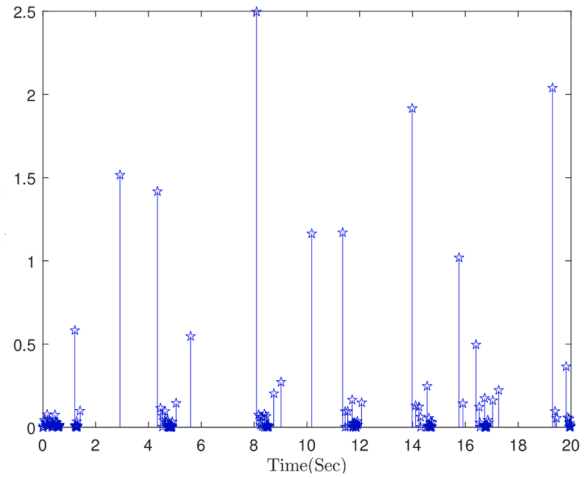

Fig. 7. Event-triggering time interval.

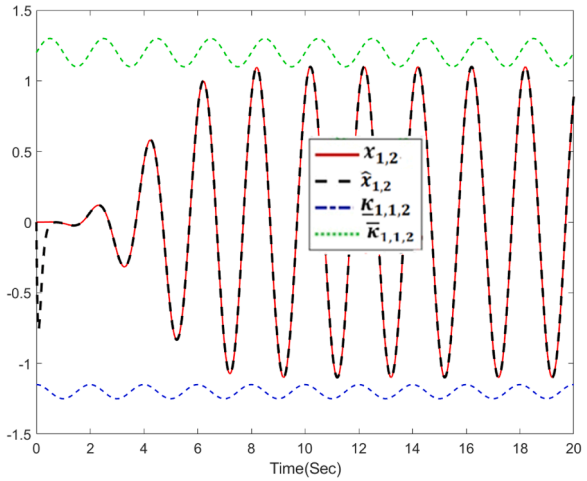

Fig. 8. Pseudo-state $\boldsymbol{x}_{1,2}$ and Pseudo-state observer $\widehat{\boldsymbol{x}}_{1,2}$.

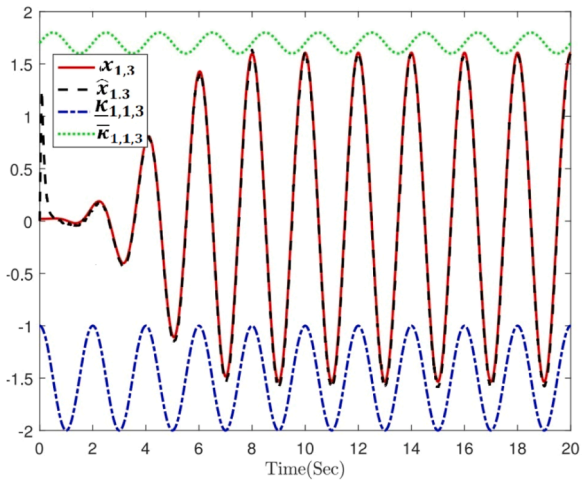

Fig. 9. Pseudo-state $\boldsymbol{x}_{1,3}$ and Pseudo-state observer $\widehat{\boldsymbol{x}}_{1,3}$.

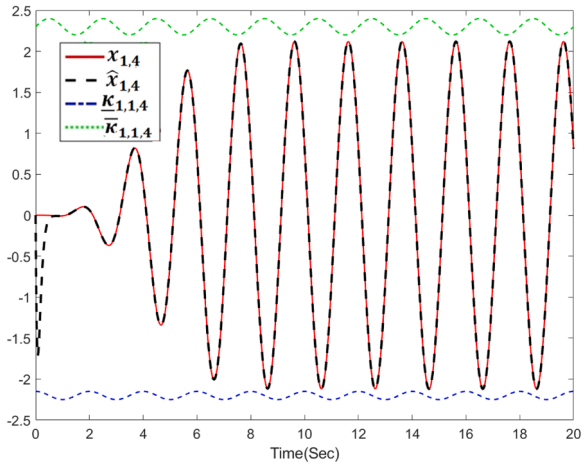

Fig. 10. Pseudo-state $\boldsymbol{x}_{1,4}$ and Pseudo-state observer $\widehat{\boldsymbol{x}}_{1,4}$.

The simulation is run by selecting the initial conditions as $\widehat{\boldsymbol{x}}_{1j_1}(0)=0,\ \widehat{\boldsymbol{W}}_{1j_1}(0)=[0,\ \ 0,\ \ 0,\ \ 0,\ \ 0,\ \ 0\ ]^{\boldsymbol{T}},\ \widehat{\Theta}(0)=0,\ \boldsymbol{\varsigma}_{1j_1}(0)=1,$ 01 and $\boldsymbol{\alpha}_{1j_1-1}(0)=0,$ **for** $\boldsymbol{j}_1=1,\ldots,6$.

Remark 35. A mathematical formula denoted by an exclamation mark "!" is the factorial function.

Remark 36. It is simple to determine $\boldsymbol{P}_1,\ \boldsymbol{Q}_1,\ \hbar_1$and $\mathrm{K}_{1j_1},\ \boldsymbol{j}_1=1,\ldots,6$ using the tools of MATLAB,

The obtained results for the proposed observer (6) and controller (11) with the event-triggered mechanism (2) are shown in Figs. 3-10. Specifically, Fig. 3 exhibits that the system output $\boldsymbol{y}_1$ successfully follows the reference signal $\boldsymbol{y}_{\boldsymbol{d}_1}$ with a minimal error within an extremely short time. Fig. 4 illustrates that the tracking error tends to zero in finite time. Fig. 5 displays the responses of intermediate continuous control $\varpi_1(\boldsymbol{t})$ and event-triggered control$\boldsymbol{u}_1(\boldsymbol{t})$. In Fig. 6, the trajectories of control input $\boldsymbol{u}_1(\boldsymbol{t})$ and actuator nonlinearity output $\boldsymbol{\nu}_1(\boldsymbol{t})$ are plotted. Fig. 7 depicts the timing of the released interval of triggered events. Figs. 8-10 give pseudo-state observer performance of $\widehat{\boldsymbol{x}}_{1,2}\ \widehat{\boldsymbol{x}}_{1,3},\ \widehat{\boldsymbol{x}}_{1,4}$, respectively.

The subsequent conclusions are drawn from the simulation results:

- All the signals in the closed-loop systems are bounded.
- The full Pseudo state constraints are not overstepped.
- Zeno behavior does not exhibit during the simulation process.
- The update frequency of control input is considerably reduced (The number of events triggered in **20 s***is* **250**, being significantly fewer than $2.10^5=\frac{20}{10^{-4}}$ which is the total number of communication with the fundamental control approach (11)).
- The proposed controller is able to track a reference signal and has strong robustness in the attendance of unknown control directions, uncertain dynamics, disturbances, asymmetric time-varying Pseudo-state constraints, and actuator nonlinearities.

Thus, our theoretical findings in Theorem 1 are successfully demonstrated and confirmed by these simulation results.

Example 2. (A Practical system: A single-link robot [36,47])

Based on Caputo fractional derivative definitions and Properties (see Definitions 2 and Property 1), the dynamic equation of a single-link robot arm consisting of a rigid link coupled through a gear train to a Direct Current (DC) motor can be expressed by

$$\begin{cases} \boldsymbol{D}_t^{\delta_{1j_1}}\boldsymbol{x}_{1j_1}=\boldsymbol{f}_{1j_1}(\boldsymbol{x},\ \boldsymbol{d}),\ \boldsymbol{j}_1=1,\cdots,5 \\ \boldsymbol{D}_t^{\delta_{1,6}}\boldsymbol{x}_{1,6}=\boldsymbol{f}_{1,6}(\boldsymbol{x},\ \boldsymbol{\nu}_1,\ \boldsymbol{d}) \\ \boldsymbol{y}_1=\boldsymbol{x}_{1,1} \end{cases} \tag{21}$$

where

- $\boldsymbol{\delta}_{1,1}=0.3,\ \boldsymbol{\delta}_{1,2}=0.3,\ \boldsymbol{\delta}_{1,3}=0.4,\ \boldsymbol{\delta}_{1,4}=0.3,\ \boldsymbol{\delta}_{1,5}=0.35$ and $\boldsymbol{\delta}_{1,6}=0.35$ denote the fractional orders of system (21).
- $\boldsymbol{x}=\boldsymbol{x}_1=\left[\boldsymbol{x}_{1,1},\ \boldsymbol{x}_{1,2},\ \ \boldsymbol{x}_{1,3},\ \boldsymbol{x}_{1,4},\ \boldsymbol{x}_{1,5},\ \boldsymbol{x}_{1,6}\right]^{\boldsymbol{T}}\in\mathbb{R}^6,\ \boldsymbol{y}=\boldsymbol{y}_1\in\mathbb{R}$ and $\boldsymbol{u}=\boldsymbol{u}_1\in\mathbb{R}$ are the system pseudo-state, output, and input, respectively,
- $\boldsymbol{x}_{1,1}$ is the angle of the rigid link.
- $\boldsymbol{x}_{1,4}$ is the angular velocity.
- $\boldsymbol{D}_t^{\delta_{1,6}}\boldsymbol{x}_{1,6}$ is the angular acceleration.
- $\boldsymbol{f}_{1,1}(\boldsymbol{x},\ \boldsymbol{d})=\boldsymbol{x}_{1,2}+\boldsymbol{d}_{1,1},\ \boldsymbol{f}_{1,2}(\boldsymbol{x},\ \boldsymbol{d})=\boldsymbol{x}_{1,3}+\boldsymbol{d}_{1,2},\ \boldsymbol{f}_{1,3}(\boldsymbol{x},\ \boldsymbol{d})=\boldsymbol{x}_{1,4}+\boldsymbol{d}_{1,3},\ \boldsymbol{f}_{1,4}(\boldsymbol{x},\ \boldsymbol{d})=\boldsymbol{x}_{1,5}+\boldsymbol{d}_{1,4},\ \boldsymbol{f}_{1,5}(\boldsymbol{x},\ \boldsymbol{d})=\boldsymbol{x}_{1,6}+\boldsymbol{d}_{1,5}$ and $\boldsymbol{f}_{1,6}(\boldsymbol{x},\ \boldsymbol{\nu}_1,\ \boldsymbol{d})=-2\boldsymbol{x}_{1,4}-10\ \mathbf{sin}(\boldsymbol{x}_{1,1})+\boldsymbol{\nu}_1+\boldsymbol{d}_{1,6}$ are continuously differentiable functions.
- $\boldsymbol{d}_{1,1}=\frac{0.015\ \mathbf{sin}\left(\frac{\pi t}{8}\right)}{1+2\|\boldsymbol{x}\|},\ \ \boldsymbol{d}_{1,2}=\frac{0.012\ \mathbf{cos}\left(\frac{\pi t}{9}\right)}{1+3\|\boldsymbol{x}\|},\ \boldsymbol{d}_{1,3}=\frac{0.02\ \mathbf{sin}\left(\frac{\pi t}{8}\right)}{1+4\|\boldsymbol{x}\|},\ \boldsymbol{d}_{1,4}=\frac{0.011\ \mathbf{cos}\left(\frac{\pi t}{8}\right)}{1+6\|\boldsymbol{x}\|},\ \boldsymbol{d}_{1,5}=\frac{0.012\ \mathbf{sin}\left(\frac{\pi t}{9}\right)}{2+4\|\boldsymbol{x}\|}$ and $\boldsymbol{d}_{1,6}=\frac{0.035\ \mathbf{sin}\left(\frac{\pi t}{11}\right)}{3+2\|\boldsymbol{x}\|}$ are external disturbances with $\boldsymbol{d}=\boldsymbol{d}_1=\left[\boldsymbol{d}_{1,1},\ \ \boldsymbol{d}_{1,2},\ \ \boldsymbol{d}_{1,3},\ \ \boldsymbol{d}_{1,4},\ \ \boldsymbol{d}_{1,5}\ ,\ \ \boldsymbol{d}_{1,6}\right]^{\boldsymbol{T}}\in\mathbb{R}^6$.
- $\boldsymbol{\nu}=\boldsymbol{\nu}_1=\begin{cases}\left(1+\frac{|\mathbf{sin}(\pi\mathbf{t})|}{8+5\boldsymbol{t}}\right)16, & \textit{if}\ \ \boldsymbol{u}_1>16\\ \left(1+\frac{|\mathbf{sin}(\pi\mathbf{t})|}{8+5\boldsymbol{t}}\right)\boldsymbol{u}_1, & \textit{if}\ \ -12\le\boldsymbol{u}_1\le16\\ -12\left(1+\frac{|\mathbf{sin}(\pi t)|}{8+5\boldsymbol{t}}\right), & \textit{if}\ \ \boldsymbol{u}_1<-12\end{cases}$ represents the input nonlinearities.
- $\begin{cases}\boldsymbol{u}_1=\varpi_1(\boldsymbol{t}_k)\ \forall\ \ \boldsymbol{t}_k\le t<\boldsymbol{t}_{k+1}\\ \boldsymbol{t}_{k+1}=\textit{inf}\ \{\boldsymbol{t}>\boldsymbol{t}_k|\ |\boldsymbol{\zeta}_1(\boldsymbol{t})|>\boldsymbol{\beta}_1|\boldsymbol{u}_1(\boldsymbol{t})|+\boldsymbol{r}_1\}\\ \boldsymbol{\zeta}_1(\boldsymbol{t})=\varpi_1(\boldsymbol{t})-\boldsymbol{u}_1(\boldsymbol{t})\end{cases}$ is the event-triggered mechanism with $\boldsymbol{\beta}_1=0.89$ and $\boldsymbol{r}_1=1.3$ being event-triggered parameters.
- The pseudo-states $\boldsymbol{x}_{1,2},\ \ \boldsymbol{x}_{1,3},\ \boldsymbol{x}_{1,4},\ \boldsymbol{x}_{1,5},\ \boldsymbol{x}_{1,6}$ are unmeasured, but the output $\boldsymbol{y}_1$ is measured.

Table 2
Single-link robot Parameters.

Description	Value	Unit
Damping coefficient	**2**	**N.s/m**
Mass of rigid link	**1.02**	**kg**
Gravitational acceleration	**9.8**	m/s^2
Rotational inertia of motor	**1**	$kg.m^2$
Distance between the joint axis and the mass center	**1**	**m**

- The initial conditions of pseudo-state are chosen as $\boldsymbol{x}_{1,1}(0) = 0.3,\ \boldsymbol{x}_{1,2}(0) = 0.2,\ \boldsymbol{x}_{1,3}(0) = 0.2,\ \boldsymbol{x}_{1,4}(0) = 0.1,\ \ \boldsymbol{x}_{1,5}(0) = -0.3$ and $\boldsymbol{x}_{1,6}(0) = -0.3$.
- The time-varying pseudo-state constraints are defined as $\underline{\boldsymbol{\kappa}}_{1,1j_1} < \boldsymbol{x}_{1j_1} < \bar{\boldsymbol{\kappa}}_{1,1j_1},\ \boldsymbol{j}_1 = 1,\cdots,6$

with

$\underline{\boldsymbol{\kappa}}_{1,1,1} = 0.4\mathbf{sin}(\boldsymbol{t}) - 0.5,\ \bar{\boldsymbol{\kappa}}_{1,1,1} = 0.1\mathbf{cos}(\boldsymbol{t}) + 0.6,\ \underline{\boldsymbol{\kappa}}_{1,1,2} = 0.2\mathbf{sin}\left(\frac{\pi}{15}\boldsymbol{t}\right) - 1.15,\ \bar{\boldsymbol{\kappa}}_{1,1,2} = 0.1\mathbf{cos}\left(\frac{\pi}{5}\boldsymbol{t}\right) + 1.75,\ \underline{\boldsymbol{\kappa}}_{1,1,3} = 0.2\ \mathbf{sin}\left(\frac{\pi}{8}\boldsymbol{t}\right) - 1.4,\ \bar{\boldsymbol{\kappa}}_{1,1,3} = 0.1\ \mathbf{cos}\left(\frac{\pi}{4}\boldsymbol{t}\right) + 1.85,\ \underline{\boldsymbol{\kappa}}_{1,1,4} = -1.35 - 0.05\mathbf{cos}(\pi\boldsymbol{t}),\ \bar{\boldsymbol{\kappa}}_{1,1,4} = 0.55.\ \underline{\boldsymbol{\kappa}}_{1,1,5} = 0.4\ \mathbf{sin}\left(\frac{\pi}{15}\boldsymbol{t}\right) - 2,\ \bar{\boldsymbol{\kappa}}_{1,1,5} = 0.5\ \mathbf{cos}\left(\frac{\pi}{8}\boldsymbol{t}\right) + 1.8,\ \underline{\boldsymbol{\kappa}}_{1,1,6} = 0.4\mathbf{sin}\left(\frac{\pi}{10}\boldsymbol{t}\right) - 2.5$ and $\bar{\boldsymbol{\kappa}}_{1,1,6} = 0.5\mathbf{cos}\left(\frac{\pi}{9}\boldsymbol{t}\right) + 1.35$.

Similar to [34-37], the input nonlinearities can be rewritten as

$$\boldsymbol{\nu}_1 = \Delta_{1,1}\boldsymbol{\eta}_1(\boldsymbol{u}_1) + \Delta_{2,1} \tag{22}$$

where $\Delta_{1,1} = 2 + 14\mathbf{sign}(\boldsymbol{u}_1)$ is a bounded function with $\mathbf{sign}(,)$ being the standard sign function. $\boldsymbol{\eta}_1(\boldsymbol{u}_1) = \left(1 + \frac{|\mathbf{sin}(\pi t)|}{8+5t}\right)\boldsymbol{erf}\left(\frac{\sqrt{\pi}}{2\Delta_{1,1}}\boldsymbol{u}_1\right)$ is a continuously differentiable function with $\boldsymbol{erf}(\boldsymbol{t}) = \frac{2}{\sqrt{\pi}}\int_0^t \boldsymbol{exp}(-\boldsymbol{\tau}^2)\boldsymbol{d\tau}$ being the gauss error function. $\Delta_{2,1}$ is a bounded function.

The physical parameters of the single-link robot are specified in Table 2.

The major goal of this example is to make the system output $\boldsymbol{y}_1$ track the desired trajectory $\boldsymbol{y}_{\boldsymbol{d}_1} = 0.5\mathbf{sin}(\boldsymbol{t})$ without violating the constraints and exhibiting Zeno behavior, due to the controller presented in Section 3.

It is obvious from this example that Assumptions 1-–2 hold.

SubSection 3.6 describes the proposed observer and controller design algorithm.

In this example, Radial basis function neural networks are used to estimate the unknown continuous function.

Then, the proposed observer (6) and controller (11) are applied to the system (21) with the event-triggered mechanism (2), and design parameters are selected as:

- $\boldsymbol{\delta}_{1,7} = 0.4,\ \boldsymbol{\delta}_{1,8} = 0.6,\ \ \boldsymbol{l}_{1j_1} = 0.001,\ \boldsymbol{b}_{1,1,7} = 8,\ \boldsymbol{b}_{1,1,8} = 7,\ \boldsymbol{b}_{2,1j_1-1} = 9,\ \boldsymbol{\phi}_{1,1j_1} = 15,\ \ \boldsymbol{\phi}_{2,1j_1} = 17,\ \boldsymbol{\phi}_3 = 8.5,\ \ \mathrm{K}_{1j_1} = \frac{8!}{(8-j_1)!\,j_1!},\ \boldsymbol{b}_1 = 136,\ \hbar_1 = 1.1,\ \boldsymbol{for}\ \boldsymbol{j}_1 = 1,\cdots,8.$
- The symmetric definite positive matrices $\boldsymbol{P}_1 = \begin{bmatrix} 97.4 & -0.5 & -24.7 & 0.5 & 12.1 & -0.5 & -9.6 & 0.5 \\ -0.5 & 24.7 & -0.5 & -12.1 & 0.5 & 9.6 & -0.5 & -12.1 \\ -24.7 & -0.5 & 12.1 & -0.5 & -9.6 & 0.5 & 12.1 & -0.5 \\ 0.5 & -12.5 & -0.5 & 9.6 & -0.5 & -12.1 & 0.5 & 24.7 \\ 12.1 & 0.5 & -9.6 & -0.5 & 12.1 & -0.5 & -24.7 & 0.5 \\ -0.5 & 9.6 & 0.5 & -12.1 & -0.5 & 24.7 & -0.5 & -97.4 \\ -9.6 & -0.5 & 12.1 & 0.5 & -24.7 & -0.5 & 97.4 & -0.5 \\ 0.5 & -12.1 & -0.5 & 24.7 & 0.5 & -97.4 & -0.5 & 1324 \end{bmatrix}$

and $\boldsymbol{Q}_1 = \begin{bmatrix} 1 & 0 & 0 & 0 & 0 & 0 & 0 & 0 \\ 0 & 1 & 0 & 0 & 0 & 0 & 0 & 0 \\ 0 & 0 & 1 & 0 & 0 & 0 & 0 & 0 \\ 0 & 0 & 0 & 1 & 0 & 0 & 0 & 0 \\ 0 & 0 & 0 & 0 & 1 & 0 & 0 & 0 \\ 0 & 0 & 0 & 0 & 0 & 1 & 0 & 0 \\ 0 & 0 & 0 & 0 & 0 & 0 & 1 & 0 \\ 0 & 0 & 0 & 0 & 0 & 0 & 0 & 1 \end{bmatrix}$.

- the appropriate function $\boldsymbol{\sigma} = 0.01\boldsymbol{exp}(-8\boldsymbol{t})$,
- The neural node number $\boldsymbol{q}_{1j_1} = 8$, for $\boldsymbol{j}_1 = 1,\cdots,8$.
- The hidden-layer activation function of the neural network $\boldsymbol{\xi}_{\boldsymbol{ij}_i}(.)$ is a Radial basis function, $\boldsymbol{j}_1 = 1,\cdots,8$.
- The Radial basis function centers are evenly distributed over the area of $[-0.5,\quad 0.5\ ] \times \cdots \times [-0.5,\quad 0.5\ ] \subset \mathbb{R}^8$ and the widths are all equal to 10.
- The total execution time of the complete system $\boldsymbol{T} = 20$.

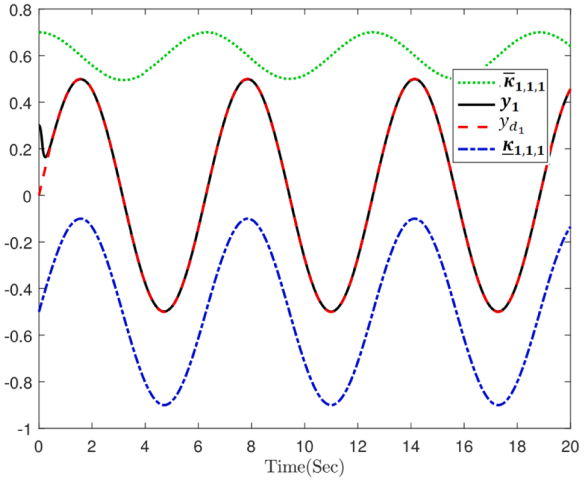

Fig. 11. System output y_1 , Reference signaly_{d_1} and constraints.

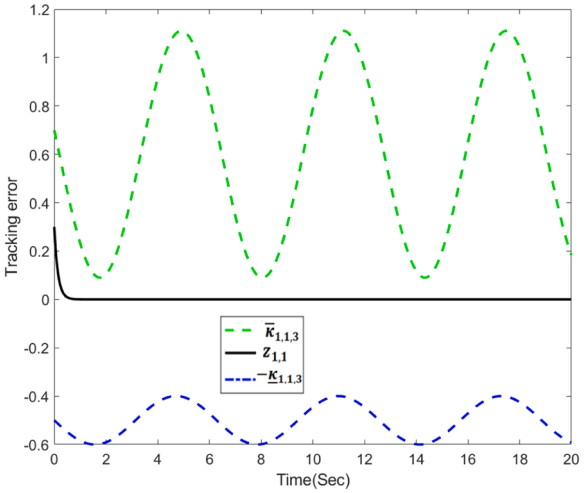

Fig. 12. Tracking error $z_{1,1}$.

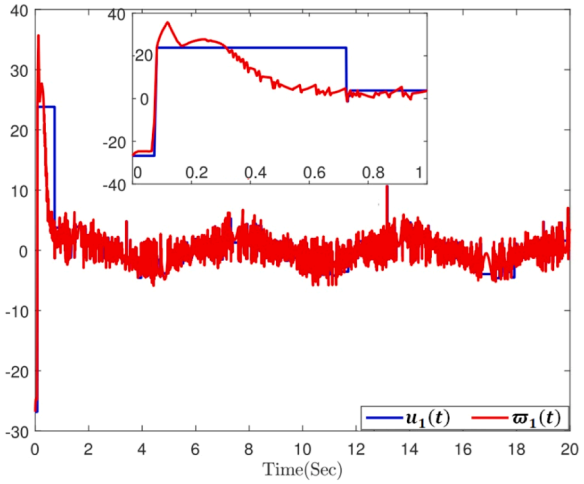

Fig. 13. Event-triggered control signal $u_1(t)$ and Intermediate control signal $\varpi_1(t)$.

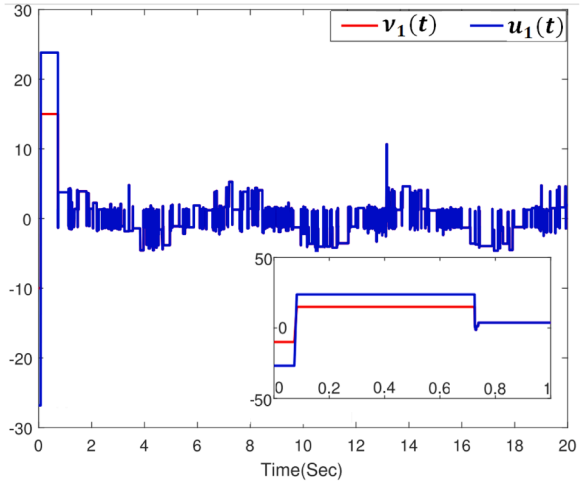

Fig. 14. Output of nonsmooth input nonlinearities $\nu_1(t)$ and Control input $u_1(t)$.

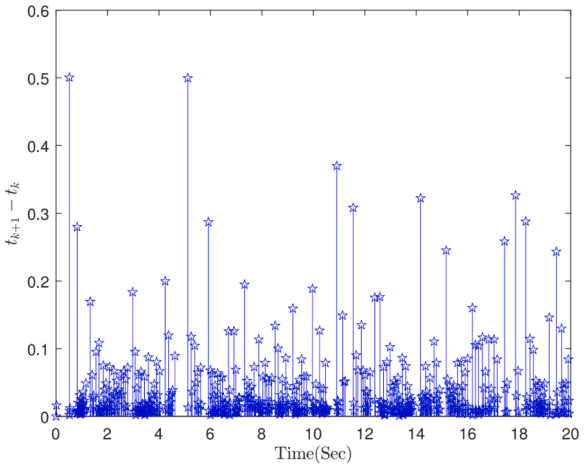

Fig. 15. Event-triggering time interval.

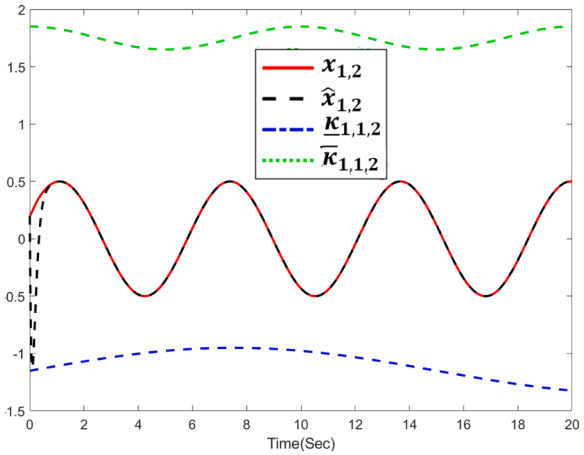

Fig. 16. Pseudo-state $x_{1,2}$ and Pseudo-state observer $\hat{x}_{1,2}$.

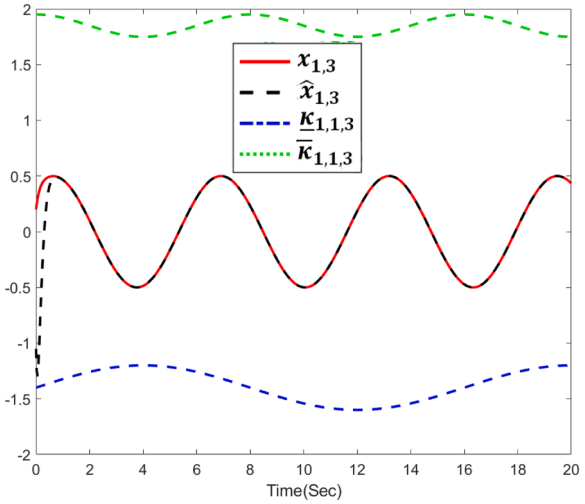

Fig. 17. Pseudo-state $x_{1,3}$ and Pseudo-state observer $\widehat{x}_{1,3}$.

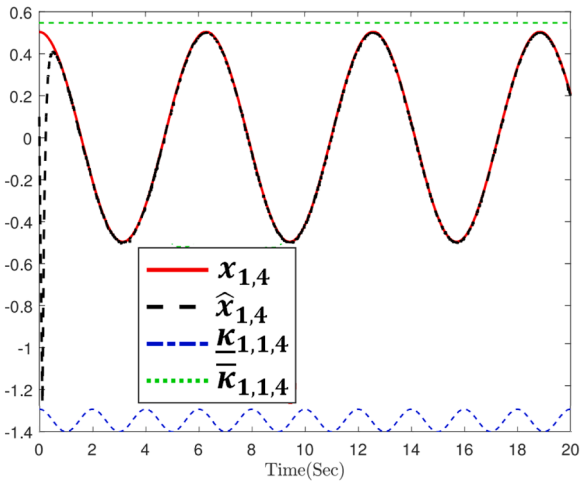

Fig. 18. Pseudo-state $x_{1,4}$ and Pseudo-state observer $\widehat{x}_{1,4}$.

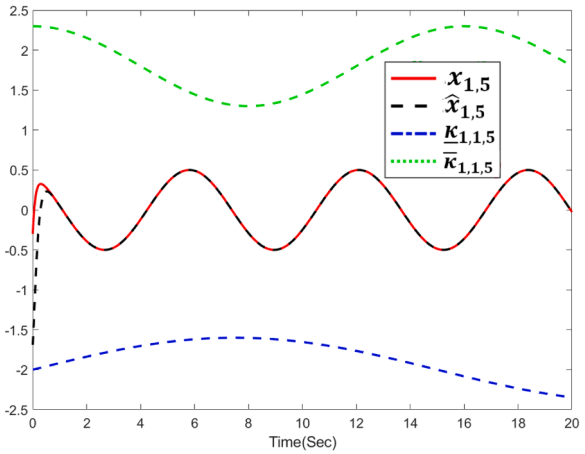

Fig. 19. Pseudo-state $x_{1,5}$ and Pseudo-state observer $\widehat{x}_{1,5}$.

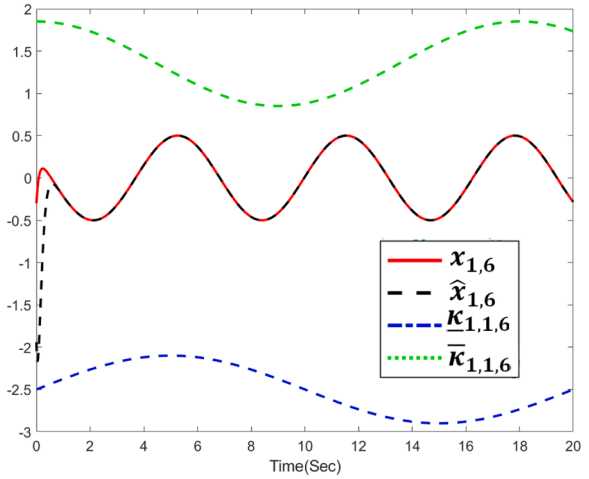

Fig. 20. Pseudo-state $x_{1,6}$ and Pseudo-state observer $\hat{x}_{1,6}$.

The simulation is run by choosing the initial conditions as follows

$$\hat{x}_{1,1}(0) = 0,\ \hat{x}_{1,2}(0) = 0.2,\ \hat{x}_{1,3}(0) = -0.9,\ \hat{x}_{1,4}(0) = 0,\ \hat{x}_{1,5}(0) = -1.6,\ \hat{x}_{1,6}(0) = -1.9$$

$$\widehat{W}_{1,j_1}(0) = [0,\ 0,\ 0,\ 0,\ 0,\ 0\ ,\ 0,\ 0]^T,\ \hat{\theta}(0) = 0,\ \varsigma_{1,j_1}(0) = 1,03$$

and $\alpha_{1,j_1-1}(0) = 0$, **for** $j_1 = 1,\ldots,8$.

The obtained results under the proposed observer (6) and controller (11) with the event-triggered mechanism (2) are displayed in Figs. 11-20. In particular, Fig. 11 indicates that the system output y_1 precisely tracks the reference signal y_{d_1} with little error over a very short period and does not transgress its constraints. Moreover, we can see with Fig. 12 that the tracking error converges to zero in finite time. The trajectories of event-triggered control $u_1(t)$ and intermediate continuous control $\varpi_1(t)$ are plotted in Fig. 13. The curves of input nonlinearity output $\nu_1(t)$ and control input $u_1(t)$ are presented in Fig. 14. Fig. 15 depicts the event triggered intervals. In addition, the pseudo-state observer performance of $\hat{x}_{1,2}$ $\hat{x}_{1,3}$, $\hat{x}_{1,4}$, $\hat{x}_{1,5}$ $\hat{x}_{1,6}$ are given in Figs. 16-20, respectively.

The simulation results: lead to the following conclusions:

- All the signals in the closed-loop systems are bounded.
- The full Pseudo state constraints are not violated.
- Zeno behavior does not exhibit throughout the simulation process.
- The number of events triggered in **20 s** is **850**, being significantly less than $2.10^5 = \frac{20}{10^{-4}}$ which is the total number of communication with the fundamental control approach (11), i.e., the update frequency of control input is significantly reduced
- The suggested controller has the ability to follow a reference signal with strong robustness in the attendance of unknown control directions, uncertain dynamics, disturbances, asymmetric time-varying Pseudo-state constraints, and input nonlinearities.
- Dynamic disturbance, asymmetric time-varying Pseudo-state constraints, unknown control directions, unmodeled dynamics, and input nonlinearities all harm system performance, especially at the start of the control period.
- These harmful effects are effectively overcome by the designed control strategy.

As a consequence, the simulation results clearly validate and verify our theoretical conclusions in Theorem 1.

Remark 37. In light of earlier research [2,3,15,22-25,27,38,39,42,43,52,56,62], our theoretical analysis suggests that despite the event-triggered control $u_1(t)$ not being identical to the intermediate continuous control $\varpi_1(t)$, the tracking errors are continuously small. As a consequence, Figs. 4 and 12 confirm both our theoretical findings and those reported in [22-25,27,38,39,42,43,52,56].

5. Conclusions and future works

This paper has largely focused on a finite-Time Output Feedback Event-Triggered Adaptive neural Control scheme for non-integer order systems subject to input nonlinearities, dynamic disturbances, asymmetric time-varying Pseudo-state constraints and unmodeled dynamics in nonaffine non-strict feedback forms. Firstly, by using Caputo fractional derivative definitions, auxiliary non-integer order integrators, novel continuous functions and the mean value theorem, the original non-affine system has been transformed into an augmented affine system. Secondly, neural networks, a high-gain observer and Nussbaum-type functions have been introduced to cope with the unknown functions, the immeasurable pseudo-states and the unknown control directions, respectively. In addition, based on fractional order filters, the dynamic surface control technique has been used to prevent the "explosion of complexity". Furthermore,

Algorithm 1
Implementation procedure of observer (7) and controller (12) Algorithm.

Step 1: Initialize k and t_k as 0. Choose the symmetric definite positive matrices P_i , Q_i, the strictly positive constants $\beta_i, r_i, \delta_{i,n_i+1}$, δ_{i,n_i+2} , K_{i,j_i}, l_{i,j_i} , b_i, b_{1,i,n_i+1}, b_{1,i,n_i+2}, b_{2,i,j_i-1}, $\hbar_i, \phi_{1,i,j_i}, \phi_{2,i,j_i}, \phi_3$, the appropriate function σ, the neural node number q_{i,j_i} and the hidden-layer activation function of the neural network $\xi_{i,j_i}(.)$. Set the initial values of the pseudo-state $\widehat{x}_{i,j_i}(0)$, the neural weight vector $\widehat{W}_{i,j_i}(0)$, the parameters $\widehat{\Theta}(0)$, $\varsigma_{i,j_i}(0)$ and the virtual control signal $\alpha_{i,j_i-1}(0)$, **for** $j_i = 1,\ldots,n_i + 2$, $i = 1,\ldots,p$. Fix the total execution time of the whole system T.

Step 2: if $t \le T$, then go to step 3.
else, go to step 20
Step 3: Update $i = 1$
Step 4: if $i \le p$ then go to step 5.
else, go to step 17
Step 5: Update $j_i = 1$
Step 6: if $j_i \le n_i + 2$ then go to step 7
else, go to step 13
Step 7: Calculate the pseudo-state $\widehat{x}_{i,j_i}(t)$, according to the Eq. (6).
Step 8: Determine the error surface $z_{i,j_i}(t)$ and the output of the fractional order filter $\alpha^c_{i,j_i-1}(t)$, using the Eq. (8).
Step 9: Calculate $E_{i,j_i}(t)$, according to the Eq. (9) with $\overline{\kappa}_{3,i,j_i} = \overline{\kappa}_{1,i,j_i} - \alpha_{i,j_i-1}$, $\underline{\kappa}_{3,i,1} = \alpha_{i,j_i-1} - \underline{\kappa}_{1,i,j_i}$ and $\alpha_{i,0} = y_{d_i}$.
Step 10: Determine the vector $\Im_{i,j_i}(t)$, according to the Eq. (10).
Step 11: Calculate the parameters $(\varsigma_{i,j_i}(t), \widehat{W}_{i,j_i}(t), \widehat{\Theta}(t))$ and the virtual controller $\alpha_{i,j_i}(t)$, using the Eq. (11).
Step 12: Update $j_i = j_i + 1$. Then, return to Step 6.
Step 13: Compute the intermediate control $\varpi_i(t)$, $i = 1,\ldots,p$ using the Eqs. (4) and (11).
Step 14: Determine the control input $u_i(t)$ and the measurement error $\zeta_i(t)$, according the Eq. (2).
Step 15: Update $i = i + 1$, Then, return to Step 4.
Step 16: if $t > t_k$ then go to step 17.
else, go to step 20.
Step 17: if $\left((|\zeta_1(t)| > \beta_1|u_1(t)| + r_1)\cdots\text{or}\ (|\zeta_p(t)| > \beta_p|u_p(t)| + r_p)\right)$ then go to step 18.
(This signifies that the event-triggered mechanism (2) is activated)
else, go to step 19.
Step 18: Update $k = k + 1$
Update $t_k = t$
Step 19: Apply the proposed observer and controller to system (1) and measure the outputs $y_i(t)$, $i = 1,\ldots,p$.
Then, Return to Step 2 for the next sampling time interval.
Step 20: End of execution

time-varying asymmetric barrier Lyapunov functions with error variables have been widely applied to arrest the violation of pseudo-State constraints. On the other hand, an event-triggered mechanism has been added into the control design process to decrease the amount of data sending out and the times of controller update. Based on the Lyapunov stability theory, it has been demonstrated that the boundedness of the closed-loop system and the error tracking performance has been guaranteed in finite time and the Zeno behavior has been excluded without any constraint breaches. Finally, Simulation studies have been provided to demonstrate the efficacy of the proposed control scheme. In our future works, we will deeply investigate and significantly extend the results obtained in this article to a more general group of fractional-order systems with input nonlinearities and time-varying deferred constraints. Furthermore, we will focus on the areas of machine learning and reinforcement learning, which have several points of overlap and complementarily with adaptive control.

Eq. (1), Eq. (14)-(15), Eq. (17)-(22), Eq. (D1.1)-(D3.1), Eq. (L1.1)-(L5.1), Eq. (P1.1)-(P2.1), Algorithm 1

CRediT authorship contribution statement

Farouk ZOUARI: Conceptualization, Formal analysis, Investigation, Methodology, Software, Writing – original draft. **Asier Ibeas:** Supervision, Validation, Writing – review & editing. **Abdesselem Boulkroune:** Supervision, Validation, Writing – review & editing. **Jinde Cao:** Validation, Writing – review & editing.

Declaration of competing interest

The authors declare that they have no known competing financial interests or personal relationships that could have appeared to influence the work reported in this paper.

Data availability

No data was used for the research described in the article.

References

[1] Xu Z, Liu Q, Yao J. Funnel function-based adaptive prescribed performance output feedback control of hydraulic systems with disturbance observers. ISA Transac 2023;136:701–14.
[2] Wei M, Li Y-X, Tong S. Event-triggered adaptive neural control of fractional-order nonlinear systems with full-state constraints. Neurocomputing 2020;412:320–6.
[3] Yue H, Feng S, Li J. Event-triggered adaptive control for stochastic nonlinear systems with time-varying full state constraints and output dead-zone. J Franklin Inst 2023;360(16):11965–94.
[4] Rigatos G, Zouari F, Cuccurullo G, Siano P, Ghosh T. Flatness-based adaptive fuzzy control for the Uzawa-Lucas endogenous growth model. In: *AIP Conference Proceedings* 2293, 310003; 2020. https://doi.org/10.1063/5.0026520.
[5] Shahvali M, Azarbahram A, Naghibi-Sistani MB, Askari Javad. Bipartite consensus control for fractional-order nonlinear multi-agent systems: an output constraint approach. Neurocomputing 2020;397:212–23.
[6] Wu Z, Rincon D, Christofides PD. Real-Time Adaptive Machine-Learning-Based Predictive Control of Nonlinear Processes. Indust Engineer Chem Res, Amer Chem Soc 2020. https://doi.org/10.1021/acs.iecr.9b03055.
[7] Wang Z-M, Zhao X, Li X, Wei A. Finite-time adaptive control for uncertain switched port-controlled Hamiltonian systems. Communic Nonlin Sci Numer Simul 2023;119:107129.
[8] Boulkroune A, Hamel S, Zouari F, Boukabou A, Ibeas A. Output-Feedback Controller Based Projective Lag-Synchronization of Uncertain Chaotic Systems in the Presence of Input Nonlinearities. Mathem Probl Engineer 2017:12. https://doi.org/10.1155/2017/8045803,2017. 8045803pages.
[9] Merazka L, Zouari F, Boulkroune A. High-gain observer-based adaptive fuzzy control for a class of multivariable nonlinear systems. In: 2017 6th International Conference on Systems and Control (ICSC); 2017. https://doi.org/10.1109/ICoSC.2017.7958728.
[10] Shojaei F, Zarei J, Saif M. Observer-based adaptive dynamic surface control of time-delayed non-strict systems with input nonlinearities. J Franklin Inst 2023;360(9):6490–514.
[11] Deng X, Zhang C, Ge Y. Adaptive neural network dynamic surface control of uncertain strict-feedback nonlinear systems with unknown control direction and unknown actuator fault. J Franklin Inst 2022;359(9):4054–73.
[12] Hamel S, Boulkroune A. A generalized function projective synchronization scheme for uncertain chaotic systems subject to input nonlinearities. Int J Gen Syst 2016;45(6):689–710.
[13] Yan L, Liu Z, Chen CLP, Zhang Y, Wu Z. Reinforcement learning based adaptive optimal control for constrained nonlinear system via a novel state-dependent transformation. ISA Transac 2023;133:29–41.
[14] Debnath R, Gupta GS, Kumar D. Observer-based adaptive control and stabilization of grid-tied inverters under PLL nonlinearities and weak grid. Electr Engineer 2023;105:905–19.
[15] Meng X, Jiang B, Karimi HR, Gao C. An event-triggered mechanism to observer-based sliding mode control of fractional-order uncertain switched systems. ISA Transac 2023;135:115–29.
[16] Long L, Wang Z, Zhao J. Switched adaptive control of switched nonlinearly parameterized systems with unstable subsystems. Automatica 2015;54:217–28.
[17] Merazka L, Zouari F, Boulkroune A. Fuzzy state-feedback control of uncertain nonlinear MIMO systems. In: 2017 6th International Conference on Systems and Control (ICSC); 2017. https://doi.org/10.1109/ICoSC.2017.7958730.
[18] Haddad M, Zouari F, Boulkroune A, Hamel S. Variable-structure backstepping controller for multivariable nonlinear systems with actuator nonlinearities based on adaptive fuzzy system. Soft Comput 2019;23:12277–93.
[19] Zouari F, Ben Saad K, Benrejeb M. Adaptive backstepping control for a class of uncertain single input single output nonlinear systems. In: 10th International Multi-Conferences on Systems, Signals & Devices 2013 (SSD13); 2013. https://doi.org/10.1109/SSD.2013.6564134.
[20] Wang G, Zhao Y, Liu C, Qiao J. Data-driven robust adaptive control with deep learning for wastewater treatment process. IEEE Transac Indust Inform 2023:1–8. https://doi.org/10.1109/TII.2023.3257296.
[21] Sun L, Huang X, Song Y. Decentralized Intermittent Feedback Adaptive Control of Non-Triangular Nonlinear Time-Varying Systems. IEEE Transac Autom Control 2023:1–8. https://doi.org/10.1109/TAC.2023.3282450.
[22] Wu Y, Zhang G, Wu L-B. Command filter-based adaptive fuzzy switching event-triggered control for non-affine nonlinear systems with actuator faults. Inform Sci 2023;638:118991.
[23] Wang N, Hao F. Event-triggered sliding mode control with adaptive neural networks for uncertain nonlinear systems. Neurocomputing 2021;436:184–97.
[24] Qiao J, Sun J, Meng X. Event-triggered adaptive model predictive control of oxygen content for municipal solid waste incineration process. IEEE Transac Autom Sci Engineer 2022:1–12. https://doi.org/10.1109/TASE.2022.3227918.
[25] Jiang Yi, Shi D, Fan J, Chai T. Event-Triggered Model Reference Adaptive control for linear partially time-variant continuous-time systems with nonlinear parametric uncertainty. IEEE Transac Autom Control 2023;68(3):1878–85.
[26] Boubellouta A, Zouari F, Boulkroune A. Intelligent fuzzy controller for chaos synchronization of uncertain fractional-order chaotic systems with input nonlinearities. Int J Gen Syst 2019;48(3):211–34.
[27] Pan R, Tan Y, Du D, Fei S. Adaptive event-triggered synchronization control for complex networks with quantization and cyber-attacks. Neurocomputing 2020;382:249–58.
[28] Zouari F, Boulkroune A, Ibeas A, Arefi MM. Observer-based adaptive neural network control for a class of MIMO uncertain nonlinear time-delay non-integer-order systems with asymmetric actuator saturation. Neural Comp Applic 2017;28:993–1010. Supplement 1.
[29] Zouari F. Neural network based adaptive backstepping dynamic surface control of drug dosage regimens in cancer treatment. Neurocomputing 2019;366:248–63.
[30] Liu Z, Gao H, Yu X, Lin W, Qiu J, R.-Andina JJ. B-spline wavelet neural-network-based adaptive control for linear-motor-driven systems via a novel gradient descent algorithm. IEEE Transac Indust Electron 2024;71(2):1896–905.
[31] Pfeiffer K, Escande A, Gergondet P, Kheddar A. The hierarchical Newton's method for numerically stable prioritized dynamic control. IEEE Transac Control Syst Technol 2023;31(4):1622–35.
[32] Noman AM, Khan H, Sher HA, Almutairi SZ, Alqahtani MH, Aljumah AS. Scaled conjugate gradient artificial neural network-based ripple current correlation MPPT Algorithms for PV system. Int J Photoener 2023;2023:8. Article ID 8891052pages.
[33] Feukeu EA, Sumbwanyambe M. Using neural network and levenberg–marquardt algorithm for link adaptation strategy in vehicular Ad Hoc network. IEEE Access 2023;11:93331–40.
[34] Zouari F, Ibeas A, Boulkroune A, CAO J, Arefi MMehdi. Neural network controller design for fractional-order systems with input nonlinearities and asymmetric time-varying Pseudo-state constraints. Chaos, Soliton Fract 2021;144:1–40.
[35] Zouari F, Ibeas A, Boulkroune A, Cao J, Arefi MM. Neuro-adaptive tracking control of non-integer order systems with Input Nonlinearities and time-varying Output Constraints. Inform Sci 2019;485:170–99.
[36] Zouari F, Ibeas A, Boulkroune A, Cao J, Arefi MM. Adaptive neural output-feedback control for nonstrict-feedback time-delay fractional-order systems with output constraints and actuator nonlinearities. Neur Netw 2018;105:256–76.
[37] Zouari F, Boulkroune A, Ibeas A. Neural Adaptive quantized output-feedback control- based synchronization of uncertain time-delay incommensurate fractional-order chaotic systems with input nonlinearities. Neurocomputing 2017;237:200–25.
[38] Cao B, Nie X. Event-triggered adaptive neural networks control for fractional-order nonstrict-feedback nonlinear systems with unmodeled dynamics and input saturation. Neur Netw 2021;142:288–302.
[39] Tong S, Zhou H. Finite-time adaptive fuzzy event-triggered output-feedback containment control for nonlinear multiagent systems with input saturation. IEEE Transac Fuzzy Syst 2023;31(9):3135–47.

[40] Zhang JX, Yang G-H. Low-complexity tracking control of strict-feedback systems with unknown control directions. IEEE Transac Autom Control 2019;64(12):5175–82.
[41] Dong L, Li P, Feng W. Adaptive motion control of non-affine unmanned hovercraft under asymmetries constraints. In: 2023 IEEE International Conference on Mechatronics and Automation (ICMA); 2023. https://doi.org/10.1109/ICMA57826.2023.10215750.
[42] Liang H, Liu G, Zhang H, Huang T. Neural-network-based event-triggered adaptive control of nonaffine nonlinear multiagent systems with dynamic uncertainties. IEEE Transac Neur Netw Learn Syst 2020;32(5):2239–50.
[43] Li Y, Wang H, Zhao X, Xu N. Event-triggered adaptive tracking control for uncertain fractional-order nonstrict-feedback nonlinear systems via command filtering. Int J Robust Nonl Control 2022. https://doi.org/10.1002/rnc.6255.
[44] Meng W, Yang Q, Jagannathan S, Sun Y. Adaptive neural control of high-order uncertain nonaffine systems: a transformation to affine systems approach. Automatica 2014;50(5):1473–80.
[45] Li Y, Gao Q, Yang R, Liu H. Finite-time formation control of nonaffine nonlinear systems under directed communication interactions. J Franklin Inst 2023;360(11):7180–205. Issues.
[46] Liu Y-H, Huang L, Xiao D. Adaptive dynamic surface control for uncertain nonaffine nonlinear systems. Int J Robust Nonl Control 2016. https://doi.org/10.1002/rnc.3583.
[47] Wang C, Wu Y, Yu J. Barrier Lyapunov functions-based adaptive control for nonlinear pure-feedback systems with time-varying full state constraints. Int J Control, Autom Syst 2017;15:2714–22.
[48] Liang M, Chang Y, Zhang F, Wang S, Wang C, Lu S, Wang Y. Observer-based adaptive fuzzy output feedback control for a class of fractional-order nonlinear systems with full-state constraints. Int J Fuzzy Syst 2022;24:1046–58.
[49] Zhu Y, Dong Z, Cheng Z, Huang X, Dong Y, Zhang Z. Neural network extended state-observer for energy system monitoring. Energy 2023;263(Part A):125736.
[50] Iqbal W, Ghous I, Ansari EA, Duan Z, Imran M, Khan AA, Humayun MT. Robust nonlinear observer-based controller design for one-sided Lipschitz switched systems with time-varying delays. J Franklin Inst 2023;360(3):2046–67.
[51] Liu YJ, Shen X, Alcaide AM, Yin Y, Leon JI, Vazquez S, Wu L. Sliding mode control of grid-connected neutral-point-clamped converters via high-gain observer. IEEE Transac Industr Electron 2022;69(4):4010–21.
[52] Shoukry Y, Tabuada P. Event-triggered state observers for sparse sensor noise/attacks. IEEE Transac Autom Control 2016;61(8):2079–91.
[53] Khalil HK. High-gain observers in feedback control: application to permanent magnet synchronous motors. IEEE Control Syst Magazine 2017;37(3):25–41.
[54] Tan Y, Xiong M, Du D, Fei S. Observer-based robust control for fractional-order nonlinear uncertain systems with input saturation and measurement quantization. Hybrid Syst 2019;34:45–57.
[55] Sakthivel R, Ahn CK. Fault-tolerant resilient control for fuzzy fractional order systems. IEEE Transac Syst, Man, Cybern 2019;49(9):1797–805.
[56] Kang S, Wang H, Chen M, Liu PX. Event-triggered adaptive backstepping tracking control for a class of nonlinear fractional order systems. Int J Adap Control Sign Process 2021. https://doi.org/10.1002/acs.3211.
[57] He S, Sun K, Wang H. Dynamics of the fractional-order Lorenz system based on Adomian decomposition method and its DSP implementation. IEEE/CAA J Automatica Sinica 2016:1–6. https://doi.org/10.1109/JAS.2016.7510133.
[58] Li H, Liao X, Luo M. A novel non-equilibrium fractional-order chaotic system and its complete synchronization by circuit implementation. Nonl Dynam 2012;68:137–49.
[59] Tavazoei MS, Haeri M. Unreliability of frequency-domain approximation in recognising chaos in fractional-order systems. IET Signal Process 2007;1(4):171–81.
[60] Chen W, Dai H, Song Y, Zhang Z. Convex Lyapunov functions for stability analysis of fractional order systems. IET Control Theor Applic 2017;11(7):1070–4.
[61] Hayakawa T, Haddad Wassim M, Hovakimyan N. Neural network adaptive control for a class of nonlinear uncertain dynamical systems with asymptotic stability guarantees. IEEE Transac Neural Netw 2008;19(1):80–9.
[62] Sedghi L, Ijaz Z, N.-A-Rahim Md, Witheephanich K, Pesch D. Machine learning in event-triggered control: recent advances and open issues. IEEE Access 2022;10:74671–90.
[63] Tolba MF, Saleh H, Mohammad B, Al-Qutayri M, Elwakil AS, Radwan AG. Enhanced FPGA realization of the fractional-order derivative and application to a variable-order chaotic system. Nonl Dynam 2020;99:3143–54.
[64] Bingi K, Ibrahim R, Karsiti MN, Hassan SM, Harindran VR. Fractional-order systems and PID controllers using scilab and curve fitting based approximation techniques. Stud Syst, Decis Control 2022;264.
[65] C.López D, M.Pacheco JM, d J. R.Magdaleno J. A review of the digital implementation of continuoustime fractionalorder chaotic systems using FPGAs and embedded hardware. Arch Comput Methods Engineer 2023;30:951–83.
[66] Qiu J, Ji W, Lam H-K. A new design of fuzzy affine model-based output feedback control for discrete-time nonlinear systems. IEEE Transac Fuzzy Syst 2023;31(5):1434–44.
[67] Bi Y, T.Wang JQiu, Li M, Wei C, Yuan L. Adaptive decentralized finite-time fuzzy secure control for uncertain nonlinear CPSs under deception attacks. IEEE Transac Fuzzy Syst 2023;31(8):2568–80.
[68] Rauh A. Exponential enclosures for the verified simulation of fractional-order differential equations. Frac Fract 2022;6(10):567.
[69] Zouari F, Boubellouta A. Adaptive neural control for unknown nonlinear time-delay fractional-order systems with input saturation" igi global, advanced synchronization control and bifurcation of chaotic fractional-order systems. 2018. p. 54–98.
[70] Zouari F, Boubellouta A. Neural approximation-based adaptive control for pure-feedback fractional-order systems with output constraints and actuator nonlinearities" igi global, advanced synchronization control and bifurcation of chaotic fractional-order systems. 2018. p. 468–95.
[71] Toumia O, Zouari F. Artificial intelligence and venture capital decision-making" igi global. Fostering Innovation in Venture Capital and Startup Ecosystems. 2024. p. 16–38.